

Jimma University
Jimma Institute of Technology
Faculty of Mechanical Engineering



**Study of the Performance of Spur Gear with Backlash
and its Effect on Flash Temperature**

Submission Date

February 2020

Study of the Performance of Spur Gear with Backlash and its Effect on Flash Temperature

By
Getachew Admassie

A Thesis Submitted to the Faculty of Graduate Studies of Jimma University in Partial Fulfillment of the Requirements for the Degree of the Masters of Science in Mechanical System Design

Thesis Advisors

Main advisor: Prof. Hirpa G.Lemu (PhD)

Co advisor: Abiyou Solomon (PhD Candidate)

Approved by


External Examiner: Dr.-Ing Getachew Shunki (PhD)

Signature _____

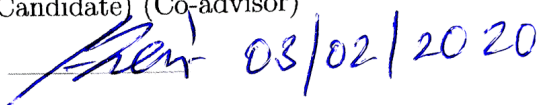
Internal Examiner: Johnson Santhosh (PhD)

Signature _____

Prof. Hirpa G.Lemu (PhD) (Main advisor)

Signature  29/1-20'

Abiyou Solomon (PhD Candidate) (Co-advisor)

Signature  03/02/2020

February 2020

Abstract

Spur gears are employed dominantly in many industrial machines and engineering products because of their simplicity in design and manufacturing. The life of a gear is limited due to time-varying tooth mesh stiffness and nonlinearities such as backlash, which is the gap between gear tooth that can be made deliberately for thermal expansion, lubrication and others. Alternatively, backlash can be introduced in gears due to manufacturing and assembly errors or as a result of modifications done on tooth thickness or center distance. In this thesis, Gear Trax has been used to model the gears with different amount of backlash and the gear models have been generated by integrating it with Autodesk Inventor. A plain strain analysis is used to predict the static transmission error, dynamic transmission error and flash temperature of spur gear with different backlash at different coefficients of friction using ABAQUS software. Flash temperature of the spur gear is analyzed using Block's equation and finite element transient coupled temperature displacement analysis for gear without backlash, and both methods are in good agreement with in the single tooth contact region. The prediction of flash temperature has been continued using finite element analysis.

The results indicate that static and dynamic transmission errors of the spur gear affect the backlash of the gear. The time-varying mesh stiffness of spur gear is dramatically influenced by a backlash, where a simple modification of gear tooth thickness leads to a huge reduction of mesh stiffness. The gear without backlash exhibits maximum flash temperature than the gear with backlash. The minimum temperature is found for a gear with 0.2 mm backlash, as the backlash increased from 0.2 to 1 mm, the flash temperature of the gear also increased, perhaps this could be the result of impact forces. Therefore, it is concluded that backlash of 0.2 mm gives an optimum result for flash temperature.

Eventually, the dynamic forces and the acceleration of the spur gear at different backlash have been examined for three loadings using ADAMS software, and the results show that the backlash has minor effects on the dynamic forces, while the effect on the acceleration is significant. Generally, backlash affects the performance of the gear.

Key words: Backlash, flash temperature, single tooth contact, transmission error.

Declaration

I, the undersigned, declare that this thesis report entitled “ Study of the Performance of Spur Gear with Backlash and its Effect on Flash Temperature ” is my original work, and has not been presented by any other people for an award of degree in this or any other University.

Name: Getachew Admassie

Signature:  _____ Date 04/02/2020

Acknowledgment

First and foremost, praises and thanks to God, the Almighty, for His shower of blessings throughout my MSc study and research work and to complete the research successfully.

I would like to express my sincere gratitude to my main advisor Prof. Hirpa G. Lemu (Ph.D.), for the continuous support of my MSc research, for his patience, motivation, and immense knowledge. His guidance helped me in all the time of research and writing of this thesis. He has taught me the methodology to carry out the research and to present the research works as clearly as possible. During the research work his punctuality amazed me every time, he gave me his time with fruitful ideas and comments, having discussions with Skype makes me feel as he is nearby me even if he abroad and he is the one that makes me realize it's possible to advise in the distance. It was a great privilege and honor to work and study under his guidance. I am extremely grateful for what he has offered me.

Furthermore, I would like to thank my Co-advisory Mr. Abiyou Solomon (Ph.D. Candidate) for his encouragement from the proposal up to the completion of this thesis.

Besides my advisors, my sincere thanks also go to Mr. Mesay Alemu (Ph.D.), for his genuine comments during this thesis writing.

Last but not the least, I would like to thank my family (specifically my mom, Wawi) and to my friends and colleagues for providing me with unfailing support and continuous encouragement throughout my years of study and through the process of researching and writing this thesis directly or indirectly. This accomplishment would not have been possible without them.

Contents

Abstract	ii
Declaration	iii
Acknowledgment	iv
List of Figures	x
List of Tables	xi
Glossary	xii
1 Introduction	1
1.1 Background	1
1.2 Motivation of the study	4
1.3 Statement of the problem	5
1.4 Questions to be addressed in this thesis	5
1.5 Objectives of the study	6
1.5.1 <i>General objective</i>	6
1.5.2 <i>Specific objectives</i>	6
1.6 Scope of the study	7
1.7 Significance of the study	7
1.8 Organization of the report	8
2 Literature Review	9
2.1 Introduction	9
2.2 General research review	10
2.2.1 <i>Research review on backlash of the gear</i>	10
2.2.2 <i>Research review on the flash temperature of the gear</i>	13
2.3 Research gaps from literature survey	17
3 Research Method and Materials	18
3.1 Introduction	18
3.2 Design and modeling of spur gear	21

3.2.1	<i>Types of gears</i>	21
3.2.2	<i>Common terminology of gears</i>	23
3.3	Geometrical design of spur gear	24
3.3.1	<i>Design for dynamic and wear load</i>	26
3.3.2	<i>Design of shafts and gear hub diameter</i>	27
3.4	Load sharing of gear	28
4	Determination of Important Contact Parameters for Spur Gear Design	30
4.1	Introduction	30
4.2	Contact length and rolling angles	31
4.3	Surface velocity and sliding velocity	32
4.4	Contact width and contact stress	34
4.4.1	<i>Contact width</i>	35
4.4.2	<i>Contact pressure</i>	37
5	Effect of Backlash on Transmission Error and Time Varying Mesh Stiffness	39
5.1	Introduction	39
5.1.1	<i>Types of transmission error</i>	40
5.1.2	<i>Methods of estimating TVMS and load sharing</i>	42
5.2	Numerical analysis of TE, TVMS and load sharing	48
5.2.1	<i>Mesh convergence</i>	48
5.2.2	<i>Static transmission error analysis of gear with backlashes</i>	50
5.2.3	<i>Dynamic transmission error analysis of gear with backlashes</i>	52
5.2.4	<i>Influence of backlash on time-varying mesh stiffness</i>	54
5.2.5	<i>Numerical analysis of torsional mesh stiffness</i>	55
5.2.6	<i>Numerical analysis of load sharing</i>	57
6	Effect of Backlash on the Flash Temperature of the Spur Gear	58
6.1	Introduction	58
6.2	Peclet number	59
6.3	Heat generation due to friction	61
6.4	Flash and conjunction temperature using Block's equation	62
6.5	Minimum film thickness	64
6.6	Numerical analysis of flash temperature	66
6.6.1	<i>Flash temperature of spur gear without backlash</i>	66

6.6.2	<i>Data regression analysis of experimental and FE result</i>	69
6.6.3	<i>Comparison of Block's equation and numerical analysis</i>	72
6.6.4	<i>Numerical analysis of flash temperature of spur gear at different backlash</i>	73
7	Dynamics of Spur Gear with Backlash	76
7.1	Introduction	76
7.2	Modeling of spur gear with different backlash	78
7.3	Boundary condition for dynamics analysis	79
7.4	Results and discussions for dynamics	80
7.4.1	<i>Contact force</i>	80
7.4.2	<i>Driving gear wheel (Pinion)</i>	83
7.4.3	<i>Driven gear wheel (Gear)</i>	88
8	Conclusions and Recommendations	93
8.1	Conclusion	93
8.2	Recommendations for future study	95
	Bibliography	96
	Appendix	102
A	Experimental data of flash temperature	102
B	Values of flexural endurance and surface endurance limit	106
C	Values of coefficients equation 5.8	108
D	Matlab code to calculate essential parameters	109
E	Matlab code for heat generation and flash temperature calculation	112
F	Matlab code for mesh stiffness calculation	113
G	Lubricant parameters	118
H	Finite Element analysis summary	119
I	Systems of consistent units	120
J	ADAMS procedures for a dynamic analysis	121

List of Figures

1.1	Illustration of backlash.	2
1.2	Backlash due to (a) tooth thickness modification and (b) center distance modification.	3
2.1	Gear tooth surface (a) pitting and (b) spall	9
3.1	Research methodology.	19
3.2	Flash temperature of spur gear obtained using experimental approach	20
3.3	3D model of (a) spur, (b) helical, (c) bevel and (d) worm gear.	22
3.4	Load sharing along line of contact	29
4.1	2D Model of spur gear.	31
4.2	Gear (a) radius of curvature and (b) velocities of gear.	33
4.3	Contact between two sectioned cylinders, general case	35
4.4	Contact width.	36
4.5	Maximum contact pressure.	37
5.1	Transmission error.	40
5.2	Geometric parameters for gear body.	43
5.3	Analytical calculation of (a) mesh stiffness and (b) time varying mesh stiffness.	45
5.4	Geometry of involute external teeth.	46
5.5	Approximate method calculation of (a) mesh stiffness and (b) load sharing.	47
5.6	FE analysis procedures.	48
5.7	Boundary condition and load.	49
5.8	von Mises stress.	49
5.9	Contact pressure.	49
5.10	Mesh convergency.	50
5.11	STE of gear with: (a) 0 mm, (b) 0.2 mm, (c) 0.4 mm, (d) 0.6 mm, (e) 0.8 mm and (f) 1 mm backlash.	51
5.12	STE of spur gear at different backlash with $\mu = 0.15$	52

5.13 DTE of gear with: (a) 0 mm, (b) 0.2 mm, (c) 0.4 mm, (d) 0.6 mm, (e) 0.8 mm and (f) 1 mm backlash.	53
5.14 TVMS of gear with: (a) 0 mm, (b) 0.2 mm, (c) 0.4 mm, (d) 0.6 mm, (e) 0.8 mm and (f) 1 mm backlash.	55
5.15 Torsional mesh stiffness at $\mu = 0.15$	56
5.16 Load sharing pattern obtained by FEA.	57
6.1 Peclet number.	60
6.2 Heat generation.	61
6.3 Gear (a) flash and (b) conjunction temperature.	63
6.4 Lubrication regimes (a) HDL, (b) ML, (c) BL and (d) Solid-film lubrication. . .	64
6.5 Film thickness.	65
6.6 Load and boundary conditions.	67
6.7 Numerical results of gear with 0 mm backlash flash temperature at: (a) mesh initiation, (b) pitch point and (c) mesh termination.	68
6.8 Experimental (by Tobe et al.[11]) and FE results	69
6.9 Data regression for experimental and FE results with in STC region	70
6.10 Comparison of FE and Block's equation spur gear with 0 mm backlash with: (a) $\mu = 0.15$, (b) $\mu = 0.2$ and (c) $\mu = 0.3$	72
6.11 Flash temperature of gear with: (a) 0 mm, (b) 0.2 mm, (c) 0.4 mm, (d) 0.6 mm, (e) 0.8 mm and (f) 1 mm backlash.	73
6.12 Flash temperature of gear at different backlash with:(a) $\mu = 0.15$, (b) $\mu = 0.2$ and (c) $\mu = 0.3$	74
7.1 Tooth profile and contact points of (a) pinion and (b) gear.	78
7.2 Boundary conditions and loading for dynamics.	80
7.3 (a) Radial and (b) Tangential loads for load case 1.	81
7.4 (a) Radial and (b) Tangential loads for load case 2.	81
7.5 (a) Radial and (b) Tangential loads for load case 3.	81
7.6 Tangential angular acceleration of pinion with: (a) 0 mm, (b) 0.2 mm, (c) 0.4 mm, (d) 0.6 mm, (e) 0.8 mm and (f) 1 mm backlash.	83
7.7 Radial angular acceleration of pinion with: (a) 0 mm, (b) 0.2 mm, (c) 0.4 mm, (d) 0.6 mm, (e) 0.8 mm and (f) 1 mm backlash.	84
7.8 Angular acceleration of pinion along Z-axis with: (a) 0 mm, (b) 0.2 mm, (c) 0.4 mm, (d) 0.6 mm, (e) 0.8 mm and (f) 1 mm backlash.	86

7.9 Tangential angular acceleration of gear with: (a) 0 mm, (b) 0.2 mm, (c) 0.4 mm,
(d) 0.6 mm, (e) 0.8 mm and (f) 1 mm backlash. 88

7.10 Radial acceleration of gear along Y-axis with: (a) 0 mm, (b) 0.2 mm, (c) 0.4
mm, (d) 0.6 mm, (e) 0.8 mm and (f) 1 mm backlash. 90

7.11 Angular angular acceleration of gear with: (a) 0 mm, (b) 0.2 mm, (c) 0.4 mm,
(d) 0.6 mm, (e) 0.8 mm and (f) 1 mm backlash. 91

List of Tables

3.1	Geometric properties and the operating conditions of the meshing gear pair . . .	24
3.2	Essential calculated gear parameters.	28
4.1	Material properties of the steel SAE-AISI 1045 at 20°C	36
6.1	Regression analysis of experimental and FE results	71
A.1	Experimental data of flash temperature of spur gear	102
B.1	Values of flexural endurance limit	106
B.2	Values of flexural endurance limit	107
B.3	Values of tooth error in action (e) verses module.	107
C.1	Values of coefficients equation 5.8	108
G.1	Lubricant parameter	118
H.1	Mesh convergency analysis	119
H.2	Finite element analysis summary	119
I.1	Systems of consistent units	120

Glossary

Nomenclature

ADAMS	Automatic Dynamic Analysis of Mechanical Systems
APDL	Ansys Parametric Design Language
BL	Boundary lubrication
CR	Contact Ratio
DTE	Dynamic Transmission Error
EHL	Elasto-Hydrodynamic Lubricant
FEA	Finite Element Analysis
GMS	Gear Mesh Stiffness
HD	Hydrodynamic Lubrication
HPSTC	Highest Point of Single Tooth Contact
KTE	Kinematic Transmission Error
LOA	Line of Action
LPSTC	Lowest Point of Single Tooth Contact
ML	Mixed Lubrication
MTE	Manufacturing Transmission Error
OLOA	Out of Line of Action
STE	Static Transmission Error
TEHL	Transient Thermal Elasto-Hydrodynamic Lubrication
TVMS	Time Varying Mesh Stiffness

Symbols

α	Pressure angle
β	Lubricant temperature viscosity coefficient
γ_c	Angular thickness of the tooth at the contact point
$\delta, \delta_h, \delta_t, \delta_f$	Total, Hertzian contact, tooth beam and tooth foundation tooth deformation respectively
$\delta_b, \delta_s, \delta_a$	Tooth deformations along LOA due to bending moment, shear force, and axial compressive force respectively
Δ_c	Difference between actual and ideal operating center distance
η	Dynamic viscosity
η_o	Ambient viscosity
κ	Thermal conductivity
μ	Coefficient of friction.
ν	Poisson ratio
ξ	Contact point parameter
ρ	Mass density
σ_e	Flexural endurance limit
ϕ_c	Backlash due to operating distance modification
ϕ_t	Backlash due to teeth thickness reduction
φ_i, φ_t	Roll approach and termination angle
$\chi_{P,G}$	Thermal diffusivity of the pinion and gear material
ψ	Lubricant pressure viscosity coefficient
a	Addendum
A_x	Area of the section of distance 'x' measured from the load application point shown in Figure 5.2.
$A_i, B_i, C_i, D_i, E_i, F_i (i = 1, 2, 3, 4)$	Parameters shown in Equation 5.8 for calculations of $L^*(i = 1), M^*(i = 2), P^*(i = 3)$ and $Q^*(i = 4)$ respectively
b	Half contact width
B	Face width of gear
c	Center distance between pinion and gear center of rotation
C	Deformation or dynamic factor
C_p	Specific heat capacity

C_s	Shear potential correction factor,for rectangular section it is 1.2
C_P	Compressibility reduction factor
C_T	Inlet shear heating reduction factor
C_V	Velocity factor
d	Dedendum
D_P, D_G	Pitch diameter of pinion and gear
e	Tooth error action
$e(y)$	Tooth thickness at the section described by y shown in Figure 5.4
E_P, E_G	Young's modulus of pinion and gear
E'	Equivalent Young's modulus
g	EHL material parameter
$G = \frac{E}{2(1+\nu)}$	Shear modulus
h_f	Ratio of r_f and r_{int} as shown in Figure 5.2
hx	Half of the tooth thickness at the integral section in Figure 5.3
h_o	Central film thickness
I_x	Area moment of inertia
J_P, J_G	Polar moment of inertia of pinion and gear
k	Factor depending up on the form of teeth
K	Material combination factor
K_a	Axial compressive stiffness
K_b	Bending stiffness
K_f	Lubricant thermal conductivity
K_s	Shear stiffness
$K_M, K(t)$	Linear and torsional mesh stiffness
l	Length of line of action
$L_{eP,G}$	Peclet number of pinion and gear
L^*, M^*, P^*, Q^*	Coefficients in Equation 5.8
m	Gear module
M_c	Contact ratio
N_P, N_G	Angular velocity of pinion and gear
P_{max}	Maximum contact pressure
Q	Ratio factor

$r_{P,G}$	Pitch radius of pinion and gear
r_c	Radius of the profile point which is in the mesh at contact point
R_P, R_G	Equivalent radii of involute of pinion and gear
R'	Equivalent radius
S_i, S_t	Length of mesh initiation and termination
S_1, S_2	Single tooth contact points
t_i	Tooth thickness on the pitch circle for ideal gearing (no backlash)
t_b	Actual tooth thickness
T_b	Bulk temperature of contacting solids before entering the contact
T_C	Maximum surface contact temperature
T_{fmax}	Maximum flash temperature
T_e	Equivalent twisting moment
T_P, T_G	Torque acting on pinion and gear
u	Entraining velocity in tooth contact
U	EHL speed parameter
$U_P, U_G, U_s(S)$	Surface velocity of pinion , gear and sliding velocities
V	Pitch line velocity
$V.R$	Velocity ratio
w	Normal tooth load per unit face width
W	Load shear distribution
W_F	EHL load parameter
W_n, W_T, W_R	Normal, tangential and radial loads
W_D, W_s	Dynamic and Static tooth loads
W_P, W_G, W_r	Pinion, gear weights and resulting load acting on the gear
y_p, y_C	Corresponding root and load section shown in Figure 5.4
Y_P	Tooth formation factor of pinion
Z_P, Z_G	Number of teeth of pinion and gear
Z_P, Z_G	Number teeth of pinion and gear

Introduction

1.1 Background

Gears play a vital role in the mechanical power transmission system. They are employed to reduce or multiply the torque for different applications. Their life will be determined due to different factors, such as, wear, backlash, amount of load, thermal load and fluctuation of the load. These factors have an effect on the dynamic characteristics of the gear boxes which in turn directly influences the performance of the system.

Gears may fail due to different internal and external excitations. The most frequent mode of failures is fatigue, followed by impact (tensile or shear), and wear (abrasive or adhesive). In an analysis of over 1500 studies, the three most frequent gear failure modes were identified to be tooth bending fatigue – 32 %, tooth bending impact – $12\frac{1}{2}$ %, and abrasive tooth wear – 10 % [1].

Non-smooth nonlinearities such as backlash, dead-zone, component failure, friction, hysteresis, saturation and time delays are common in industrial control systems. Backlash is a dynamic characteristic that exists in mechanical couplings such as gear trains, and always limits the accuracy of servo-mechanisms and other mechanical power transmission systems. Dead-zone is a static input-output relationship which for a range of input values gives no output; it also limits system performance. Dead-zone characteristics are often present in amplifiers, motors, hydraulic valves and even in bio-medical actuation systems [2].

Backlash is the gap between gears tooth at the pitch circles. This distance can be involved in the gears either deliberately or without any intention due to the manufacturing error and assembly fault. Backlash is provided deliberately for a different reason and cannot be desig-

nated without consideration of machining conditions. The general purpose of backlash is to prevent gears from jamming by making contact on both sides of their teeth simultaneously. It's also introduced intentionally for lubricant space and differential expansion between the gear components and the housing.

Backlash is built in to speed reducers to let the gears mesh without binding and to provide space for an oil film between the teeth. This prevents an overheating and tooth damage. On the other hand, if the same clearance causes lost motion between the input and output shafts as a result, it is difficult to achieve an accurate positioning in equipment for those machines or elements that need an accuracy very importantly like robots, machine tools and measuring instruments. A simple backlash model is shown in Figure 1.1, which illustrates the fact that when the difference between the motor and the load position is smaller than $\tan(\phi)$, then the two shafts are disengaged and no torque is applied to the motor or the load [3].

The basic purpose of designing backlash is to prevent locking the gears, as well as to prevent coming into contact in both sides of one tooth simultaneously. A small amount of backlash is desirable to make necessary gap for lubrication and partially expansion of gears. Also, the amount of backlash should not be increased exceedingly, because the backlash causes high manufacturing costs [3].

Backlash can be introduced in two ways; (1) by reducing the thickness of the gear and (2) by modifying the center distance between the gear mates. Backlash due to tooth thickness change is typically measured along the pitch circle. In this case either one or both of the gear mate thickness will be reduced from the designed value. Figure 1.2 (a) shows the left side of gear whose thickness is reduced. The backlash due to this effect can be expressed as follow:

$$\phi_t = t_i - t_b \tag{1.1}$$

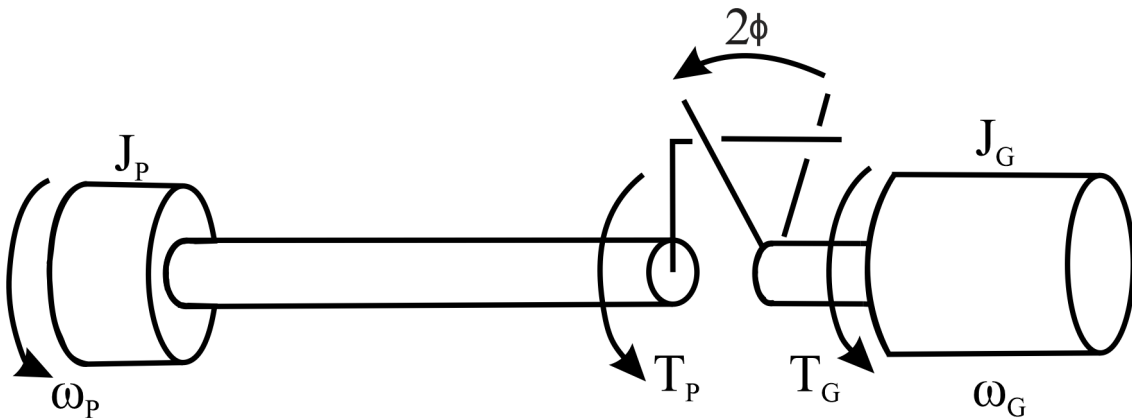


Figure 1.1: Illustration of backlash.

The second way to introduce backlash in gear is by modifying the center distance of the gear, in this case there is no contact between pitch circles of the two gears. The contact of the gear teeth exists on addendum. The backlash that is created due to modified center distance is show in Figure 1.2 (b). The thickness of the gear tooth will decrease from pitch circle to the top face of the gear. So, there will be a gap between these teeth again, and this can be expressed as follows.

$$\phi_c = 2(\Delta c)\tan\alpha \quad (1.2)$$

According to ISO/TR 10064-2-1996 [4], the value of minimum backlash can be expressed as in Equation 1.3. Therefore, the gear mates should have at least a minimum backlash value, but too large backlash will have another problem on the gear such as the impact of the gear and vibration.

$$\phi_{min} = 2 \frac{(0.06 + 0.0005c + 0.03m)}{3} \quad (1.3)$$

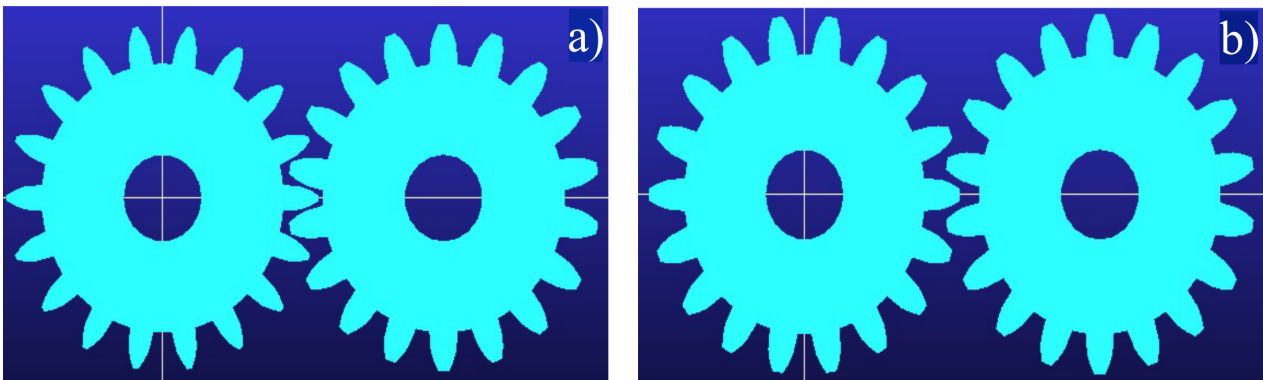


Figure 1.2: Backlash due to (a) tooth thickness modification and (b) center distance modification.

Backlash affects the dynamics of the system because it disturbs the smooth operation of the system. Prajapat et al. [5] investigated the effect of backlash on the doubly-fed induction generator based wind turbine. A small amount of backlash is recommended for smooth operations. If un-optimized amount of backlash is involved with gears then the smooth operation will be affected. In addition to this, the backlash affects the wear rate of the gear surfaces. Pitting wear is one of the prominent types of the wear that repeatedly occurs on gears. It is the surface failure of the gear material as a result of stress developed that exceeds the endurance or fatigue limit of the material.

Ghazaly et al. [6] investigated the influence of shaft misalignment and backlash on the stress generated on the spur gear using FEM. They reached on a conclusion of, when misalignment

angle increases the deformation will increase, while the stress generated at contact and root areas decreases.

Scuffing or scoring is a failure mode of gears when there is a direct contact between the gear mates [7]. To prevent these contacts some small gaps or backlash should be provided initially, so that the lubricant will have space to separate a direct asperity to asperity contacts of the gear mates. Many researchers have done a lot on it, and the minimum oil film thickness should be revealed to enhance the performance of the gear. When the gears are in contact, only a certain portion of the surface area will be in contact. The gears without the load have a line contact but when the load increases this line will change in to small area. The machine elements such as spherical bearings and gears have elliptical contact [8].

1.2 Motivation of the study

Mechanical power is transmitted through shafts, shaft couplings, gears, disc brakes, and others. Each of the above mechanical elements has its own distinct functions, for instance, gears are employed for different purposes, like increasing or decreasing the torque and reversing the direction of power transmission. In addition to that, when the power transmission is considered, it is very impressive to realize that the power will only be transmitted through a single gear tooth or one and fraction gear tooth. The gears may fail due to direct overload, heat load, and other reasons.

Even though these are the main causes of failure of mechanical elements, it is possible to overcome them by an extensive design. However, there are some non-linearities like backlash, which cannot be easily overcome. Analyzing the effect of this backlash on the performance of the gear will reveal something to understand the effect of non-linearity on different parameters

1.3 Statement of the problem

The gears may fail due to internal and external excitations. The internal excitation should be controlled to prolong the life of the gear. The main source of internal excitations is time-varying mesh stiffness and backlash. The backlash has a strong effect on the dynamics of the gears. If an excessive amount of backlash is introduced then the impact between gears tooth will increase, on another hand if there is no enough amount of backlash the wear will increase and also the friction between the tooth mates will generate much amount of heat and this may cause failure due to thermal stress and changing the material property of the gears. The effect of backlash on TE, dynamics response and flash temperature of the gears should be studied. Taking this concept into account the following hypotheses are formulated:

- As the backlash increases the flash temperature will be decreased because there is enough amount of gap so that there is no continuous contact of the gear tooth.
- As the backlash increases the impact load becomes more because the tooth is separate as a result there is continuous striking of the tooth due to the load. This might increase the flash temperature of the gear surfaces.

1.4 Questions to be addressed in this thesis

This thesis will address the following questions:

- How does the backlash affect TE, smooth operation and flash temperature ?
- What kind of boundary conditions are necessary for coupled temperature displacement and TE of gear analysis ?
- To what extent does the backlash size influence the performance or the functioning life of the gear in terms of transmission error ?
- How will the friction coefficient of material affect the flash temperature in addition to the backlash ?

1.5 Objectives of the study

1.5.1 *General objective*

The general objective of this thesis is to study the performance of spur gear with backlash and its effect on flash temperature with different coefficient of friction.

1.5.2 *Specific objectives*

The specific objectives of the study are to:

- Design and modeling of spur gear with different amount of backlash.
- Analyzing the effect of backlash on transmission error, and time varying mesh stiffness.
- Coupled temperature displacement analysis of each gears with different coefficient of friction using ABAQUS CAE.
- Simulating a 3D gear with backlash using MSC ADAMS to understand the effect of backlash on the smooth operation of the gear.

1.6 Scope of the study

The main aim of this thesis is limited to study of the effect of backlash on the flash temperature, TE and dynamics of the gear body. Using the Gear Trax AI-2017 software the 2D model will be produced by changing the parameters such as backlash and then the 3D model will be generated by coupling them with Auto Desk Inventor. In Gear Trax AI-2017 the backlash will be specified from zero to 1 mm by 0.2 mm increment. The coupled thermal displacement analysis will be conducted using ABAQUS CAE by importing the gears. In addition to that, the study will also include the analysis of the gears with a different coefficient of friction for TE and TVMS and finally, the effect of backlash on the dynamics of the system will be shown using ADAMS software.

1.7 Significance of the study

Gear trains are used in many mechanical power transmission systems such as in automobiles, wind power plants, helicopters, bucket wheel excavators and milling machines. The transmission of motion might not be uniform, and it can include changes in direction and torque. The life of the gear mates should be improved. As a result, this research will reveal the effects of backlash on the flash temperature, TE and dynamics of the gear.

1.8 Organization of the report

Following this chapter, which is intended to provide the general introduction on gear transmission, backlash and flash temperature, the remaining part of the thesis is divided in to seven chapter.

Literature review and research methodology are provided in the second and third chapter respectively. The basic parameters of the contact gear mates such as surface velocity, sliding velocity, contact width and pressure are provided in the fourth chapter. The fifth chapter deals with load sharing, transmission error, and time-varying mesh stiffness of spur gear with different backlash, and in this chapter, the effect of backlash on transmission error and time-varying mesh stiffness are discussed in detail. The effect of backlash on the flash temperature of spur gear are analyzed using the numerical method. In addition, the Blocks equation and FE results are compared to understand the level of agreement of the two methods, this is discussed in the sixth chapter. The seventh chapters is about the dynamics of spur gear, where the gear with different amount of backlash is modeled and simulated using ADAMS to understand the effect of backlash on contact load and angular acceleration of the gear mates. The last chapter of this thesis report is the conclusion and recommendations. The effect of backlash on the performance of the gear are concluded in this chapter. In addition, future works are provided in this chapter.

Literature Review

2.1 Introduction

Gear systems or gear trains tend to play a very vital role in all industries and in our day-to-day life, any failure to the gear system leads to the total system failure. Pitting and tooth breakage is the most mode of failures of the gear. Pitting is a major cause of gear failure accounting for nearly 60 % of the gear failures [9].

Pitting is the formation of craters on the gear tooth surface. These craters are formed due to the high amount of compressive contact stresses in the gear surface occurring during transmission of the torque or in simple terms due to compressive fatigue on the gear tooth surface [10]. Pitting and scuffing of a gear tooth appearance are shown in Figure 2.1.

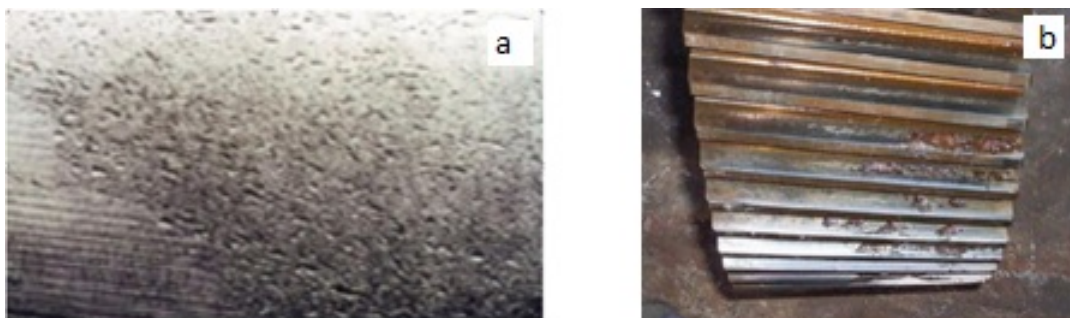


Figure 2.1: Gear tooth surface (a) pitting and (b) spall [7].

Xihui Liang et al. [10] reviewed on dynamic modeling of a gearbox fault and they mention that gear tooth pitting is the most common failure mode of gears. The main cause of tooth pitting or spalling which is large pit formed when the pits are joined together are subsurface

cracks caused by foreign or inclusions in the gear materials, metal to metal contact of asperities or defects due to low lubricant film thickness and foreign particle contamination of lubricant. Metal to metal contacts will occur when the oil film is broken, the reason of oil film breaking is low viscosity of the lubricant at the beginning or high flash temperature of the gear. High temperature will reduce the viscosity of the lubricant and then when the gear rotates it will splash easily and break down. Therefore, pitting will occur.

Conjugate action of gear teeth in mesh consists primarily of sliding and rolling motions. At the pitch line, sliding velocity is zero; however, sliding velocity increases when the conjugated tooth contact line travels away from the pitch line in both directions. Heat is generated by sliding friction of tooth surfaces. The temperature distribution is proportional to the distribution of contact pressure and sliding velocity.

Taburdagitan and Akko [11] studied on determination of surface temperature rise with thermo-elastic analysis of spur gears, and they found that the surface temperature rises on spur gear teeth pair along the pressure line are highest at the very beginning of the meshing and the surface temperatures at the initial contacts can be decreased by profile modification at the tip of the tooth. The low contact temperature of the optimized design can significantly contribute to prevent tooth surface damage under “no-lubricant” operating conditions was done by Wink and Mantri [12].

2.2 General research review

In this section the research review has been made by categorizing in to two parts, (1) research review on the effect and advantages of backlash of the gear and (2) research review on the flash temperature of the gear. The reviews are presented in the following subsections.

2.2.1 *Research review on backlash of the gear*

In industrial drives, elements like gear boxes and flexible couplings introduce backlash. For instance, a commonly used flexible coupling gives a backlash of about 10 degrees that can be partly filed with rubber [2]. Papageorgiou et al. [3] estimated the backlash for industrial drive-train system. Backlash plays an important function in many systems and it is one of the most important non-linearities that limit the performance of speed and position control in industrial, robotics, automotive, automation and other applications [13].

Observing the effect of backlash on friction, Lichtsinder and Gutman [14] concluded that when the backlash gap is decreased by mechanical means, friction is generally increased, and vice versa. Hence, there is a lower bound to all possible friction-backlash combinations defining a Feasibility Area. Gear transmission system is one of the most important components of the mechanical system. Gear systems are widely used in various power transmission applications due to their distinguished merits of accurate transmission ratio, large power range, high transmission efficiency and stable operation quality [15, 16].

Lagerber and Egardt [17] conducted experimental validation for backlash estimation in automotive power train. Merzouki and Cadiou [18] did the same thing to estimate the backlash for electro mechanical actuators.

Ravanbod-Shirazi and Besançon-Voda [19] proposed a new approach for estimating the backlash amplitude, characterized by dead zone model identification is achieved in two main steps. In the first step, a pre-estimation of the backlash amplitude, is performed based on the existing physical relation between the amplitude of the backlash, instant of commutation, the motor and the load speeds. In the second step, a least square criterion based on the model of the motor speed (non-linear regression model) is minimized around the pre-estimation. The comparison between the backlash identification made by this approach and an approach that doesn't use the pre-estimation illustrates that the first method is considerably advantageous.

Nordin et al. [2] proposed a new model for an inertia free elastic shaft with internal damping connected to a backlash. They found that the new model gives a negligible torque error in comparison with the exact torque solution.

Shinde and Mangrulkar [20] studied the effect of backlash on bending stresses in spur gears. They found that as the backlash increases the maximum von Mises stress increases slightly initially and after that it increases very much and after that it nearly remains constant. In addition, the maximum deflection is nearly proportional to the backlash.

Moradi and Salarieh [21] analyzed the nonlinear oscillations in spur gear pairs with approximated modelling of backlash nonlinearity. Backlash is included as a displacement-type nonlinear function and approximated with a third-order polynomial of DTE as a cubic nonlinearity.

Chen et al. [22] investigated how the backlash affect the performance of the gears based on the factorial theory. In order to get reasonable and precise dynamic analytic result, the fractal theory is employed here to express the backlash instead of the existed way of setting backlash as a fixed value or a steady random number that meets the normal distribution.

Three methods of gear backlash evaluation, i.e (1) fractal, (2) fixed value and (3) normal distribution methods were compared and clearly concluded that fractal method is more effective and reasonable than the latter two ways, because they both have the shortcoming of missing to reflect the influence by the changing backlash. Therefore, the normal distribution method can't get the unique answer when average backlash is set, while the fractal method doesn't have these drawbacks.

Lotfi et al. [23] developed an algorithm to minimize or eliminate the effect of backlash on the accuracy of the motion of the gear. The algorithm is formulated using a rotating coordinate system and has been shown to be able to produce backlash free motions for a wide range of geometrical paths including those with very sharp edges.

Walha [24] investigated dynamics of a two-stage gear system involving backlash and time dependent mesh stiffness. Gear contact is characterized by a periodically changing stiffness and a backlash which can lead to loss of the contact. The nonlinear dynamic response of the system is studied using a linearization technique, which decomposes the nonlinear system into some linear systems satisfying some conditions. For low rotational speeds, the system is characterized by a discontinuity of movement which is due to the discontinuous transfer of the kinetic energy from the input wheel to the output receiving wheel.

Vörös [25] developed a new analytic form of backlash characteristic description. The backlash parameters in the model equation are separated; hence their estimation can be solved as a quasi-linear problem using an iterative method with internal variable estimation. Also, the identification of cascaded systems consisting of an input backlash followed by a linear dynamic system is presented. Simulation studies of backlash and cascaded systems identification are included.

Ji [26] studied the torsional vibrations of wind turbine gearbox having two planetary gear stages and one parallel gear stage. The nonlinear dynamic model developed considers the factors such as time-varying mesh stiffness, damping, and static transmission error and gear backlash. Dynamic responses of internal components in the gearbox were predicted with the variations of factors such as the static transmission error (STE), mean-to-alternating force ratio and mesh stiffness ratio, adjusted for parametric studies. The increase of the external excitation fluctuation would lead to the large magnitude variation for gearbox components. In addition, compared to the static transmission error, the mesh stiffness was found to have more effect on the torsional vibrations of gearbox components. This is because increase of the fluctuating mesh stiffness could change the dynamic responses significantly.

Kacalak et al. [27] developed newest designs of worm gear drives which allow to adjust or decrease the amount of backlash. Results of numerical research performed with the finite element method and also the results of experimental research on the innovative worm gear drive with an axially adaptive worm. The results analysis has led to the conclusion that the described solutions allow reduction of backlash to percent , and even greater reduction of its standard deviation – that is 5 – 10 % of their initial values.

Baumann and Bertsche [28] reached on a conclusion that the reduction of gear rattle noise level can be achieved by avoiding meshing impacts, e.g. by minimizing the traction coefficient of the gear oil or high lubrication film thickness at the gear mesh. In addition to this Fernandez-Del-Rincon et al. [29] shown the effect of lubricant entrance in the contact area plays a decisive role in the dynamic behavior. An experiment also conducted on helical gear pairs from an automotive gear box in the “idle gear rattle” condition by varying the lubrication mechanism by Russo [30] to reveal the effect of lubrication on gear rattling.

2.2.2 Research review on the flash temperature of the gear

Friction will occur when two or more bodies come in contact and having a relative motion. Friction can be generated due to different mechanisms such as when one body tries to make sliding, pure rolling or rolling/sliding motion over the other. The mechanical energy due to the friction will be converted to a heat energy and this causes increasing the temperature of the bodies those are in dynamic motion. Kennedy [31] investigated that almost 95 % of energy dissipation occurs due to friction that has a 5 μm roughness amplitude .

When there is a substantial sliding between a lubricated rolling gears, excessive temperature will be generated and this in turn break down the oil film. After that the asperities of the rolling elements or gear will come in contact and then if they cannot carry the load they will be deformed plastically. This will facilitate the wear and the wear rate becomes rapid as the load continuously increases. This kind of phenomenon is called scuffing, and the best possible way of remedy of this failure is just minimizing the working temperature as well as the flash temperature of the rolling bodies. Shipley [32] shows that the gear can fail by scuffing at the tip and root areas of gear by taking a medium hardened spur gear. There is a sliding motion at the tip and roots of gears rather than having a rolling motion, there is a high friction at those locations and then the temperature will raise and the oil film thickness will break down then the gear will fail by scuffing.

Srirattayawong and Gao. [33] studied on the surface roughness effects on fluid flow between two rotating cylinders, and they concluded that thermal effects play an important role on the viscosity of the lubricant, as the viscosity decreases when the temperature increases. In addition, the influence of surface roughness is increased when the temperature increases due to the reduction in viscosity.

Li and Anisetti [34] investigated the effect of load, surface roughness, lubricant viscosity on the flash temperature. Based on their results they concluded that the flash temperature will increase as the torque increase. In addition, the vibration motion also influences the flash temperature not only on line of action (LOA), it also affects out of line of action (OLOA).

Wang et al. [35] developed a computer analysis of an involute spur gear to anticipate the variation of dynamic load, surface temperature and lubricant film thickness along line of action when the gear tooth are meshed. They didn't couple the above analysis together, rather they analyzed the dynamic load analysis independently and oil film thickness, flash temperature, bulk temperature are done by iterative method.

Elastohydrodynamic lubrication (EHL) can be defined as a form of hydrodynamic lubrication where the elastic deformation of the contacting bodies and the changes of viscosity with pressure play fundamental roles. A substantial amount of work was devoted to resolving elastohydrodynamics and the first realistic model which provided an albeit approximate solution for elastohydrodynamic film thickness was proposed by Ertel and Grubin [8].

Hua and his colleges investigated the effect of gear ratio and module on the film thickness and pressure of the gear by employing EHL theory. They concluded that as the gear ratio increase, the central oil film thickness increases markedly at the recess end, but they found that there is only a very small reduction at the approach end. In addition, if the module is doubled without changing the gear size, the oil film thickness would decrease slightly at the recess end of the gear [36].

Surface conjunction temperature is the temperature at the interface of two contacting and mutually sliding solid objects. For any specific part of the sliding surface, frictional temperature rises are very short duration and the temperature generated is called flash temperature, it was originally formulated by Blok in 1937 and developed further by Jaeger 1944 and Archard in 1958 [8].

According to Blok, Jaeger and Archard's theory [8], the flash temperature is the temperature rise above the temperature of the solids entering the contact which is called the bulk tem-

perature. The maximum contact temperature (T_c) is the sum of bulk temperature (T_b) and maximum flash temperature (T_{fmax}) expressed as:

$$T_c = T_b + T_{fmax} \quad (2.1)$$

Depending on the velocities of the rotating elements or gears the flash temperature will be calculated in different equations. A non-dimensional measure of the speed at which the 'heat source' moves across the surface called the 'Peclet number' has been introduced as a criterion allowing the differentiation between various speed regimes.

The Peclet number is an indicator of the heat penetration into the bulk of the contacting solid, i.e. it describes whether there is sufficient time for the surface temperature distribution of the contact to diffuse into the stationary solid. A higher Peclet number indicates a higher surface velocity for constant material characteristics. Flash temperature equations are given in terms of the heat supply over the contact area, the velocity, and the thermal properties of the material. They are applicable in many practical cases such as gears, roller bearings, cutting tools and others.

The critical surface temperature of the gear for scoring lies between 443 K and 447 K under the conditions of tooth material and lubricant used. The scoring resistance of gears can be accurately estimated by evaluating the critical surface temperature. Scoring resistance of the gear may be affected by quantity of lubricant, thermal and mechanical properties of the gear material, geometrical errors and surface roughness of the gear, and dynamic load. Terauchi and Nadano [37] have done a research on the effect of tooth profile modification of the scoring resistance of spur gears, and they draw the following conclusions:

- Small modification of addendum will significantly affect the scoring resistance of the gear.
- The scoring resistance of gears can be accurately estimated by evaluating the critical surface temperature.

Dhanasekaran and Gnanamoorthy [38] conducted research on gear tooth wear in sintered spur gears under dry running conditions, they revealed that the maximum wear is occurred in the dedendum and addendum regions even though the gear wear depends on the material hardness and strength of the gear material. In addition, Walton and Goodwin [39] also work on the wear of unlubricated metallic spur gear and they draw the following conclusion, temperature measurements of the gear bulk body revealed an almost linear increase with speed up to about 500 rev/min, where the temperatures of the driver and driven were almost equal.

A 2D coupled thermo-elastic analysis has been carried out by Taburdagitan and Akkok [11], to investigate the tooth surface temperature rise of the spur gears. They consider heat generation from the contact tooth pairs in addition to load sharing between contacting tooth pairs and elastic deformation. As the friction coefficient and load increases the tooth contact also increase, so that the tooth surface scuffing will be highly probably caused by high tooth contact temperature [40]. To minimize the contact temperature either of the load or frictional coefficient should be minimized, when the gear is subjected to a high load the frictional coefficient should be minimized.

Dong et al. [41] studied on temperature analysis of involute gear based on mixed elasto-hydrodynamic lubrication theory considering tribo-dynamic behaviors. They concluded that the surface of the pinion has a higher temperature in the approaching stage compared with that of the wheel while this is reversed after the pitch point and the temperatures at two ends of the gear tooth width are obviously higher than that in the middle part due to the stress concentration. The film temperature in mid layer is much higher than the temperature on the surfaces. For heavy-load gear systems, the temperature of film center is much higher than that of two boundaries. The temperature of the boundary increases until close to the outlet and then slightly decreases. The distribution of maximum flash temperature and minimum film thickness is in respective consistent with that of Blok flash temperature and thickness of Dowson in meshing cycle. The flash temperature from transient thermal elasto-hydrodynamic lubrication, TEHL is higher in the dedendum region and lower in the addendum region compared to that from Blok theory [8, 42, 43].

Luo and Li [44] studied on the influence factors on bulk temperature field of gear using parametric design APDL. Tooth profile modification will affect the distribution of the bulk temperature field; therefore, the bulk temperature can be reduced by the tooth profile modification in addition to this they also conclude that the initial temperature of the lubricant oil will determine the bulk temperature.

If the initial temperature of the lubricant is high, then the bulk temperature of the gear also high. This concept is supported by, Taburdagitan and Akkok [11] conducted an experiment and numerical analysis of spur gear, they saw that the numerical results that found by FEA is relatively higher that of the experimental results. This is because splashing lubricated conditions and the coefficient of friction may not be constant as assumed constant in the FEA.

2.3 Research gaps from literature survey

Many researchers have used experimental and numerical methods to study the performance of the gear as we have seen in the literature review. The STE, DTE and TVMS of the gear have been studied by many researchers by introducing different shape and size of the crack, but in this thesis the transmission error and time-varying mesh stiffness of the spur gear by introducing a backlash (modifying the tooth thickness) will be studied.

The flash temperature of the gear can be determined using FE, Block's equation and experimental methods, in this thesis the flash temperature of the spur gear at different amounts of backlash will be studied using FEA. But flash temperature for the gear with 0 mm backlash will compare to the experimental results to see the goodness of the FE approach fit with the experimental results obtained by Tobe and his colleagues. The dynamics of the spur gear with different amounts of backlash will be studied using ADAMS.

In general, the effect of backlash on TE, TVMS, flash temperature and dynamics of the spur gear by introducing different amounts of backlash using the methodology that explained above is not clearly drew a conclusion in the previous studies. Taking this as a research gap and the performance of the gear that relates to STE, DTE, TVMS, Flash temperature and dynamics of the spur gear will be studied in this thesis work.

Research Method and Materials

3.1 Introduction

The research methodology begins by looking for related articles, conference proceedings, and books on backlash, flash temperature, transmission error of the gears. This will pave a way to understand the details of the backlash on the performance of the gear. In addition to that, it will also reveal the current status and research work of the study.

The second step is gathering data about a specific spur gear dimension and parameters that have been done previously, these will include geometrical dimensions, material properties of gear, loads and operating conditions.

Once the parameters are collected, preparing a 2D gear model can be proceed using Gear Trax 2017 software, and then the 2D gear model converted to a 3D gear model using Auto desk Inventor 2017 Pro. by integrating the two packages. The Gear Trax allows modeling different type of gears by modifying the parameters such as number of teeth, module, backlash, face width, and others, and the other's advantage of this software is the 3D model can be generated by integrating with other modeling software such as Auto Desk Inventor, Solid Work, and others.

Backlash is the main parameter of this thesis work, six gear models have been produced by changing the backlash values of the gear. The first spur gear is modeled with zero-backlash and the rest five gears are modeled by 0.2 mm backlash increments.

The research methodology that has been implemented in this thesis work is explained in detail in Figure 3.1.

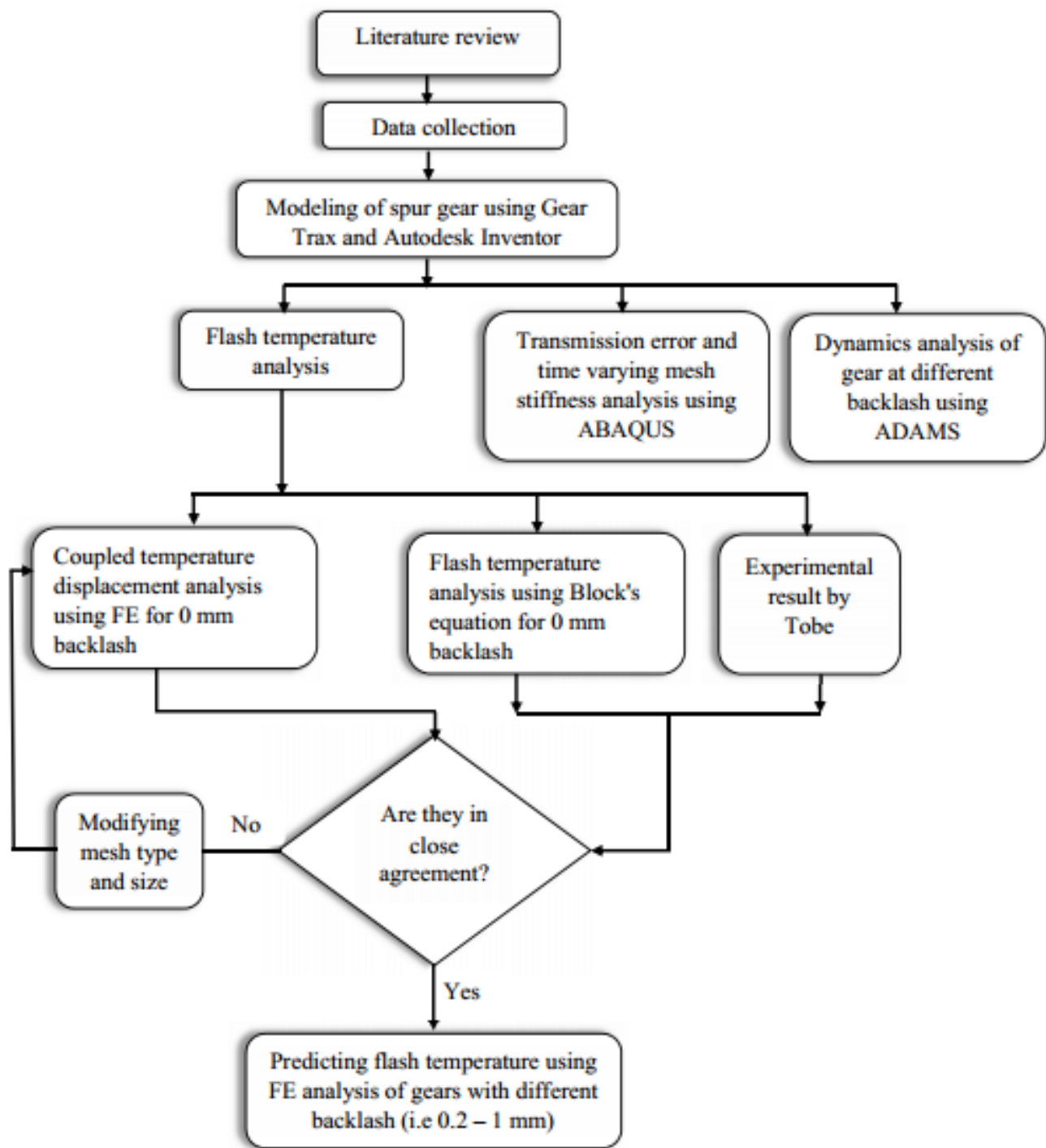


Figure 3.1: Research methodology.

A coupled displacement temperature analysis will be conducted to investigate the effect of backlash on the flash temperature of the gear surfaces using ABAQUS/Standard CAE 2017 software. Plane strain is a stress condition in linear elastic fracture mechanics in which zero strain in the direction normal to the axis of applied tensile stress and direction of crack growth. It is achieved in a thick plate, along a direction parallel to the plate. While a plane stress is a stress condition in linear elastic fracture mechanics in which stress in the thickness direction is

zero. It is achieved in loading thin steel along a direction parallel to the surface of a sheet.

The flash temperature of two sliding components can be calculated using Block's equation, the sliding velocity, normal contact load, and friction coefficients are the main parameters for calculation of the flash temperature of contacting bodies.

Therefore, determining the load sharing is very essential to analyze the flash temperature of the gear. Load sharing is directly related to the contact length, which is the sum of the length of from mesh initiation to a pitch point and from pitch point to a mesh termination, it is also used to find the sliding velocities of the gear sets.

Load sharing can be determined using FEM, analytical potential energy method and approximate method, for analytical calculation a liner load shear graph is used. Once these parameters are determined the flash temperature can be analytically calculated using Block's equation.

Tobe and his colleges conducted an experimental work for determining the flash temperature of spur gear [11], this experimental graph is extracted using Engauge digitizer software and then compared the results with a Block's and FE results. The experimental data of flash temperature of spur gear is given in Appendix - A versus time and mesh position, actually the data is given with flash temperature versus time, but using the common points (the mesh initiation is 0 msec and when the plotted data touches the horizontal line (time axis) is a pitch point and at final time is a mesh termination) it can be plotted with mesh position to as shown in Figure 3.2.

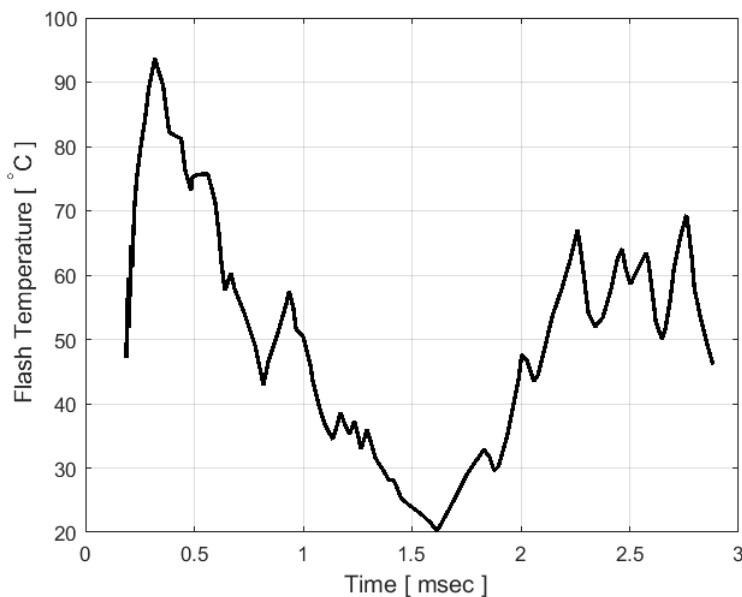


Figure 3.2: Flash temperature of spur gear obtained using experimental approach by Tobe et al. (adopted from [11])

Eventually, the comparison of experimental, FEA and Block's equation results will be compared for 0 mm backlash gear with 0.15, 0.2 and 0.3 coefficient of frictions. Then predicting the flash temperature of spur gear with different coefficient of friction at different backlashes will be carry on.

The noise and vibration of gear are the results of transmission error, determining the transmission error can help to understand the system dynamics. The transmission error has been determined using FE method because FE considers the system as a flexible body and this will give better results. The transmission error of the gear at the different amounts of the backlash has been examined.

The last part of this document is analyzing the effect of backlash on the dynamics of the gear using ADAMS 2018. Using an incorporating machinery tool on ADAMS the gear sets will modeled and then applying the material property, loading and operating conditions and analyzing it. All the graph that shows in this document is plotted using MATLAB and Corell draw. The numerical data obtained from the ABAQUS and ADAMS are imported to MATLAB, this helps to draw easily many figures together. Using the above methodology the effect of backlash on the performance of the spur gear has been studied.

3.2 Design and modeling of spur gear

The main purpose of gear is to transmit motion and power from one shaft to another. If there is error on the gears due to design, manufacturing and working conditions, the motion will not be transmitted as it intended to transmit. This transmission error will cause a vibration and this may lead the distraction of the gear and the components nearby.

Therefore, designing a spur gear in a proper way plays a vital role in minimizing the faults, that are shown in the gearbox like transmission error. In this section, the spur gear is designed based on the specifically given load, module, and a number of teeth, and eventually, it has been modeled for further analysis of the gear.

3.2.1 *Types of gears*

There are many different types of gears used in industry, but all these gears share the same purpose, which is to transmit, multiply or reduce the load and motion from one shaft to another. Generally, gearing consists of a pair of gears with an axis that is either parallel or perpendicular.

The most commonly used gears are spur gear, helical gear, bevel gear, and worm gears.

A spur gear is considered as the simplest form of gear, and it consists of teeth parallel to the axis of rotation as shown in Figure 3.3 (a). Spur gear can be designed with different pressure angles. The spur gear with a low-pressure angle is smoother and quieter tooth action, on contrary a gear with larger pressure angle is rather noisy, but it has a better load carrying capacity.

Helical gears (Figure 3.3 (b)) consist of teeth that are cut at an angle and inclined with the axis of rotation. Helical gears essentially have the same applications as spur gears. However, because of their gradual engagement of the teeth during meshing, helical gears tend to be less noisy. In addition, the inclined tooth develops thrust loads and bending couples, which are not present in the spur gear.

Bevel gears (Figure 3.3 (c)) teeth are formed on conical surfaces, and unlike spur and helical gears, bevel gears are used for transmitting motion between intersecting shafts. There are different types of bevel gears, but all of them establish thrust, radial, and tangential loads on their support bearings.

Worm gearing (Figure 3.3 (d)) consists of the worm and worm gear. In general, worm gear sets are more efficient when the speed ratios of the two shafts are high. Basically, in worm gearing, higher speed equals better efficiency. The following figure demonstrates the four most common types of gears in the industry.

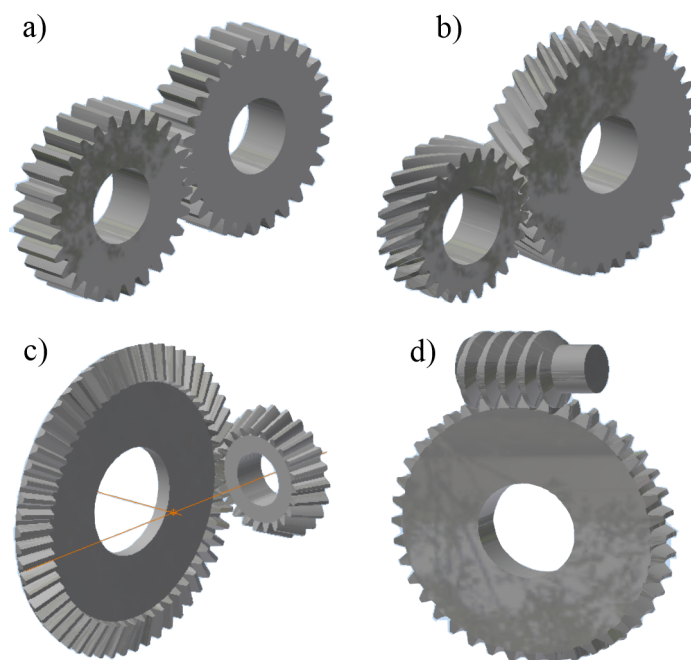


Figure 3.3: 3D model of (a) spur, (b) helical, (c) bevel and (d) worm gear.

3.2.2 *Common terminology of gears*

Since spur gears are the most common form of gearing, it will be used to illustrate the nomenclature of gear teeth. One of the most important parameters on the gear teeth is the pitch circle since all calculations are based on this theoretical circle. The diameter of the pitch circle is called the pitch diameter d . When a pair of gears are mated together, the pitch circles of the gears are tangent to each other. The circular pitch is the distance on the circumference of the pitch circle between the corresponding points of adjacent teeth. Therefore, the circular pitch is the sum of the tooth thickness and the width of a space.

The addendum is the radial distance between the pitch circle and the top of the tooth. Dedendum is the radial distance between the pitch circle and the bottom of the tooth space. Clearance is the amount by which the dedendum in a given gear exceeds the addendum of its mating gear.

The diametral pitch P is the ratio of the number of gear teeth to each inch of the pitch diameter. The module m is the ratio of the pitch diameter to the number of teeth, and the unit of the module is usually millimeter.

$$P = \frac{N}{d} \quad (3.1a)$$

$$m = \frac{d}{N} \quad (3.1b)$$

$$p = \frac{\pi d}{N} = \pi m \quad (3.1c)$$

When gear teeth are meshing against each other, it will generate rotary motion. Also, when a curved surface pushes against another, the point of contact appears where the two surfaces are tangent to each other. The imaginary line that passes through this contact point with the characteristic of being common normal to the surfaces. Then, the forces at any instant are directed along this line, and this line represents the direction of the forces. This is called the line of action or pressure line.

Furthermore, the line of action will intersect the line of centers which is formed by the gears centers at point. This point is called a pitch point. The pitch point can be found by drawing the pitch circles of the gears since they are supposed to come in contact as soon as the gears have meshed together.

3.3 Geometrical design of spur gear

For modeling purposes, the gear dimensions should be determined first. Table 3.1 shows the given geometrical properties and operating conditions of the gear pairs, these parameters are used to design the gears. The same geometrical properties and operating conditions have been taken to compare with a Taburdagitan et al. results.

Table 3.1: Geometric properties and the operating conditions of the meshing gear pair [11].

Parameter	Value	Unit
Module, m	4	mm
Pressure angle, α	20	degree
Number of teeth, Z_P and Z_G	14 and 22	
Face width, B	6	mm
Normal tooth load per unit face width, w	75.5	N/mm
Angular velocity of pinion, ω_P	2090	RPM

Dimensions of the gear is given by:

$$D_{P,G} = Z_{P,G} \times m \quad (3.2)$$

The pitch diameter of both pinion and gear can be calculated from Equation 3.2, and the values are, $D_P = 56 \text{ mm}$ and $D_G = 88 \text{ mm}$ and center distance, $c = r_P + r_G = 72 \text{ mm}$. The essential gear parameters of the spur gear is summarized in Table 3.2.

The load is given as a function of face width, so multiplying the load by face width will give the normal tooth load acting on the gear tooth, $W_n = w \times B = 453 \text{ N}$. The normal load can be resolved in to tangential and radial load. These loads are given by Equation 4.3:

$$W_T = W_n \times \cos\alpha \quad (3.3a)$$

$$W_R = W_n \times \sin\alpha \quad (3.3b)$$

Tangential (W_T) and radial (W_R) loads based on the above formula is calculated as 425.68 N and 154.935 N respectively.

The torque distributed on pinion and gear can be calculated by multiplying the tangential load with their respective pitch radius. Torque acting on the pinion and gear is given by:

$$T_{P,G} = W_T \times r_{P,G} \quad (3.4)$$

Using Equation (3.4) $T_P = 11919.04 \text{ Nmm}$ and $T_G = 18729.92 \text{ Nmm}$. Since both gears are made of the same material, pinion is the weaker, then the design will be based up on the pinion. The static load should be determined first to check for dynamic and wear loading.

Pitch line velocity of the pinion,

$$V = \frac{\pi D_P N_P}{60} \quad (3.5)$$

Using Equation (3.5), $V = 6.1282 \text{ m/s}$. Since the pitch line velocity is less than 12.5 m/s , therefore the velocity factor is given by the following equation [45]:

$$C_V = \frac{3}{3 + V} \quad (3.6)$$

From the above Equation (3.6), $C_V = 0.3286$

Tooth formation factor for the pinion,

$$Y_P = \frac{0.175 - 0.841}{Z_P} \quad (3.7)$$

Using the above equation $Y_P = 0.1149$

Static tooth load or endurance strength of the tooth:

$$W_s = \sigma_e B \pi m Y_P \quad (3.8)$$

The flexural endurance limit (σ_e) of steel with a hardness of 200 BHN is 350 MPa it shown in Appendix B, Table B.1, and the static tooth load from Equation 3.8 yields 3032.13956 N .

3.3.1 Design for dynamic and wear load

In this section the design of the gear will checking the gears for the dynamic and wear load. Dynamic and maximum or limiting load for wear is given by Equation 3.9 (a) and (b) respectively:

$$W_D = W_T + \frac{21 \times V(B \times C + W_T)}{21 \times V + \sqrt{B \times C + W_T}} \quad (3.9a)$$

$$W_W = D_P \times B \times Q \times K \quad (3.9b)$$

Deformation or dynamic factor C is given by:

$$C = \frac{k \times e}{\frac{1}{E_P} + \frac{1}{E_G}} \quad (3.10)$$

Tooth error action (e) for first class commercial gears having module 4 mm is 0.051 as given in Appendix B, Table B.3. While the factor for form of teeth is taken as $k = 0.111$ for 20° involute tooth [45]. From Equation 3.10, the deformation load factor is obtained as $C = 772.7265$ N/mm.

Ratio factor and the velocity ratio is given in Equation 3.11 (a) and (b) respectively,

$$Q = \frac{2V.R}{V.R + 1} \quad (3.11a)$$

$$V.R = \frac{D_G}{D_P} \quad (3.11b)$$

According to Buckingham, the load stress factor or material combination factor for the wear, K is given by Equation 3.12:

$$K = \frac{\sigma_{es}^2 \sin \alpha}{1.4} \left[\frac{1}{E_P} + \frac{1}{E_G} \right] \quad (3.12)$$

The surface endurance limit of steel, σ_{es} with 200 BHN is given in Appendix B, Table B.2 and it is 490 N/mm². The equation yield $K = 0.429717$, and this value enable to determine the limiting load for wear.

Based on the above equations the dynamic and maximum limiting load is 2308.698 N and 176.438 N respectively. Since $W_D < W_S$ and $W_W < W_S$, the design is safe for both dynamic loading and wear loading.

3.3.2 Design of shafts and gear hub diameter

The shaft of the gear enables us to calculate the the hub diameters of the gear. It primarily subjected to the normal load and twisting loads due to external load and weight of the gear. The weight of the gear wheels is given by Equation 3.13:

$$W_{P,G} = 0.00118 \times Z_{P,G} \times B \times m^2(N) \quad (3.13)$$

From the above equation the weight of pinion and gear is 1.58592 N and 2.492 N respectively. The resultant load is given by Equation 3.14, and the resultant load for pinion and gear is obtained as 454.49 N and 455.34 N respectively.

$$W_r = \sqrt{W_W^2 + W_{P,G}^2 + 2W_N W_{P,G} \cos\alpha} \quad (3.14)$$

If the gear is overhang on the shaft, then bending moment on the shaft due to the resultant load is given by the resultant load multiply by the overhang distance. If the distance between center of the gears and center of the bearing, assume $x = 100 \text{ mm}$, then the bending moment for pinion and gear is obtained as 45449 Nmm and 455534 Nmm respectively.

Twisting moment on the shaft is the obtained by multiplying the tangential load and the radius, and the twisting moment of pinion and gear shafts is calculated as 11919 Nmm and 118729.92 Nmm respectively. Equivalent twisting moment is the results of bending and twisting moments and is given by Equation 3.15 and it gives 46.9859 $kNmm$ and 49.2357 $kNmm$ for pinion and gear shafts.

$$T_e = \sqrt{M^2 + T^2} \quad (3.15)$$

The relation between shaft diameter and Equivalent twisting moment is given by Equation 3.16, for the given material by assuming the safe stress as 40 MPa and shaft diameters for pinion and gear is calculated as 20 mm and 25 mm respectively.

$$T_e = \frac{\pi \tau d^3}{16} \quad (3.16)$$

Diameter of the hub is given by relation, $1.8d_{P,G}$, and 36 mm and 45 mm are obtained for diameter of pinion and gear respectively. For FE analysis the gear is modeled with the bore that equal to the hub diameter to reduce the computation time.

Table 3.2: Essential calculated gear parameters.

Calculated parameter	Formula	Value (mm)
Pitch circle radius of pinion, r_P	$r_P = \frac{D_P}{2}$	28
Pitch circle radius of gear, r_G	$r_G = \frac{D_G}{2}$	44
Addendum, a	$a = 1m$	4
Dedendum, d	$d = 1.25m$	5
Pinion addendum circle radius, r_{aP}	$r_{aP} = r_P + a$	32
Pinion base circle radius, r_{bP}	$r_{bP} = r_P \times \cos\alpha$	26.311
Gear addendum circle radius, r_{aG}	$r_{aG} = r_G + a$	48
Gear base circle radius, r_{bG}	$r_{bG} = r_G \times \cos\alpha$	41.35
Base pitch, P_b	$P_b = P_n = \pi m \cos\alpha$	11.808

3.4 Load sharing of gear

The contact pressure is a function of the area of contact and the load distribution. The load distribution profile along the gear contact is not uniform and it should be determined properly.

Single tooth gear contact occurs between lowest point of single tooth contact (LPSTC) and highest point of single tooth contact (HPSTC), these points are illustrated in Section 4.1 with Figure 4.1. At the gear mesh, there is more than one pair in contact below the LPSTC and above HPSTC. To understand the load sharing the following simplified equation is used.

$$W(s) = \frac{\lambda T_P}{B r_P \cos\alpha} \quad (3.17)$$

$$\lambda = \begin{cases} 0.5 & S_i \leq S \leq S_1 \text{ or } S_2 \leq S \leq S_t \\ 1 & S_1 < S < S_2 \end{cases} \quad (3.18)$$

Taburdagitan et al. [11] find the load sharing using FEA and change into a linear graph as shown in Figure 3.5. For analytical solutions such as contact pressure and flash temperature,

load sharing is better to be a linear load sharing, this will simplify the calculation. This load sharing is used to calculate contact width and pressure.

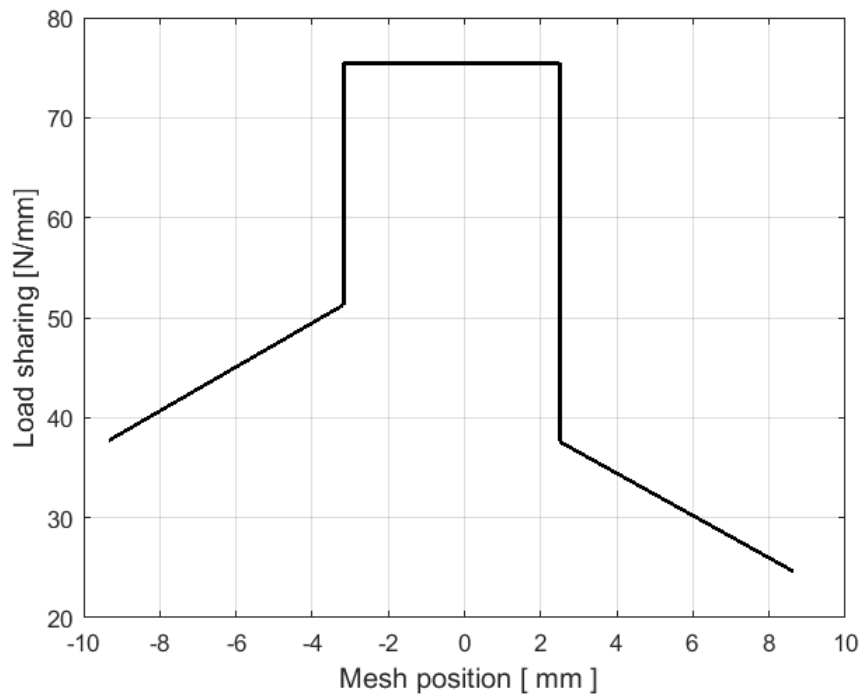


Figure 3.4: Load sharing along line of contact (adopted from [11]).

Figure 3.4 shows that the load sharing is increased from mesh initiation to LPSTC region, and then the gear tooth holds the full load. Double tooth contact begins at a point HPSTC around $38 N/mm$ and decreases to $25 N/mm$ at the mesh termination. The figure clearly shows that the load share is for mesh initiation is lower than the load shear for mesh termination. The load sharing of the gear using approximate equations is also discussed in Section 5.1.2 and 5.3.

Determination of Important Contact Parameters for Spur Gear Design

4.1 Introduction

The motion and power are transmitted through a successive contact of gear tooth surfaces. The gear mates have a maximum of two teeth in contact this is called contact ratio, and the distance from one contact pair of gear to the other contact gear tooth pair is called contact length. In simple expression, the contact length is an imaginary line that passes through pitch point from the mesh initiation to mesh termination points.

The load is distributed through the contact length of the gear, which has a strong influence on the performance of the gear. The gear with a longest contact length has less chance to fail early than the gear with the shortest contact length unless manufacturing and other situations affect the system. To illustrate this, the spur gear has the shortest contact length than helical gear, therefore, the spur gear can fail early than helical gear if both gears subjected to same load and operating conditions. In this section the length of mesh initiation and termination, contact ratio, surface and sliding velocity of the gear will be determined.

Figure 4.1 shows the length of contact, recess and approach angles for a mesh. The length from point A to C and from C to E is called the length of mesh initiation (approach) and length of mesh termination (recess) respectively. A single gear tooth contact will show between a point B to D, while in a length between A to B and D to E double tooth contact will occur. The full mesh cycle can be got by summing up the roll angle approach and termination angles. In other words point, B and D are called the Lowest point of single tooth contact (LPSTC)

and the highest point of single tooth contact (HPSTC) respectively.

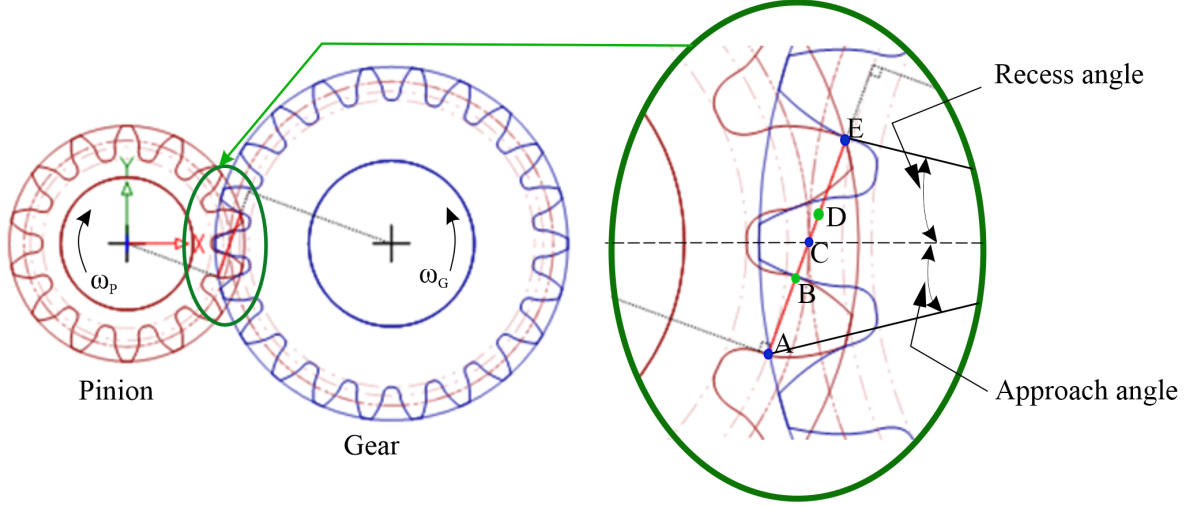


Figure 4.1: 2D Model of spur gear.

4.2 Contact length and rolling angles

Length of meshing initiation is the distance from the beginning of contact until the point of contact arrives at the pitch point, While the length of mesh termination is the distance from the pitch point to the end of contact arrives at the point and it is calculated as -9.327 mm and 8.638 mm respectively using Equation 4.1 (a) and (b).

$$S_i = -\sqrt{(r_{aG}^2 - r_{bG}^2) - r_G \sin \alpha} \quad (4.1a)$$

$$S_t = \sqrt{(r_{aP}^2 - r_{bP}^2) - r_P \sin \alpha} \quad (4.1b)$$

The other important parameter is the rolling approach angle and angle of termination. Roll approach angle is the angle between the horizontal line and the line that begin from center of rotation and passes through the mesh initiation point. While, recess roll angle is the angle between the horizontal line and the line that begin form center of rotation and pass through the mesh termination point. These both parameters can be determined from the Equations 4.2 (a) and (b) as 12.93° and 18.81° .

$$\varphi_i = -\frac{S_i}{r_{bG}} \quad (4.2a)$$

$$\varphi_t = -\frac{S_t}{r_{bP}} \quad (4.2b)$$

Length of line of action is the sum of length of mesh initiation and termination and is given by Equation 4.3, and it is calculated as 17.965 mm .

$$l = S_i + S_t \quad (4.3)$$

The contact ratio is given by Equation 4.4. A contact ratio of 1 means that only one tooth pair is engaged at all times during the course of action. The gear tooth may not carry the load as good as the gear tooth that there are more than one pair of tooth contact, this is undesirable because slight errors in the tooth spacing will cause oscillations in the velocity, vibration, and noise. For the satisfactory performance of power transmitting gears, a value of 1.4 is used as a practical minimum. A lower contact ratio also necessitates a higher degree of accuracy in meshing to ensure quiet running of the gear set, but from Equation 4.4 the contact ratio is 1.52 and this indicates that one pair of teeth are always in contact, and the second pair of teeth are in contact 52% of the time Norton et al. [45].

Low-contact-ratio spur gears suffer from abrupt changes in the transmitted load because of the continuous engagement and disengagement of teeth in a meshing cycle. These changes generate noise and vibrations, resulting in poor lubrication and increased tooth wear, and can even cause tooth breakage.

$$M_c = CR = \frac{l}{P_b} \quad (4.4)$$

From Figure 4.1, it is shown that a single tooth contact is occurred between points B and D. This indicates that the single tooth contact starts at length AB (S_1) and ends at length AD (S_2) from mesh initiation (point A). The pitch point (C) can be taken as a reference and then the length along the right side of this can be considered as a positive and along the left side negative. These distances, S_1 and S_2 can be calculated by:

$$S_1 = \frac{S_i + (M_c - 1)S_t}{M_c} \quad (4.5a)$$

$$S_2 = \frac{S_i(M_c - 1) + S_t}{M_c} \quad (4.5b)$$

From the above equation $S_1 = -3.18 \text{ mm}$ and $S_2 = 2.49 \text{ mm}$. In other word, there is a single meshing pair when $-3.18 \text{ mm} < S < 2.49 \text{ mm}$, and there are a two meshing pairs when the meshing position is in the range of $S_i \leq S \leq S_1$ or $S_2 \leq S \leq S_t$.

Point S_1 and S_2 along the line of action are called the lowest point of single tooth contact and the highest point of single tooth contact respectively.

4.3 Surface velocity and sliding velocity

The gear is constrained at the center and subjected to a constant rotational load. The gear surfaces will contact along line of action, the surface velocity will vary from the beginning of mesh to mesh termination due to the length from the center of the rotational axis.

Radii of the two equivalent cylinders at a given meshing position are given by

$$R_{P,G} = r_{P,G} \sin \alpha \pm S \quad (4.6)$$

The equivalent radius of the elastohydrodynamic lubrication (EHL) contact is given by:

$$R'(S) = \frac{(R_P R_G)}{(R_P + R_G)} = \frac{(r_P \sin \alpha + S)(r_G \sin \alpha - S)}{c \sin \alpha} \quad (4.7)$$

The surface velocities of the two cylinders are given by

$$U_{P,G}(S) = \omega_{P,G} R_{P,G} \quad (4.8)$$

The entraining velocity of the EHL contact

$$U(S) = \frac{(U_P + U_G)}{2} = \omega_P r_P \sin \alpha + \frac{(\omega_P - \omega_G)S}{2} \quad (4.9)$$

Sliding velocity is the relative velocity in a transverse plane of a common contact point between mating gear teeth and is given by Equation 4.10.

$$U_S(s) = U_P - U_G = (\omega_P + \omega_G)S \quad (4.10)$$

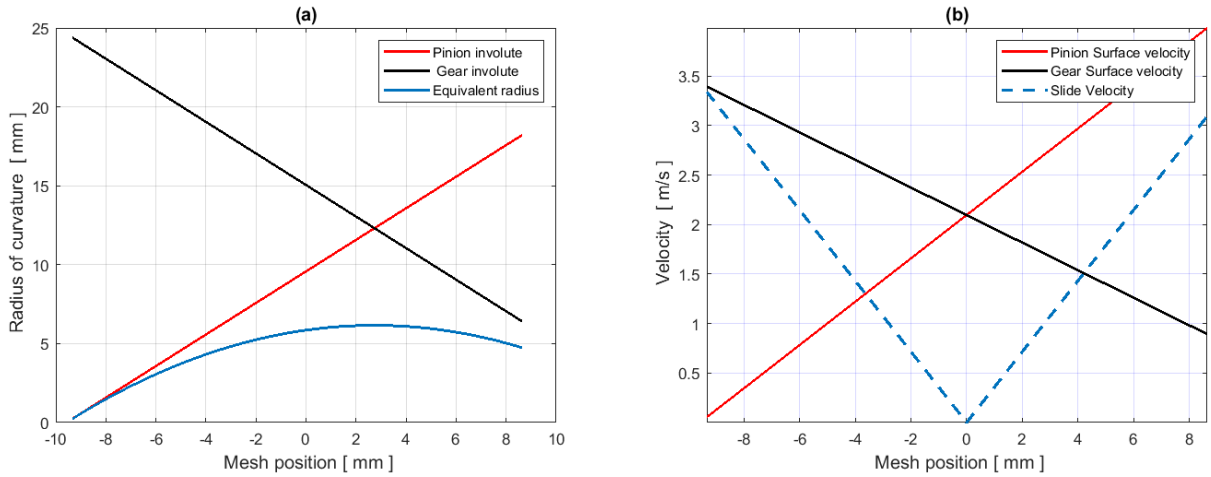


Figure 4.2: Gear (a) radius of curvature and (b) velocities of gear.

The radius of the curvature of the involute of gear tooth for both pinion and gear is shown in Figure 4.2 (a). It shows that the radius of curvature of pinion gear tooth is minimum at the mesh initiation and increased to the maximum value as it is shown in the figure, on the other hand, the radius of curvature of the gear involute tooth is maximum at the mesh initiation and decrease to the minimum value at the mesh termination. The pinion and gear radius of curvature is equal at 2.85 mm mesh position along the line of action. The equivalent radius of

curvature also shown in the figure and it increases gently from mesh initiation till it reaches to the point where the pinion and gear have the same radius of curvature and then it starts to decrease gently, it has a downward parabolic shape. These radii of curvatures are used to determine the surface and sliding velocities of the gear.

The contact of the gear tooth shows a rolling and sliding velocities. Both surface velocities for pinion and gear and sliding velocities are shown in Figure 4.2 (b). The surface velocity of the pinion is increased from 0.2 m/s to a maximum value of 4 m/s, this indicates that the radius of involute at the mesh initiation is very small and as it goes from this point it increases. The surface velocity of the gear is maximum as mesh initiation and decrease to 0.8 m/s at the mesh termination point.

In addition, at the pitch point the surface velocities of pinion and gear are the same, in other words there is a pure rolling at the pitch circle.

4.4 Contact width and contact stress

In mechanical engineering and tribology, Hertzian contact stress is a description of the stress between mating parts. Theoretically, the contact area of two spheres is a point, and it is a line for two parallel cylinders. As a result, the contact pressure between two curved surfaces should be infinite for both of these two cases, which will cause immediate yielding of both surfaces. However, a small contact area is being created through elastic deformation in reality due to deformation at the contact surfaces.

Figure 4.3 shows the Hertz contact components of sectional two elastic objects for general cases. When the contacting components are subjected to a load there is a point contact and then as the load increases the stress induced in the contacting bodies increases and as a result, the contacting area will grow as an elliptical shape. The maximum contact pressure, P_{max} is found at the center and it decreases as it goes away from the center. The contact width, b is measured from the semi-minor axis of the elliptical geometry as shown in the graph.

The gear tooth has a cylindrical shape and the Hertz contact theory can be applied. Conjugate action of gear teeth in mesh consists primarily of sliding and rolling motions. At the pitch line, sliding velocity is zero; however, sliding velocity increases when the conjugated tooth contact line travels away from the pitch line in both directions. The contact pressure of gear teeth in mesh also changes along the line of action. In this thesis cylindrical contact object is considered for the analysis of spur gear contact width and pressure.

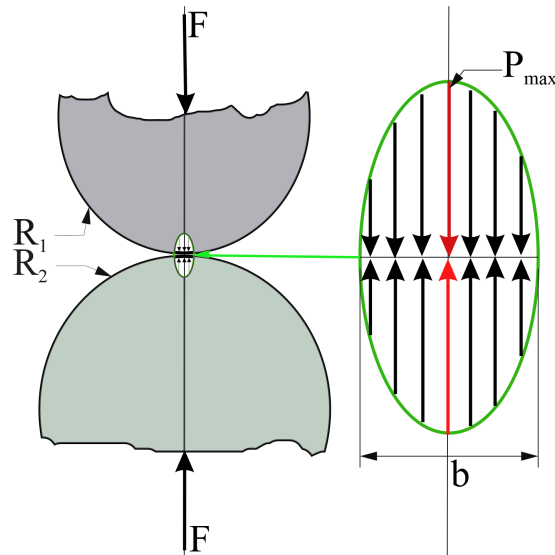


Figure 4.3: Contact between two sectioned cylinders, general case

4.4.1 Contact width

Contact width is used to determine the contact pressure of mating pairs. Contact width is given by Equation 4.11, and it shows that it is directly proportional to the equivalent radius of curvature and inversely proportional to the equivalent elastic of module.

Equivalent radius is calculated in Section 4.3, Equation 4.7, it varies along the line of action. The equivalent modulus is given by Equation 4.12, in this thesis report the both mating components of gear have the same modulus of elasticity as given in Table 4.1. Both gear and pinion are made from steel SAE-AISI 1045 at 20 °C. The units also used as it shown in the table, for numerical analysis, there is no unit in built in ABAQUS. Therefore the unit should be consistent and it is given in Appendix-I. The MATLAB code for contact width and pressure is given in Appendix - D.

$$b = \sqrt{\frac{8WR'}{\pi E'}} = \sqrt{\frac{8 \times W \times R'}{\pi E'}} \quad (4.11)$$

$$\frac{1}{E'} = \frac{1}{2} \left[\frac{1 - \nu_P^2}{E_P} + \frac{1 - \nu_G^2}{E_G} \right] \quad (4.12)$$

Table 4.1: Material properties of the steel SAE-AISI 1045 at 20°C [11].

Parameter	Value	Unit
Mass density, ρ	7.86×10^{-6}	Kg/mm^3
Modulus of elasticity, E_P & E_G	207×10^3	N/mm^2
Poisson ration, ν	0.3	
Specific heat, C_p	485×10^3	$(Nmm)/Kg^\circ C$
Thermal conductivity, κ	42.3	$(Nmm)/mm^\circ C$

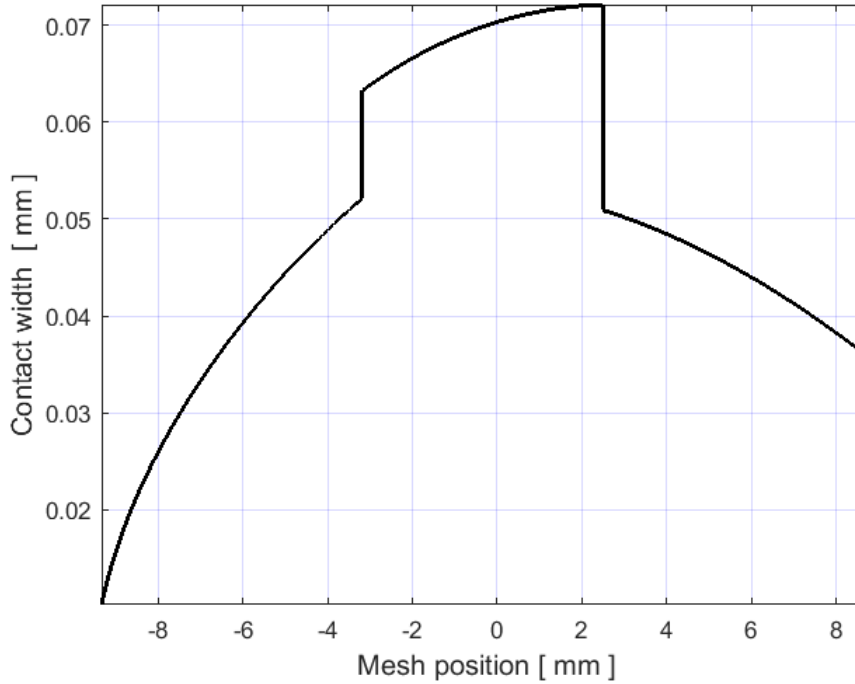


Figure 4.4: Contact width.

Figure 4.4 shows that the contact width increased from the point where the meshing of gear sets start to the LPSTC, and the maximum contact width has occurred at HPSTC 0.073 mm, and at mesh termination point the contact width is around 0.0375 mm. The contact width is maximum under single tooth contact, i.e between - 3.18 to 2.49 mm. This shows that the contact width is maximum under the single tooth contact region.

The gear width is proportional to the load that applied on the gear, the load is shared into two teeth in the double tooth contact region. Near to the pitch point, the width is maximum. This

is because the gear load is carried by a single tooth only, this indicates that, the more the load subjected the more the deformed width will be produced. Once the gear width is determined the maximum contact pressure can be determined, and this show in the next section.

4.4.2 Contact pressure

The contact stresses on the gear surfaces can be estimated by analytical equations based on the frictionless elastic theory developed by Hertz in 1881 [10]. The gear contact is analyzed with the assumption that the contact is between two cylinders with radii equal to the radius of the curvature of the teeth. The contact geometry between the two elastic contact bodies in general cases is as shown in Figure 4.3. The Hertz equations can be utilized to calculate the contact pressure at the tooth surfaces of two mating spur gears.

The contact pressure is the ratio of the normal load to the true contact area. Contact stress is generally the deciding factor for the determination of the required dimensions of gears. The maximum and average contact pressure of the two cylindrical contact bodies is given by Equation 4.13 (a) and (b). In this thesis the maximum pressure is calculated as shown in Figure 4.5.

$$P_{max} = \frac{2W}{\pi b} \quad (4.13a)$$

$$P_{average} = \frac{W}{4b} \quad (4.13b)$$

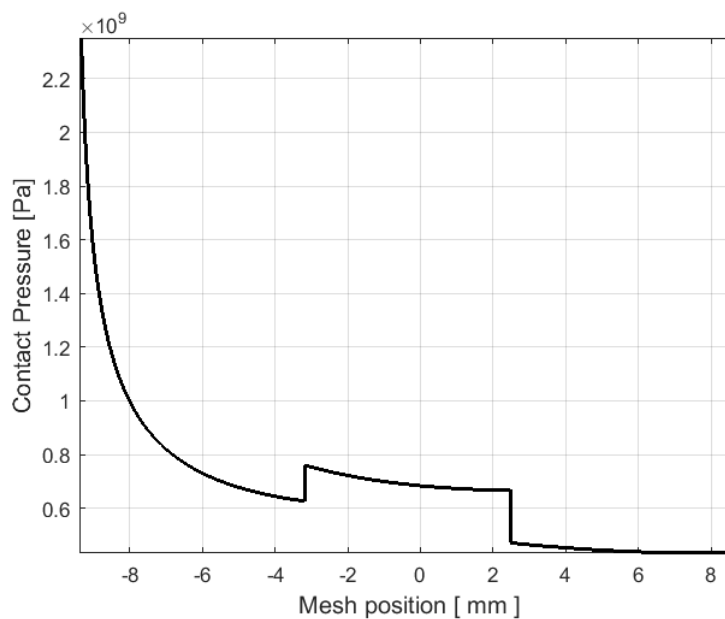


Figure 4.5: Maximum contact pressure.

As shown in Figure 4.5, the maximum contact pressure (2.4 GPa) is obtained around the tip of the gear tooth, and it decreases gently to 610 MPa at the LPSTC region, and then it increases to 780 MPa without change of mesh position, and then it decreases gently to a point HPSTC region which is almost 680 MPa . and then the minimum contact pressure is occurred at the mesh termination which is almost 500 MPa .

If the gear tooth profile is modified the maximum contact pressure will occur on a single tooth contact region. Maximum contact pressure is occurred at the LPSTC and then decreases gently to the point of HPSTC.

In this chapter the important contact parameters have been determined. The radius of involute is used to determine the sliding velocity of the gear, and the equivalent radius of curvature is maximum at above pitch point. The sliding velocity of the spur gear is maximum at the mesh initiation and decreases and eventually it gets zero at the pitch point and it increases again. The other main point of this chapter is its about the contact width and pressure, the cylindrical contact bodies have been considered to analyzed the gear contact width and maximum pressure. Maximum contact width is found on the single tooth contact region. The maximum contact pressure is maximum at the mesh initiation and it decreases gently until it reach on the LPSTC region. The maximum contact pressure can be found on the single tooth contact region if the tip of the gear tooth is modified.

Effect of Backlash on Transmission Error and Time Varying Mesh Stiffness

5.1 Introduction

The transmission error has been defined in different ways, according to Harris [46], it is the difference between the angular position that the out put shaft of the driven would occupy if the drive were perfect and the actual position of the output.

The deviation in position of the driver gear (pinion) for any given position of the driving gear, the actual angular position of the gear is not perfect, due to the deformation of gear tooth, tooth profile error and assembly and installation error of the gear pair, so the actual angular position of the output gear will not be exact with the theoretical and actual position.

The transmission error (TE) would be zero if a pair of meshing gears with rigid, perfect, uniformly spaced involute teeth would transmit exactly uniform angular motion this was expressed by [47]. The angular transmission error is given by Equation (5.1):

$$TE(\omega) = \theta_P(\omega) - \frac{N_G}{N_P} \times \theta_2(\omega) \quad (5.1)$$

The transmission error can also be expressed in a linear form as given in Equation 5.2.

$$TE(\mu m) = \frac{D_P}{2} \left[\theta_P - \frac{N_G}{N_P} \theta_G \right] = \frac{1}{2} [D_P \theta_P - D_G \theta_G] \quad (5.2)$$

Power and motion cannot transmitted exactly basically due to the geometrical imperfection and deformation due to the applied torque, this is called the transmission error. If the gear mates are perfect geometrically and un-deformed then the torque and the motion will be transmitted without any deviation.

Munro [48] defined transmission error, “The deviation in position of the driven gear (for any given position of the driving gear), relative to the position that the driven gear would occupy if both gears were geometrically perfect and un-deformed”.

As explained above, the source of the transmission error is geometrical imperfection and deflection due to the load applied on the gear. The geometry error mainly arises from manufacturing error and assembling the gear system. It is difficult to get a perfect involute profile as per design unless the advanced technologies are used to manufacturing it.

The transmission error could also occur due to assembly error. In addition, when the gear is operating after a certain time the flank face starts to wear out or it could fail due to different gear failure modes, such as pitting, scuffing and others. When the gears are worn out, the thickness of the gear and shape will deviate from the original gear thickness and shape. Minimization of thickness due to wear or manufacturing error can be considered as a backlash and study the effect on the transmission error and time-varying mesh stiffness.

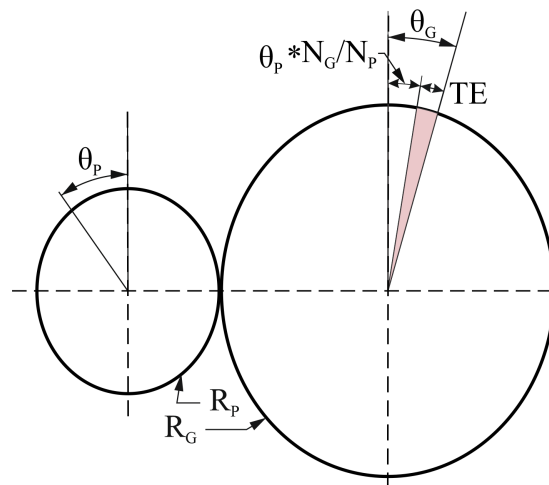


Figure 5.1: Transmission error.

5.1.1 *Types of transmission error*

Based on the source, the transmission error can be grouped into four main groups. These are manufacturing transmission error (MTE), static transmission error (STE), dynamic transmission error (DTE), and Kinematic transmission error (KTE), each of them will be discussed below.

a. Manufacturing transmission error

It is the simplest type of TE, which is caused by an error during the manufacturing of the gear that generally makes the tooth profile deviate from the perfect involute profile that it should follow. If the teeth don't have a perfect involute profile, this will make the transmission of torque not perfectly uniform. But MTE also accounts for the uneven spacing of the teeth along the pitch circle, errors during the assembly of the gearbox which may lead to the distance between gears not be the correct one, or even to a misalignment in the shafts which will make the axes not parallel to each other. This MTE is directly linked to the quality of the gears and its manufacturing process.

MTE is measured by running the gear pairs with out the application of load or light load and at low speed. This is done in order to avoid any deformations that may occur under load and to avoid a dynamic load respectively.

b. Static transmission error

When the gear mates are subjected to a low load or speed, there is still a transmission error that is called static transmission error. This kind of error results from manufacturing error and tooth deflection due to the load. The small loading will produce an elastic deformation of the system, and the dynamic effects are ignored. Determining this will pave a way to examine the whine noise of the gear transmission system.

c. Kinematic transmission error

The load is transmitted through the contact of tooth of the gear, at a small load the contacts could be a line contact if the flank face is smoothed enough and when the load is increased the line width will increase and then it will become a surface contact. If there is uneven surface then there will be an asperity contact. When the load is applied then this asperities will deformed till the contact area increases to the area that can withstand the load. Kinematic transmission also result from the manufacturing error.

d. Dynamic transmission error

Dynamic transmission error is the cumulative error due to inertia of the gears, dynamics and load of the gear. It is the most important one because it considers all the variables that affect the

system during its working life since it includes all manufacturing error, the static deformation of the system, but also the effects of the masses and inertial forces of the system, that generate also dynamic deformations.

To measure DTE, the TE is measured under load and at a high-speed condition, which is generally the working condition of many gears. So, it accounts for all the possible reasons of transmission error.

Gear dynamics is an important method to predict dynamic performance as well as to monitor the status of a gear system. The time-varying mesh stiffness caused by alternately changing the gear pairs in mesh plays a crucial role in dynamic responses. The basic methods of determining the TE will be discussed in the next section.

5.1.2 *Methods of estimating TVMS and load sharing*

The time varying mesh stiffness (TVMS) can be estimating primarily in three main methods and these are (1) analytical, (2) finite element and (3) approximate methods, and these are explained briefly as follows.

1. Analytical approach

According to Braunschweig [49], three contributing factors need to be considered when analytically calculating the tooth deformation (or deflection) in the line of action (LOA) at a contact point subjected to a certain mesh force and these are: local deformation caused by the Hertzian contact; beam deflection caused by tooth considered as a cantilever beam; and deflection caused by the flexibility of the foundation of the gear body. These deformations are discussed in detail as follows.

a. Hertzian contact deformation, δ_h

The Hertzian contact deformation δ_h between the meshing tooth surfaces of a mating tooth pair is nonlinear and various approximate formulas for the calculation of δ_h , have been found by Kiekbusch et al. [50].

A simplified nonlinear contact deformation based on the semi-empirical equation developed by Palmgren [51] had been adopted by many researchers such as Zeng et al. [52]. It's expressed as :

$$\delta_h = \frac{1.275F^{0.9}}{E^{0.9}l^{0.8}} \quad (5.3)$$

b. Tooth beam induced deformation

The tooth beam induced deformation δ_t can be determined by considering it as a non-uniform cantilever beam and it considered as it is rigidly fixed at its foundation. The potential energy method is widely used to derive the tooth beam deflection under a contact load. In general, when a tooth beam is under the action of the mesh force F at point P (as shown in Figure 5.2), there will be potential energy stored in the tooth beam due to the bending moment M , the shear force F_s and the axial compressive force F_a . Therefore, the total tooth deformation consists of bending moment induced δ_b , shear force induced δ_s and axial compressive force induced δ_a , which can be expressed as [52]:

$$\delta_t = \delta_b + \delta_s + \delta_a \quad (5.4)$$

$$\frac{1}{\delta_b} = F * \int_0^l \frac{((l-x)\cos(\alpha) - h\sin(\alpha))^2}{EI_x} dx \quad (5.5)$$

$$\frac{1}{\delta_s} = F * \int_0^l \frac{1.2\cos^2(\alpha)}{GA_x} dx \quad (5.6)$$

$$\frac{1}{\delta_a} = F * \int_0^l \frac{\sin^2(\alpha)}{EA_x} dx \quad (5.7)$$

where l , x , h and α are shown in Figure 5.2. For a tooth with no crack, I_x and A_x are calculated on the whole section:

$$I_x = \frac{(h_x+h_x)^3}{12} dB, A_x = (h_x + h_x)dB$$

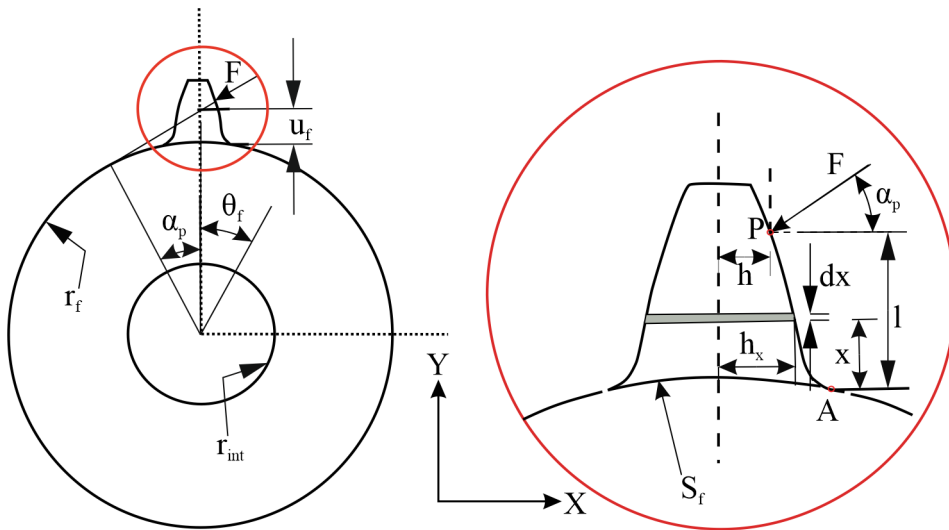


Figure 5.2: Geometric parameters for gear body.

c. Tooth foundation induced deformation

Foundation induced deflection can be calculated from Shao et al.[53].

Sainsot et al. [54] studied the effect of fillet foundation deflection on the gear mesh stiffness, derived this deflection, and applied it for a gear body. The fillet foundation deflection can be calculated as in Equation 5.8:

$$\delta_f = \frac{F \cdot \cos^2(\alpha_m)}{W \cdot E} \left\{ L^* \left(\frac{u_f}{S_f} \right)^2 + M^* \left(\frac{u_f}{S_f} \right) + P^* \left(1 + Q^* \tan^2(\alpha_m) \right) \right\} \quad (5.8)$$

where the following notations are used: α is the pressure angle. u_f , and S_f are illustrated in Figure 5.2.

Q^* , P^* , M^* , and L^* can be approximated using polynomial functions as follows:

$$X_i^*(h_f, \theta_f) = \frac{A_i}{\theta_f^2} + B_i h_{fi}^2 + \frac{C_i h_{fi}}{\theta_f} + \frac{D_i}{\theta_f} + E_i h_{fi} + F_i \quad (5.9)$$

X_i^* represents the coefficients L^* , M^* , P^* , Q^* , and this values of the coefficients are listed in Appendix C.

The value of h_{fi} is calculated from r_f/r_{int} , and r_f , r_{int} and θ_f are illustrated in Figure 5.2.

Then the stiffness due to fillet foundation deflection can be obtained as:

$$\frac{1}{K_f} = \frac{\delta_f}{F} \quad (5.10)$$

d. Mesh stiffness (MS) model based on the analytical methods

The equivalent mesh stiffness of a mating gear pair is calculated by direct summation of equivalent mesh stiffness of tooth pairs in contact:

$$K(t) = \sum_{i=1}^N K^i|_j \quad (5.11)$$

where N denotes the number of tooth pairs in mesh simultaneously; $K^i|_j$ is the equivalent stiffness of the i'th tooth pair at the contact point j (at time instant t), which is expressed as:

$$K^i = \frac{F}{\delta_{fP} + \delta_{tP} + \delta_h + \delta_{fG} + \delta_{tG}} \quad (5.12)$$

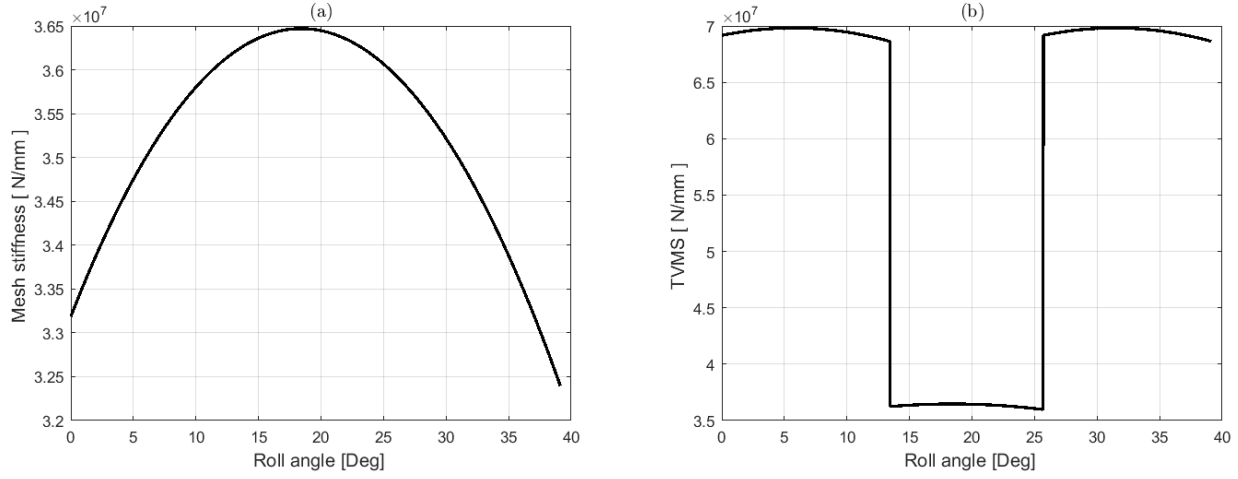


Figure 5.3: Analytical calculation of (a) mesh stiffness and (b) time varying mesh stiffness.

Figure 5.3 shows mesh stiffness (a) and time varying mesh stiffness (b) calculation using analytical method. Maximum mesh stiffness is found at the pitch point as it is shown in Figure (a). The minimum time varying mesh stiffness is found in a single tooth contact region the mesh stiffness which is 36 MN/mm. In double tooth contact region the TVMS is 70 MN/mm, this is shown in Figure (b). MATLAB code is written for this analysis and is given in appendix-E.

Time varying mesh stiffness is responsible for the failure of the gear. The stiffness of the gear varies between 36 and 70 MN/mm with time or roll angle. This is due to the load variation along line of action.

2. Finite element approach

FE models are the primary tools used to obtain gear mesh stiffness due to their significant advantage in representing the crucial tooth contact behavior. Two-dimensional (2D) models and three dimensional (3D) models are both common in the literature. Time varying mesh stiffness of the gear with different backlash will be examined using plain strain FE analysis in Section 5.2.5.

3. Approximate mesh stiffness analysis

According to Philippe [55], the hypothesis of minimum elastic potential energy, the meshing stiffness of a couple of teeth in contact at a point P of the path of contact can be expressed as:

$$K_M = \left[\left(\frac{1}{K_b} + \frac{1}{K_s} + \frac{1}{K_a} \right)_P + \left(\frac{1}{K_b} + \frac{1}{K_s} + \frac{1}{K_a} \right)_G + \frac{1}{K_H} \right]^{-1} = K_M(\xi) \quad (5.13)$$

The contact point parameter is the pinion profile parameter r corresponding to the point which is in mesh at point P of the path of contact, and is given by:

$$\xi = \frac{Z_P}{2\pi} \sqrt{\frac{r_{cP}^2}{r_{bP}^2} - 1} \quad (5.14)$$

The stiffness components can be computed from:

$$\frac{1}{K_b} = \pm \frac{12}{EB} \int_{y_p}^{y_y} [\pm(y_c - y) \cos \alpha - r_c \sin(\frac{\gamma_c}{2}) \sin \alpha]^2 \frac{dy}{e^3(y)} \quad (5.15a)$$

$$\frac{1}{K_a} = \pm \frac{1}{EB} \int_{y_p}^{y_y} \sin(\alpha)^2 \frac{dy}{e(y)} \quad (5.15b)$$

$$\frac{1}{K_s} = \pm \frac{C_s}{GB} \int_{y_p}^{y_y} \cos(\alpha)^2 \frac{dy}{e(y)} \quad (5.15c)$$

$$\frac{1}{K_H} = \frac{4}{\pi} \frac{1 - \nu^2}{EB} \quad (5.15d)$$

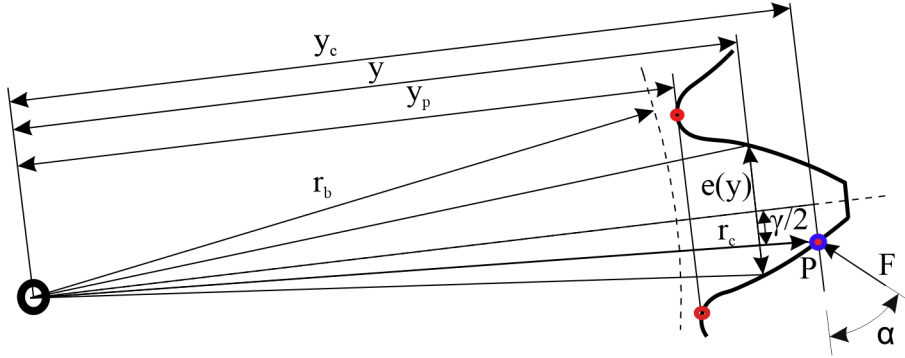


Figure 5.4: Geometry of involute external teeth.

The load sharing ratio is the fraction of the total load transmitted by a tooth pair along the multiple tooth contact interval, and can be computed as:

$$R_i = \frac{F_i}{F} = \frac{K_{Mi}}{\sum(K_{Mj})} \quad (5.16)$$

Where: F - the total transmitted load and the sum is extended to all the tooth pairs in the simultaneous contact. Mesh stiffness and load sharing can be approximately calculated using Equation 5.17 and the MATLAB code is given in Appendix-F.

$$K_M(\xi) = K_{Mmax} \cos(b_o(\xi - \xi_m)), K_{Mmax} = 1 \quad (5.17a)$$

$$b_o = \left[\frac{1}{2} \left(1 + \frac{\xi_\alpha}{2} \right)^2 - 1 \right]^{-\frac{1}{2}} \quad (5.17b)$$

$$\xi_m = \xi_{inn} + \frac{\xi_\alpha}{2} \quad (5.17c)$$

$$R(\xi) = \frac{F(\xi)}{F} = \frac{K_M(\xi)}{K_M(\xi + 1)} \quad (5.17d)$$

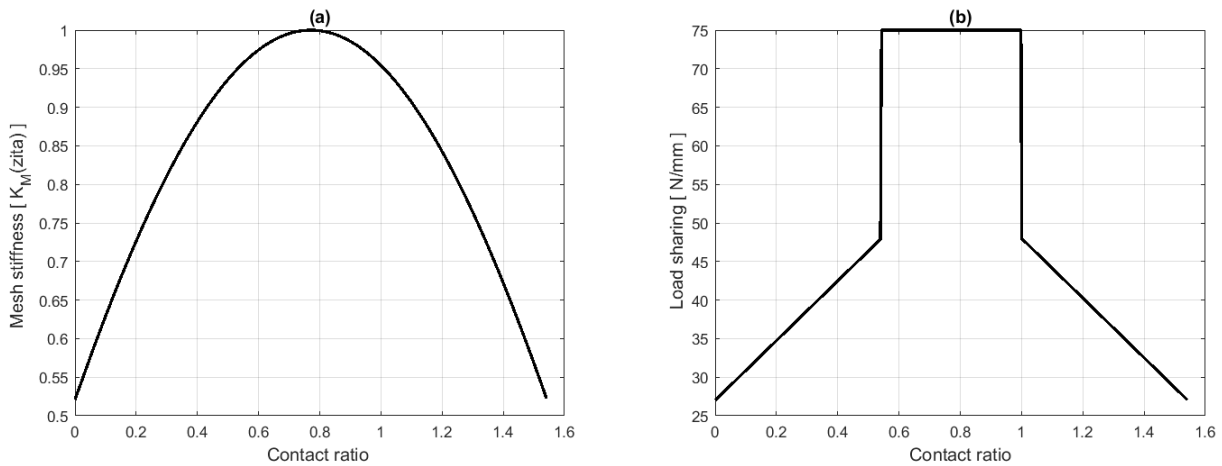


Figure 5.5: Approximate method calculation of (a) mesh stiffness and (b) load sharing.

Figure 5.5 shows the mesh stiffness and load sharing using approximate method. The stiffness of the gear is maximum when the contact ratio is 0.75 it is shown in (a), the mesh stiffness of the gear is increased (from 0.525) as the contact ratio increased till it reach at 0.75 contact ratio, and then it decrease gently and the mesh stiffness at 1.52 contact ratio of mesh termination is 0.525.

Figure 5.5 (b) shows that the load sharing is increased from 27.5 N/mm to 47.5 N/mm, this is from mesh initiation to LPSTC region, and then single tooth carry a full load. From LPSTC TO HPSTC region the load sharing is 75 N/mm, this implies that the single tooth carry full load without sharing to the other gear tooth. The load sharing decrease from HPSTC to mesh termination point.

This is an approximate method, the load sharing is deviated from the load shear that shown in Section 4.4. MATLAB code for this is shown in Appendix-F.

5.2 Numerical analysis of TE, TVMS and load sharing

In this section the TE and TVMS will be determined by FEA using appropriate mesh convergence.

5.2.1 Mesh convergence

Mesh density of the given system will determine the accuracy of the output result. If the mesh density is too small the finite element yield less accurate results and completes the given job analysis within a short time, while on the other hand if the mesh density is too large then the result is accurate, but it takes a long time relative to less mesh density.

The mesh density can be specified by comparing the results of the finite element analysis and experimental or analytical results. If the value is close enough then that mesh density is proper for the analysis. But there is a situation that enables us to find the mesh density without considering the experimental or analytical results. Take some less mesh density arbitrary and then take the output after the completion of the analysis, and then increase the mesh density and then take the output, and continue until the result become constant or nearly get constant. It's obvious that when the mesh density increases the result value increase accordingly, and after some time it becomes constant. Then by taking the last increased mesh density and then used it for the other analysis.

The sketch model of a single tooth imported to ABAQUS and then develop a geometry of gear as a plane object and applying the material property of the gear. The analysis type should be specified based on the system and the required outputs. In this case, a general static analysis is used to determine the mesh convergence, but this step is used for other kinds of analysis only bay changing the analysis procedure. The other important step is applying proper boundary conditions, the boundary condition directly affects the results of the analysis. So appropriate boundary conditions should be applied based on the analysis type. Finally, create a job and submit it then the desired output parameters can be extracted. The step of the analysis is put in Figure 5.6.

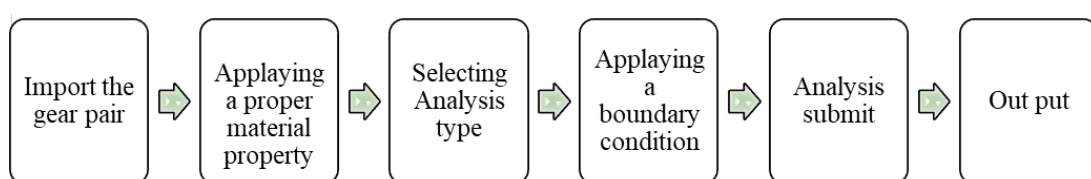


Figure 5.6: FE analysis procedures.

Mesh convergence analysis has been done for a plane strain analysis of the gear using CPE4 (A 4-node bilinear plane strain quadrilateral) element type. The mesh convergence is done by fixing all linear and angular degrees of freedom of both centers of pinion and gear except the rotational degree of freedom of gear as shown in Figure 5.7, and 3322 Nmm torque is applied on the gear.

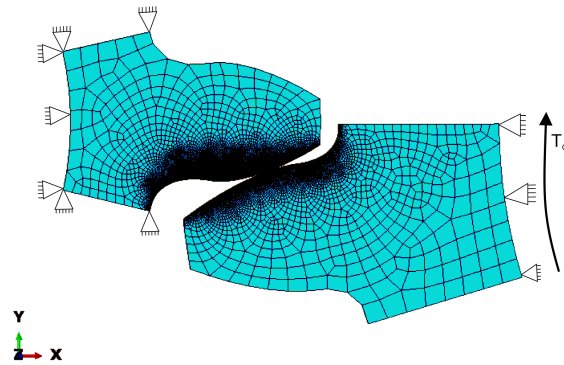


Figure 5.7: Boundary condition and load.

The mesh convergence is analyzed at the pitch point, the teeth of gear pairs contact at the pitch point. Figure 5.8 and Figure 5.9 shows the von Mises and contact stresses for 0.6 mm mesh size.

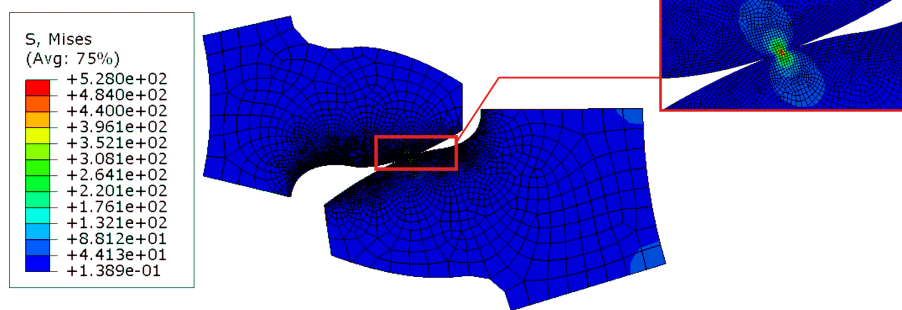


Figure 5.8: von Mises stress.

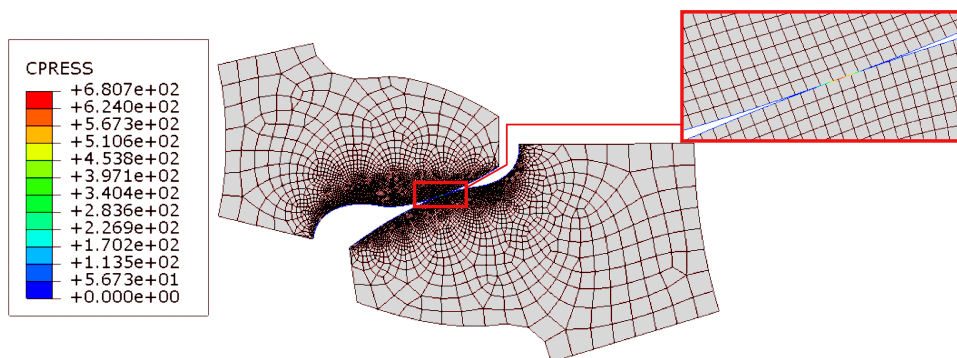


Figure 5.9: Contact pressure.

In this thesis, the contact stress and von Mises stress are used as an output to find a mesh convergence. As Figure 5.10 shows from 1.1 mm to 0.2 mm mesh size the contact pressure and Von Mises stress increase slowly and after that, it increases rapidly until 0.06 mm mesh size. And after 0.06 mm mesh size, the contact pressure and Von Mises stress slowly increase. So for the rest of the analysis 0.06 mm mesh size will be taken.

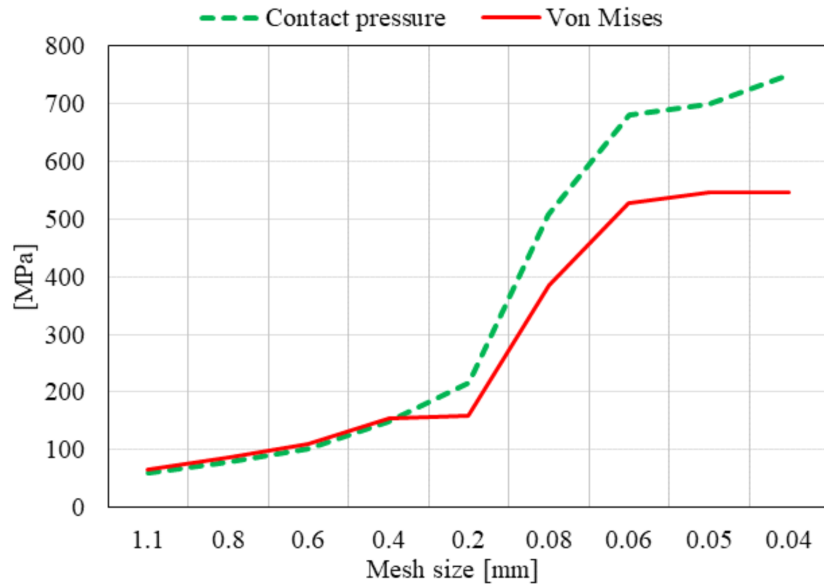


Figure 5.10: Mesh convergence.

The number of elements and nodes for each mesh sensitivity analysis have been given in Appendix H, Table H.1. Automatic time control has been implemented with 0.01, 1×10^{-5} and 0.1 seconds for initial, minimum and maximum time increments respectively and run for 1 second. In this thesis Full Newton methods have been used for solution technique.

5.2.2 *Static transmission error analysis of gear with backlashes*

In static transmission error analysis the gear is free to rotate about its axis and the pinion is fixed in all degree of freedom. The static general step is applied for this analysis. The torque is applied on the gear, and then using the Equation 5.1 and 5.2, the STE can be determined.

There are three steps needed to be implemented in ABAQUS to get the static transmission error. The first step is initial step, in which the initial conditions and boundary conditions are set before the gear sets subjected to any external load, while in the second step can be renamed as contact, in this step the torque is applied on the center of the gear to ensure the gear tooth surfaces are in contact. The third step can be renamed a rotation step in which the rotation of the pinion will be granted. The amount of rotation should be equal or greater than roll angle

to get a full mesh cycle, in this case the roll angle is 32° so the rotation is 32° is given for this analysis. The number of elements and nodes are given in Appendix H, Table H.2, this data are have been used to all analysis such as TVMS, flash temperature, except the element type for flash temperature analysis is CPE4T. The STE for different amount of backlash and friction has been obtained from FEA is shown in Figure 5.11.

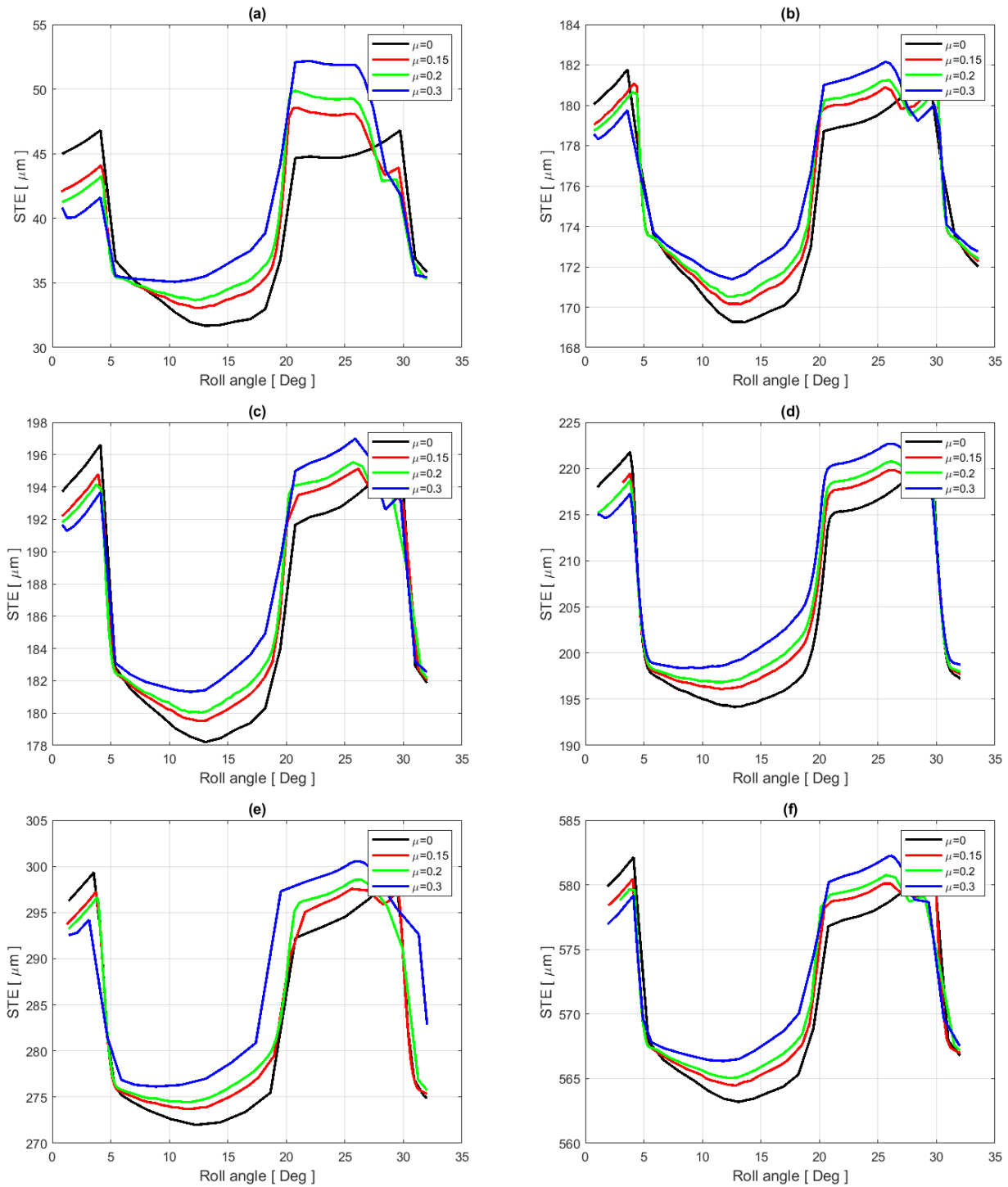


Figure 5.11: STE of gear with: (a) 0 mm, (b) 0.2 mm, (c) 0.4 mm, (d) 0.6 mm, (e) 0.8 mm and (f) 1 mm backlash.

Figure 5.11 shows that the STE at different backlash, the STE without backlash and the transmission error is maximum ($48 \mu m$) at a single tooth contact region and minimum ($43 \mu m$) at double tooth contact region for 0.15 coefficient of friction. For 0.2 friction coefficient, the STE in the single tooth contact region is around $51 \mu m$ and $34.5 \mu m$ in the double tooth contact region. For 0.3 coefficient of friction $54 \mu m$ and $36 \mu m$ transmission error is shown in Figure (a).

As the backlash increased the STE also increased, this shown Figure 5.11 (b) - (f) and for more understanding Figure 5.12 shows all the STE due to different amounts of backlash in one for 0.15 coefficient of friction. In general, backlash and friction of the gear material seriously affect the STE of the gear. The vibration of the transmission system is the result of transmission error, therefore, the backlash will seriously affect the system.

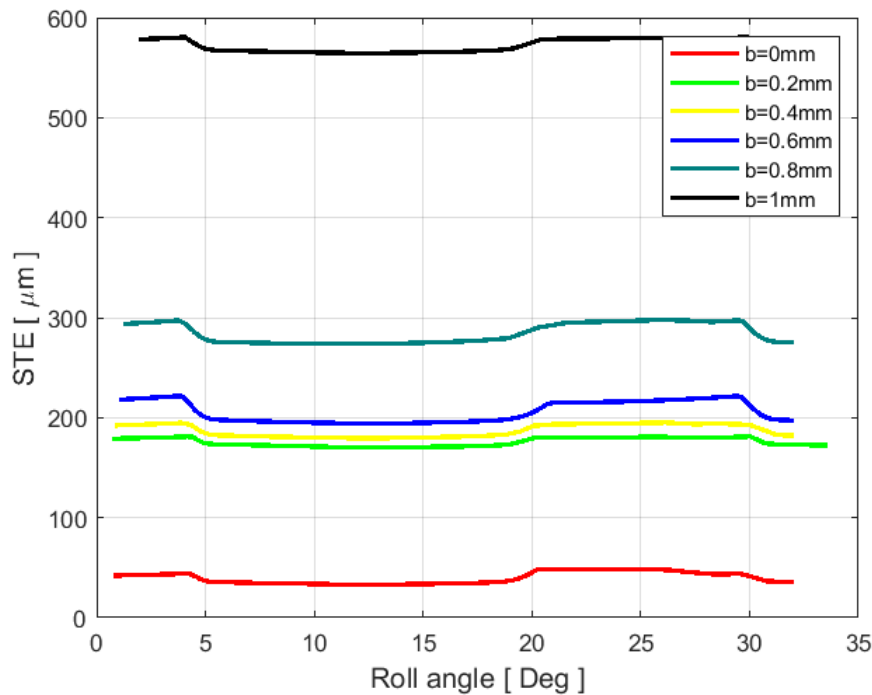


Figure 5.12: STE of spur gear at different backlash with $\mu = 0.15$.

5.2.3 *Dynamic transmission error analysis of gear with backlashes*

The boundary condition is the same as that applied for the static transmission error analysis, the only difference is in this case dynamic implicit step is used and there is only a single step beside the initial step and this can be renamed as rotation, and in this case, both the torque and the rotations are applied at the same time. DTE with different coefficient of friction is examined as follows.

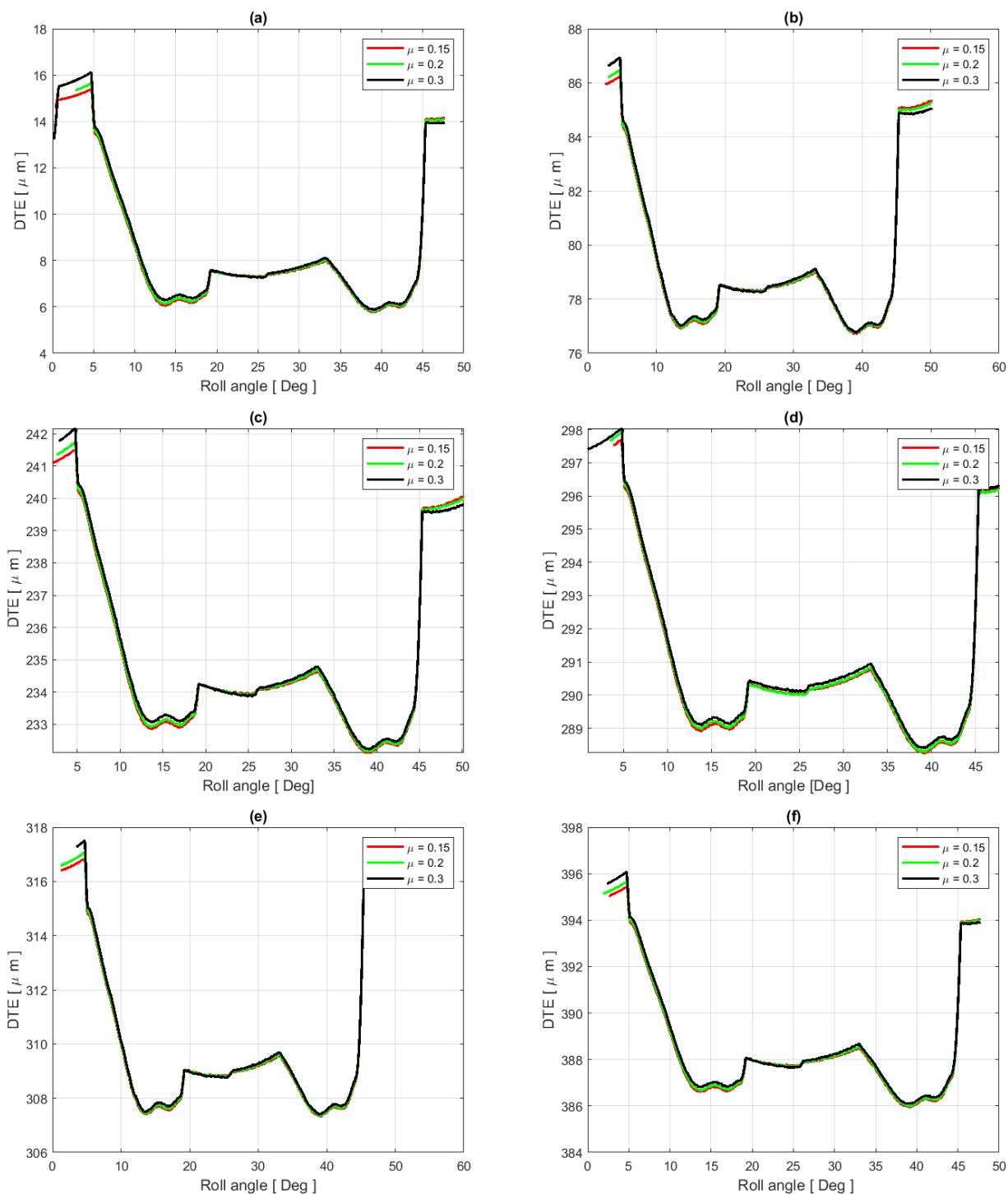


Figure 5.13: DTE of gear with: (a) 0 mm, (b) 0.2 mm, (c) 0.4 mm, (d) 0.6 mm, (e) 0.8 mm and (f) 1 mm backlash.

Figure 5.13 shows that the DTE of the gear at different backlashes with different coefficient of friction, (a) shows that the DTE of spur gear with out backlash, in this case it's lower than the gear with the backlash (b-f), and generally it shows that as the backlash increases the DTE also increase dramatically. The DTE in the double tooth contact region can be minimized by modifying the gear involute profile, Therefore, the maximum DTE can be obtained only in a

single tooth contact region. DTE increases as the coefficient of friction increases.

5.2.4 *Influence of backlash on time-varying mesh stiffness*

An effective time-varying mesh stiffness model is a basic condition to conduct a dynamic analysis. Thus, it is significant to recognize the mechanism of a gear system's shock and vibration to investigate the influence of time-varying mesh stiffness on vibration responses, especially with regard to the mechanism of the noise. The main internal excitation source of gear dynamics is time-varying gear mesh stiffness [56].

There are two types of stiffness for a pair of gears, these are rectilinear mesh stiffness and torsional mesh stiffness. Rectilinear mesh stiffness is an equivalent mesh stiffness of a pair of gears along the action line, while torsional mesh stiffness is the ratio between a torque applied on gear (the pinion body is fixed) and the corresponding angular displacement of the gear body. These two types of mesh stiffness are related to each other by Howard et al. [57] using Equation 5.18.

Rectilinear mesh stiffness can be calculated using the experimental, finite element method and potential energy methods. Torsional mesh stiffness is commonly evaluated using the finite element method [58, 59, 60].

$$K_M = \frac{K_t}{r_b^2} = \frac{T}{r_b^2 \theta(t)} \quad (5.18)$$

Where r_b - base radius of the driving gear.

The torsional mesh stiffness can also calculate using Equation 5.19 [61] and it used in this document to determine the torsional mesh stiffness and then it can be converted into a linear mesh stiffness using Equation 5.18.

$$K_t = \frac{T}{TE(\omega)} \quad (5.19)$$

5.2.5 Numerical analysis of torsional mesh stiffness

Time varying mesh stiffness (TVMS) of gears with different backlashes that obtained using Equation 5.19 is shown in Figure 5.14.

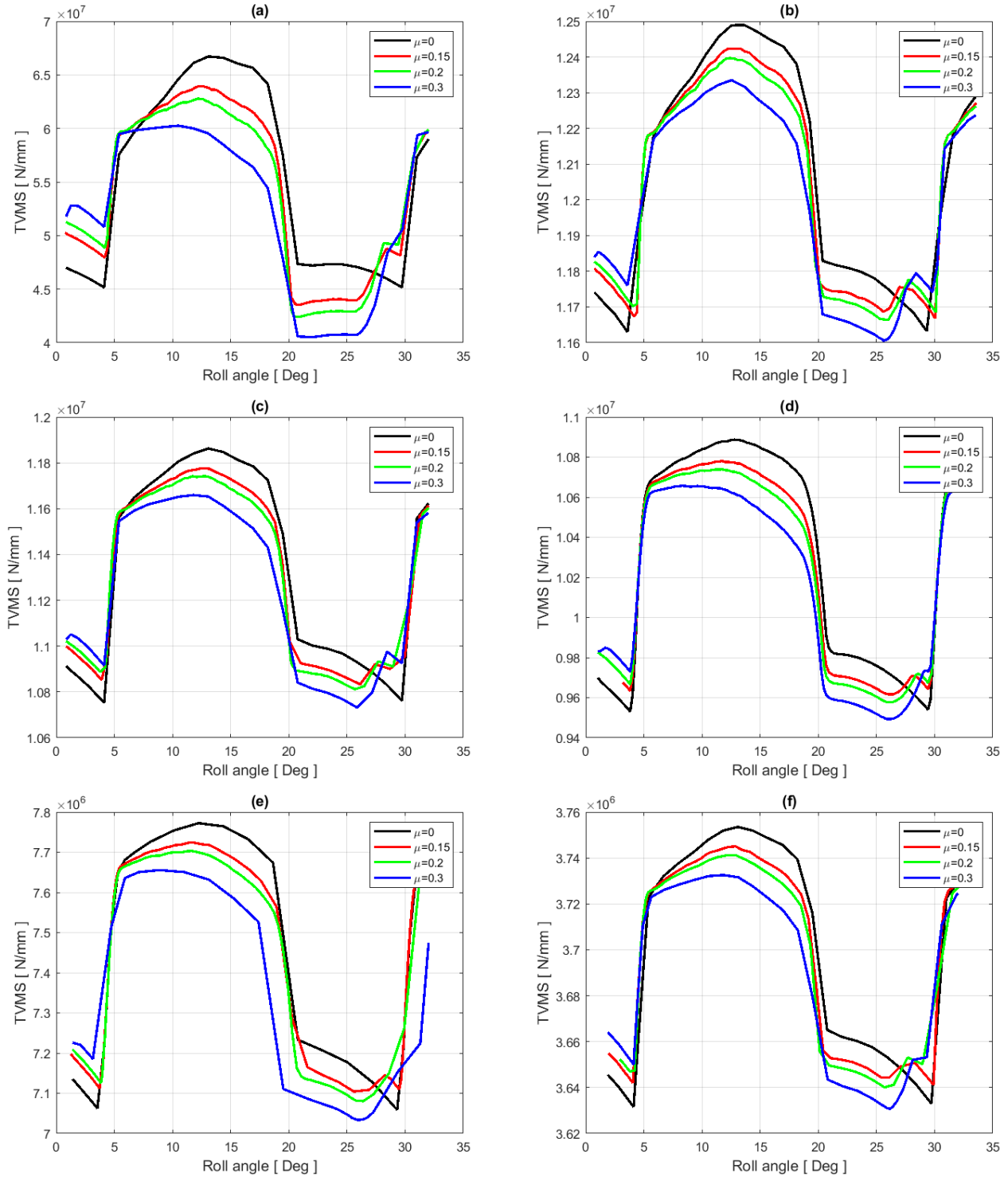


Figure 5.14: TVMS of gear with: (a) 0 mm, (b) 0.2 mm, (c) 0.4 mm, (d) 0.6 mm, (e) 0.8 mm and (f) 1 mm backlash.

Figure 5.14 shows that the time varying mesh stiffness of gear with different backlashes at different coefficients of friction. The mesh stiffness for a single tooth contact is between 46 and 45 MN/mm and for double tooth contact region it's around 67.5 MN/mm for 0 mm backlash with 0 coefficient of friction as shown in Figure 5.14 (a), it also shows that as the backlash increases the mesh stiffness decreases drastically.

Figures 5.14 (b) - (f) show a similar phenomenon with Figure 5.14 (a), but it clearly shows that the mesh stiffness decreases as the backlash of the gear increases, to clarify this Figure 5.15 shows the mesh stiffness of gear with different backlashes at 0.15 coefficient of friction.

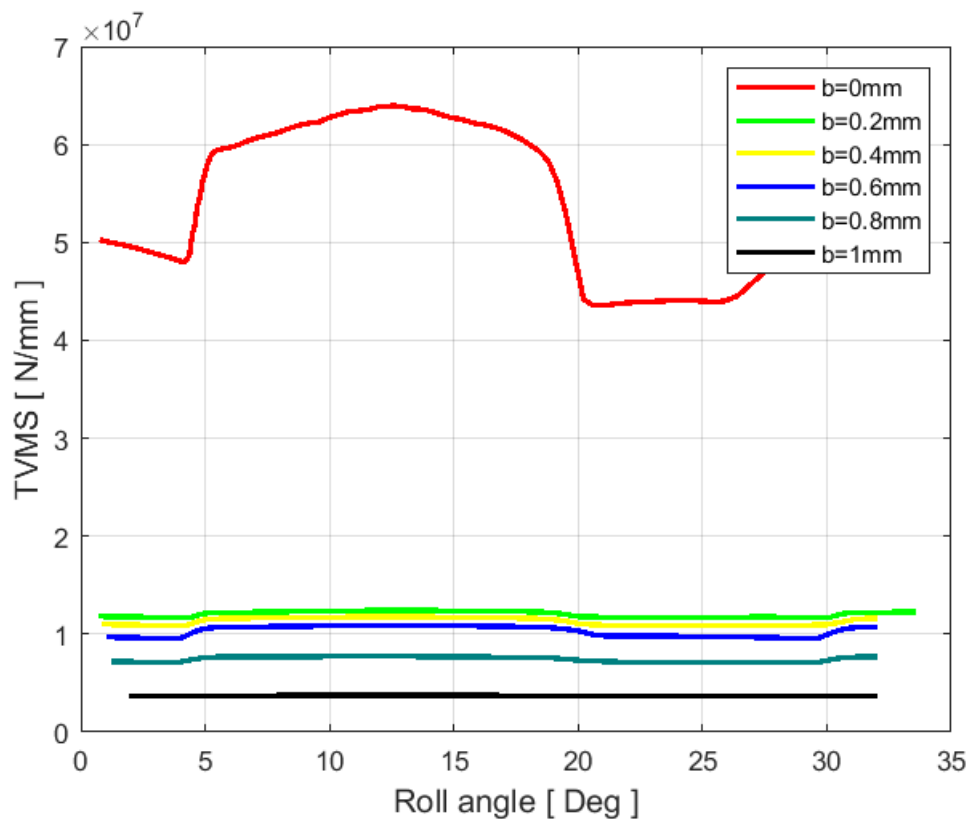


Figure 5.15: Torsional mesh stiffness at $\mu = 0.15$.

Figure 5.15 shows the mesh stiffness of the gear with out backlash is 67.3 MN/m for a single tooth contact and 45 MN/m for double tooth contact. The mesh stiffness of the gear with 0.2 mm and above have lower than 15 MN/m . In general, as the backlash increase the mesh stiffness decrease dramatically.

5.2.6 Numerical analysis of load sharing

2D models with a plane strain assumption for a thick gear body, or a plain stress assumption for a thin gear body gives better accurate results than the 3D models. But 3D models can overcome the limitations of 2D models in simulating helical gears, spur gears with modifications along the face width direction, or gears with misalignment [53]. In this section the load sharing using FEA will be discussed.

Load sharing is obtained by FE analysis for 0 mm backlash of the is shown in Figure 5.16.

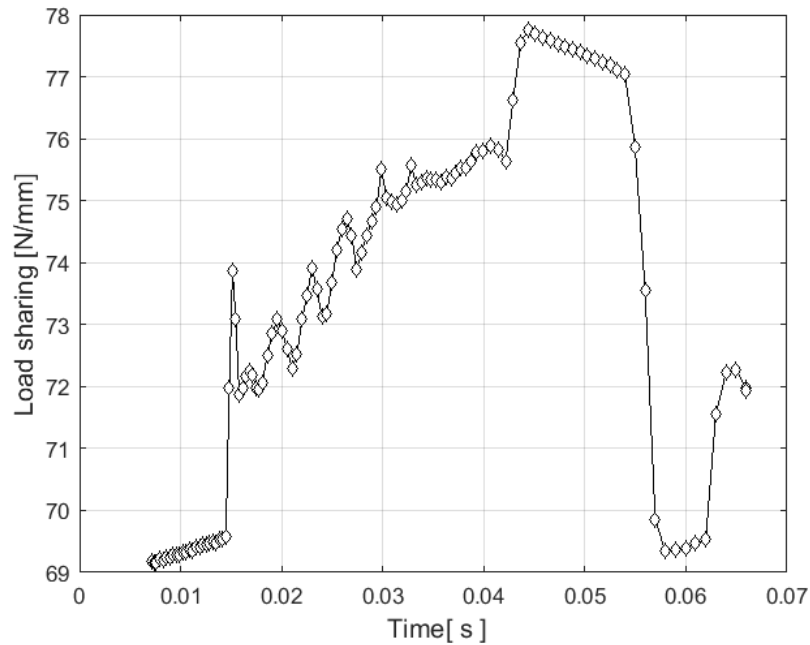


Figure 5.16: Load sharing pattern obtained by FEA.

The load sharing using FE analysis is shown in Figure 5.16, the normal contact force is taken from ABAQUS post-process and it shows that the load between time 0.015 and 0.058 seconds the load is maximum comparing to the others, therefore this region is called a single tooth contact region, while the rest is a double tooth contact region.

In this chapter the effect of backlash on TE and TVMS have been discussed, and it reveals that the STE and DTE is increases drastically as the backlash increases. In addition, the mesh stiffness of the gear is highly influenced by the backlash. When the gear tooth thickness reduced a little due to manufacturing or wear, the mesh stiffness of the gear decreases drastically.

Effect of Backlash on the Flash Temperature of the Spur Gear

6.1 Introduction

In this chapter, the effect of backlash on the flash temperature of the spur gear will be analyzed. FE analysis and Block's equation methods have been used. There is no single formula to calculate the flash temperature of contacting bodies, pecelet number is one of the non dimensional parameter that helps to determine the amount of heat generation when the gear pairs are in contact. The value of pecelet number will indicate how fast the heat source is moving.

When gears rotate about their own axes of rotation and the tooth is in contact, heat will be generated due to friction and this heat generation varies along the line of contact due to the movement of the gear. The heat source is not stationary in gear, rather it is a moving heat source.

The speed of the heat source will affect the temperature of the contact bodies. Once the heat generation is obtained the equation is selected based on the pecelet number analytically. The second method to determine the flash temperature is using FEM, when the gear is modeled without introducing backlash and then analyzing it for flash temperature using ABAQUS coupled temperature displacement analysis. Numerical value and analytical results will be compared with the experimental results that obtained by Tobe, and if the results are in good agreement, prediction of flash temperature using FEA of the spur gear with different backlash will be carry on.

Surface temperature has a strong effect on EHL, as is the case with hydrodynamic lubrication. Elevated temperatures lower the lubricating oil viscosity and usually decrease the pressure viscosity coefficient ψ . A reduction in either of these parameters will reduce the EHL film thickness which may cause lubricant failure. Excessively high temperatures may also interfere with some auxiliary mechanisms of lubrication necessary for the stable functioning of partial EHL.

6.2 Peclet number

There is no single algebraic equation giving the flash temperature for the whole range of surface velocities. Peclet number is a non-dimensional measure of the speed at which the heat source moves across the surface, and it has been introduced as a criterion allowing the differentiation between various speed regimes.

The Peclet number is an indicator of the heat penetration into the bulk of the contacting solid bodies, which means it describes whether there is sufficient time for the surface temperature distribution of the contact to diffuse into the stationary solid. A higher Peclet number indicates a higher surface velocity for constant material characteristics and can be calculated using Equation 6.1. Since all frictional heat is generated in the contact, the contact is modeled and treated as a heat source in the analysis.

Peclet number is inversely proportional to the thermal diffusivity which is the thermal conductivity divided by the density and specific heat capacity at constant pressure and is a measure the rate of transfer of heat of a substance or material from the hot side to the cold side. The thermal diffusivity is a material-specific property for characterizing unsteady heat conduction and describes how quickly a material reacts to a change in temperature. In order to predict cooling processes or to simulate temperature fields, the thermal diffusivity must be known and it is given by Equation 6.2.

$$L_{eP,G} = \frac{bU_{P,G}}{2\chi_{P,G}} \quad (6.1)$$

The value of half heat sources width (b) has been determined in Section 4.4.1. Thermal diffusivity of the pinion and gear material is calculated from Equation 6.2, it gives $11.0962 \times 10^{-6} \frac{m^2}{s}$;

$$\chi_{P,G} = \frac{\kappa}{\rho C_p} \quad (6.2)$$

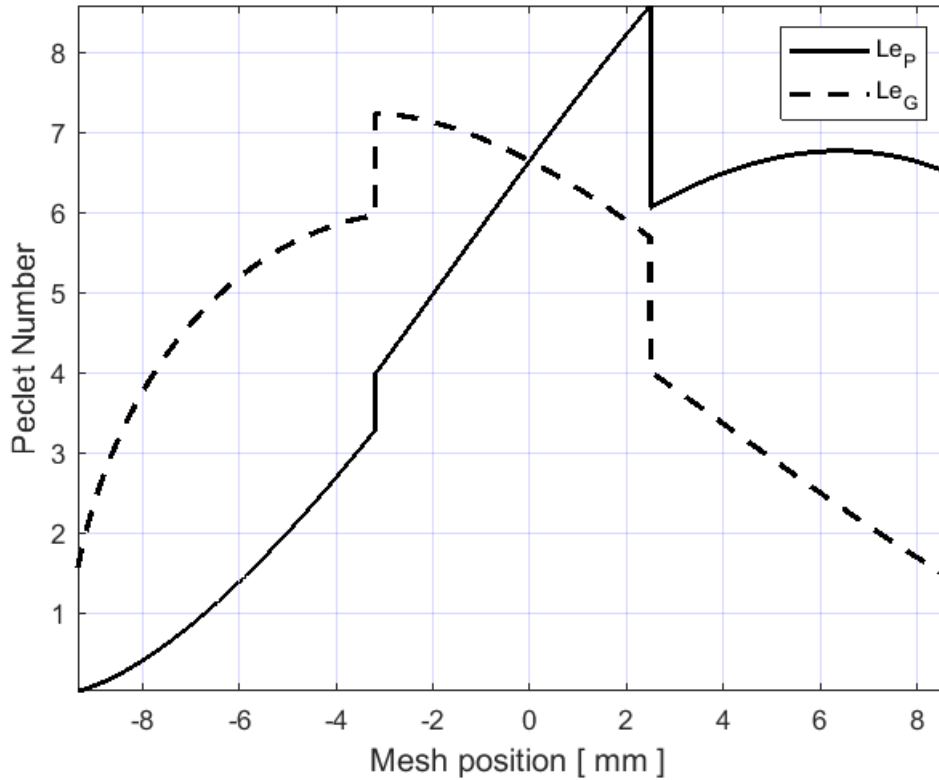


Figure 6.1: Peclet number.

Figure 6.1 shows that the peclet number of the pinion (L_{eP}) is increased slowly from 0 at mesh initiation to 3.3 at the LPSTC and after that, it increased linearly until the HPSTC its value is around 8.5. The peclet number decreases instantly at the HPSTC and increases gradually to 6.5 at mesh termination. While the peclet number of gear increases gradually from the point of contact till the LPSTC and automatically increases to 7.2 and decreases till it reaches the HPSTC it is around 5.8 and again decreases linearly to 1.5 at the mesh termination.

The pcelet number of both mating gears are equal at the pitch point. The major portion of the peclet number for both gears of double tooth contact region are less than 5, this indicates that the heat source is moving slowly. On the contrary, the major portion of the single tooth contact region for both gear sets is greater than 5, this indicates that the heat source is moving fast, there is insufficient time for the temperature distribution of the contact to be established in the stationary body and the equations of linear heat diffusion normal to the surface apply.

6.3 Heat generation due to friction

For most metallic gears, sliding friction is the dominant mechanism for the heat generation. Heat is generated by sliding friction of tooth surfaces. The temperature distribution is proportional to the distribution of contact pressure and sliding velocity. The flash temperature of tooth contact along the line of action is calculated by Blok's contact temperature theory.

The contact temperature is the sum of the maximum flash temperature along the line-of-action and bulk temperature of the gear tooth, which is the temperature of the tooth surface before it enters the contact zone.

The amount of heat generation is given by Equation 6.3, and it shows that the heat generation is proportional to the friction coefficient, normal load and the sliding velocity of contacting bodies. The sliding velocities and the contacting load has been determined in Chapter 4.

$$Q = \mu W |U_P - U_G| \quad (6.3)$$

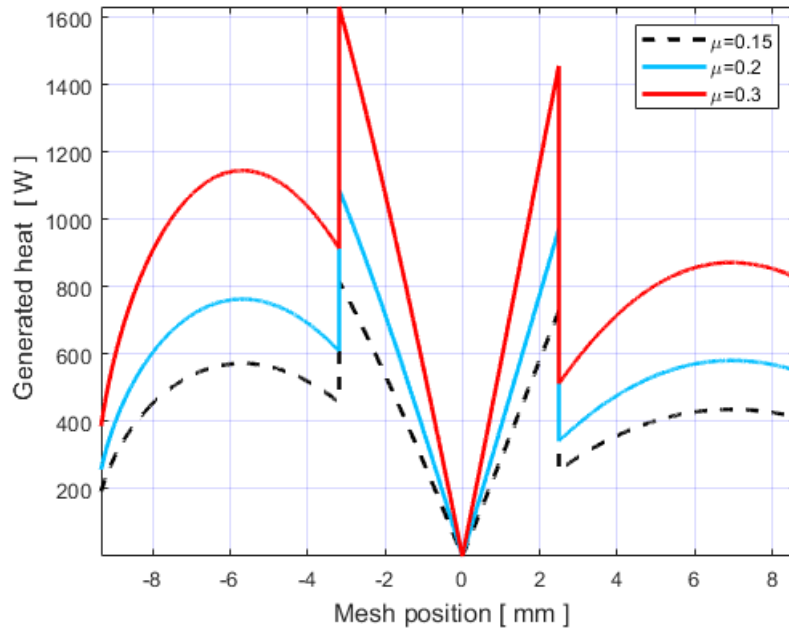


Figure 6.2: Heat generation.

Figure 6.2 shows that the heat generation is increased from zero to a maximum value till it reaches on the last point of single tooth contact, and the falls automatically and again increase slightly till the mesh termination. This is similar for mesh initiation. In addition to this as the coefficient of friction increases the amount of heat generation will also increase.

6.4 Flash and conjunction temperature using Block's equation

During the meshing of gear teeth, there is inherent sliding (with a friction of material) which produces heat generation. At the sliding contact, substantial temperatures develop for very short periods of time, due to the motion of the sliding spot along the tooth flank. These are called flash temperatures and can have very adverse effects on the gear operation.

Block's hypothesis that when this flash temperature reaches a critical value, there is a breakage of the oil film and this results from a rapid scuffing of the contact surfaces in the case of repeated contact at the same position.

Bulk temperature during operation is also important because it affects the properties of the gear materials and some materials, such as plastics, can result in general yielding and failure.

Flash temperature of the gear for $L_e > 5$ is given by Equation (6.4).

$$T_{fmax} = \frac{1.11\mu W |\sqrt{U_P} - \sqrt{U_G}|}{2l\sqrt{2b\kappa\rho C_p}} \quad (6.4)$$

The temperature when the pair of gear tooth are in contact is the sum of the flash temperature that produced due to the friction and the bulk temperature of the gear pairs.

$$T_{bnew} = \frac{1}{2}(T_{bP} + T_{bG}) + \frac{1}{2}\left(\frac{n-1}{n+1}\right)(T_{bP} - T_{bG}) \quad (6.5)$$

Where a constant $n = \sqrt{\frac{U_P\rho_P C_{pP}\kappa_P}{U_G\rho_G C_{pG}\kappa_G}}$

For $0.2 \leq n \leq 5$ the average bulk temperature can be calculated with sufficient accuracy from Equation 6.6. Pinion and gear have the same bulk temperature which equals to $20^\circ C$ it's given in the Table 4.3 as an operating condition.

$$T_{bnew} = \frac{1}{2}(T_{bP} + T_{bG}) \quad (6.6)$$

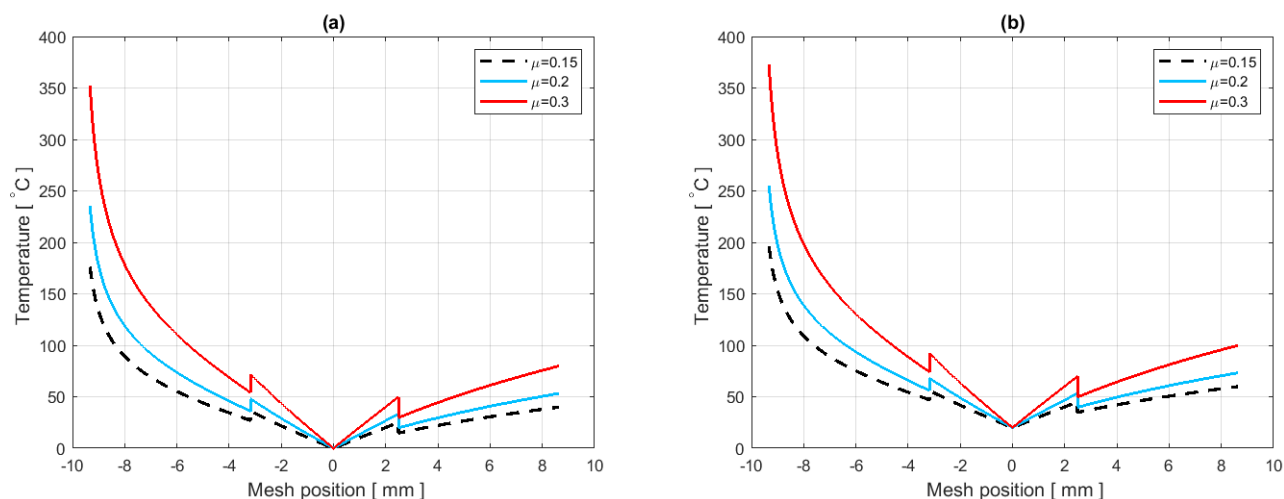


Figure 6.3: Gear (a) flash and (b) conjunction temperature.

Flash temperature distribution is shown in Figure 6.3 (a) and the maximum flash temperature which is 175, 245 and 350 °C has been found at the mesh initiation point for 0.15, 0.2 and 0.3 coefficient of friction respectively, and it decreases gently till it gets at the point of LPSTC. In the single tooth contact region, the maximum flash temperature is exhibited at LPSTC and linearly decreases and gets equal to the bulk temperature of the gear at the pitch point and it increases again in the mesh termination direction.

In general, it is maximum at mesh initiation and smoothly falls till the point where the single tooth contact occurs and it decreased linearly and gets near to zero at a pitch point. After the pitch point again the temperature increases linearly till the endpoint of single tooth mesh, and then it increases slightly.

Coefficient of friction of the gear material affect the flash temperature of the gear considerably.

Figure 6.3 (b) shows the temperature at the conjunction, the conjunction temperature exceeds the flash temperature by 20 °C , it is the sum of flash temperature and the bulk temperature.

6.5 Minimum film thickness

Lubrication regimes are basic contact conditions that predict the way the load is carried from one surface to another of contacting bodies. There are four main lubrication regimes that are commonly known.

Hydrodynamic lubrication: the contacting bodies are separated by a liquid lubricant which is thick enough to avoid any direct contact between their surfaces. The load is then carried by the pressurized lubricant and it is shown in Figure 6.4 (a). The thickness of the film (h) can lead in to another division, if $h \geq 0.25 \mu m$ is called a hydrodynamic lubrication (HDL) regime, while if $0.025 \geq h \geq 5 \mu m$ we call it elasto hydrodynamic lubrication (EHL) regime.

Mixed lubrication (ML): the average lubricant film thickness between contacting bodies is lower than the mean roughness of their surfaces. Direct contacts occur between asperities. The load is then carried partly by the lubricant, partly there is a direct contact between mating pairs as shown in Figure 6.4 (b).

Boundary lubrication (BL): No liquid lubricant is used: the load is carried by direct contact between bodies at the level of the asperities, this is shown in Figure 6.4 (c), the thickness of the film is between 1 and 3 nm.

Solid-film lubrication: the contacting bodies are separated by a solid lubricant thick enough to avoid any contact between the tool and the work piece. Figure 6.4 (d) shows that the load is fully carried by the solid lubricant.

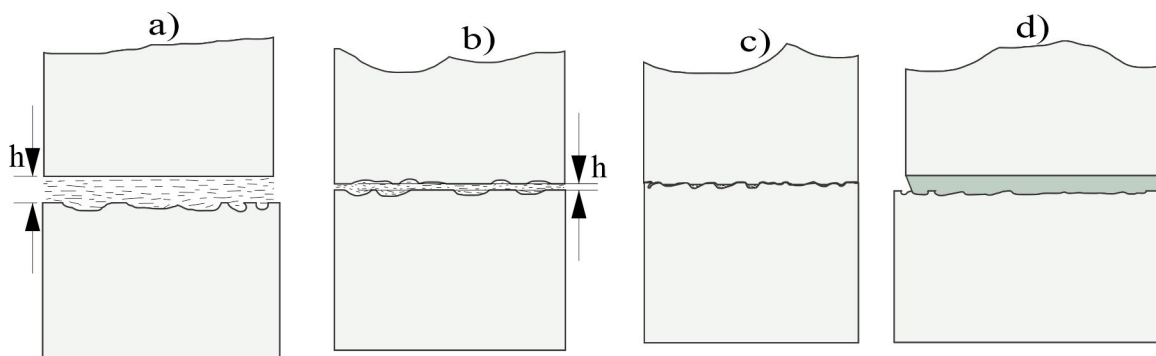


Figure 6.4: Lubrication regimes (a) HDL, (b) ML, (c) BL and (d) Solid-film lubrication.

The exact analysis of elastohydrodynamic lubrication by Hamrock and Dowson, provided the most important information about EHDL [62].

Film thickness at each meshing position is expressed in Equation 6.7:

$$h_o = 3.068C_P C_T R' U^{0.69} g^{0.56} W_F^{-0.1} \quad (6.7)$$

Compressibility reduction factor C_P and inlet shear heating reduction factor respectively C_T can be calculated by the following equations.

$$C_P = \left(1 + \frac{0.58 \times 10^{-9} P_{max}}{1 + 1.68 \times 10^{-9} P_{max}} \right)^{-1} \quad (6.8a)$$

$$C_T = \exp \left(-0.75 \beta \frac{\eta_o u^2}{4k_f} \right) \quad (6.8b)$$

$$u = \frac{U_P + U_G}{2} \quad (6.8c)$$

$$U = \frac{\eta_o u}{E' R'} \quad (6.8d)$$

$$g = \psi E' \quad (6.8e)$$

$$W_F = \frac{w}{E' R'} \quad (6.8f)$$

The lubricant pressure viscosity (ψ) and temperature viscosity (β) factors respectively. These and other parameter values are given in Appendix - G.

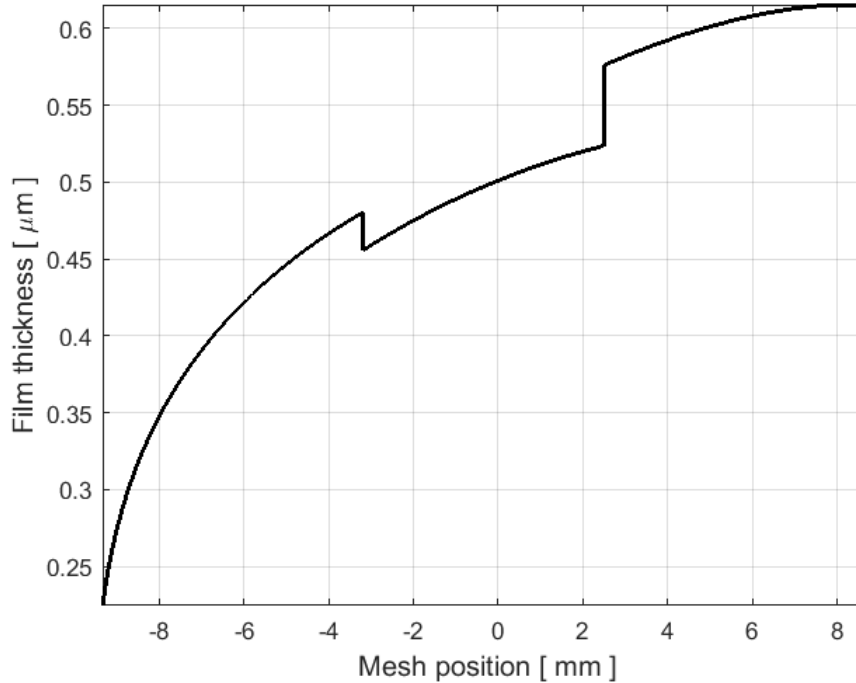


Figure 6.5: Film thickness.

Figure 6.5 shows that the film thickness increases from mesh initiation to LPSTC exponentially, then minimum film thickness is found at the mesh initiation and which is around $0.2 \mu m$.

The film thickness is decreased in a single tooth contact region and increases smoothly up to HPSTC region, and then it increases exponentially to $0.62 \mu m$ at the mesh termination. The minimum film thickness at mesh initiation can be altered by modifying the gear tooth profile, this will make the minimum film thickness lay between LPSTC and HPSTC region. In general, the minimum film thickness is found in single tooth contact region.

6.6 Numerical analysis of flash temperature

In this section, the flash temperature of the gear without backlash will be analyzed using ABAQUS at a different coefficient of frictions and compared the results with the Block's equation results. And finally, the numerical analysis for the gear with 0.2 mm to 1 mm backlash by 0.2 mm increments will be analyzed.

ABAQUS has two options to analyze the simulations, these are ABAQUS/Standard and ABAQUS/Explicit. ABAQUS standard allows to simulate a steady and transient analysis using an implicit analysis approach. Therefore, ABAQUS/ Standard has been used for this simulation. A coupled temperature displacement analysis option is used to predict the temperature of the gears.

6.6.1 *Flash temperature of spur gear without backlash*

The geometry of the spur gears have been modeled using gear Trax 2017 software and a 2D model of the gear is generated. Gear Trax is also a very efficient software to model a modified gear. A 2D sketch model is imported to ABAQUS and generates a plane strain model, in this case, plane strain analysis is implemented.

The sketch is then converted into a 2D plain strain geometry, and a thickness of 1 mm is used. The material property is given in Table 4.1 and uses a solid object for the designation of the gear. To apply loads and boundary conditions ABAQUS allows to use different steps, this will pave a way to apply different loading and boundary conditions at different time. In this case, three steps have been implemented, the first one is the initial step, in this step where the boundary conditions determined before the gear mates are subjected to any load.

The second step is the contacting step, where the torque is applied on the gear and this will make the tooth are in contact. The third step is a speed or rotation step, in this step the pinion is rotated with the specified speed, and each step is running when one step is completed.

Loading and boundary conditions

The center of both gears are coupled with points RP-1 and RP-2 as shown in Figure 6.6, and these points are restricted in all translational degree of freedoms. The pinion is restrained from rotating in the initial step while the gear is free to rotate about its rotating axis, but RP-1 is modified in rotating step, and the pinion is allowed to rotate for 5.2 seconds at 2090 RPM. The torque, 3322 Nmm is applied on gear at point RP-2 at the contacting step, and the load is propagated to the next step. The convection heat transfer coefficient of lubricant is included in the mesh model of the gear, in this analysis a film with $(750 \times 10^{-6} W/mm^2 \cdot C)$ for VG68 lubricant is applied in meshes to cool down the gear tooth faces as used by [11].

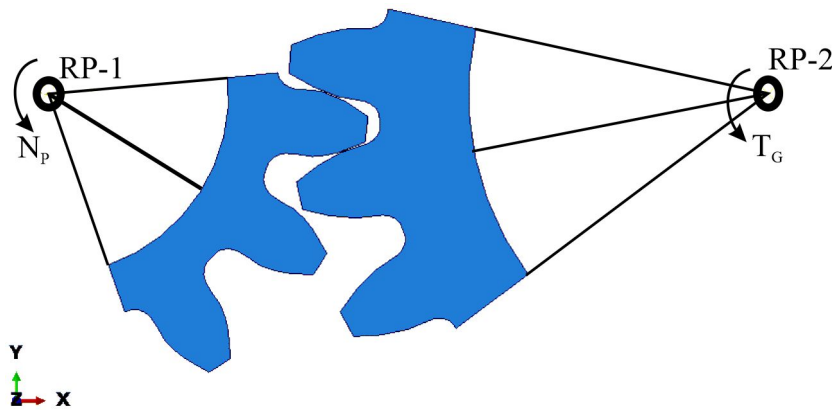


Figure 6.6: Load and boundary conditions.

CPE4T(A 4-node plane strain thermally coupled quadrilateral, bi-linear displacement and temperature) element type has been used for coupled temperature analysis and it has 62830 number of elements and 190488 number of nodes and the it runs for 5.2 seconds this will give a full role angle of the gear. The analysis takes 10.84519 hrs to complete the analysis for 0.15 coefficient of friction.

The initial condition and convective heat transfer coefficient is included in the analysis. The initial temperature of the gear sets are $20 \text{ }^\circ\text{C}$. In this analysis 1×10^{-8} , 1×10^{-20} and 1×10^{-5} seconds are used as initial, minimum and maximum time increment with automatic time control.

Results of analysis

The temperature at the mesh initiation, pitch point and mesh termination of 0 mm backlash for 0.15 coefficient of friction is shown in the contour view of Figure 6.7. The maximum temperature is achieved on the mesh initiation. At mesh initiation around $194.9 \text{ }^\circ\text{C}$ and there

is no considerable change of temperature at the pitch point with the bulk temperature of the gear, this is due to pure rolling at the pitch point. The temperature at mesh termination is found around 89.52 °C.

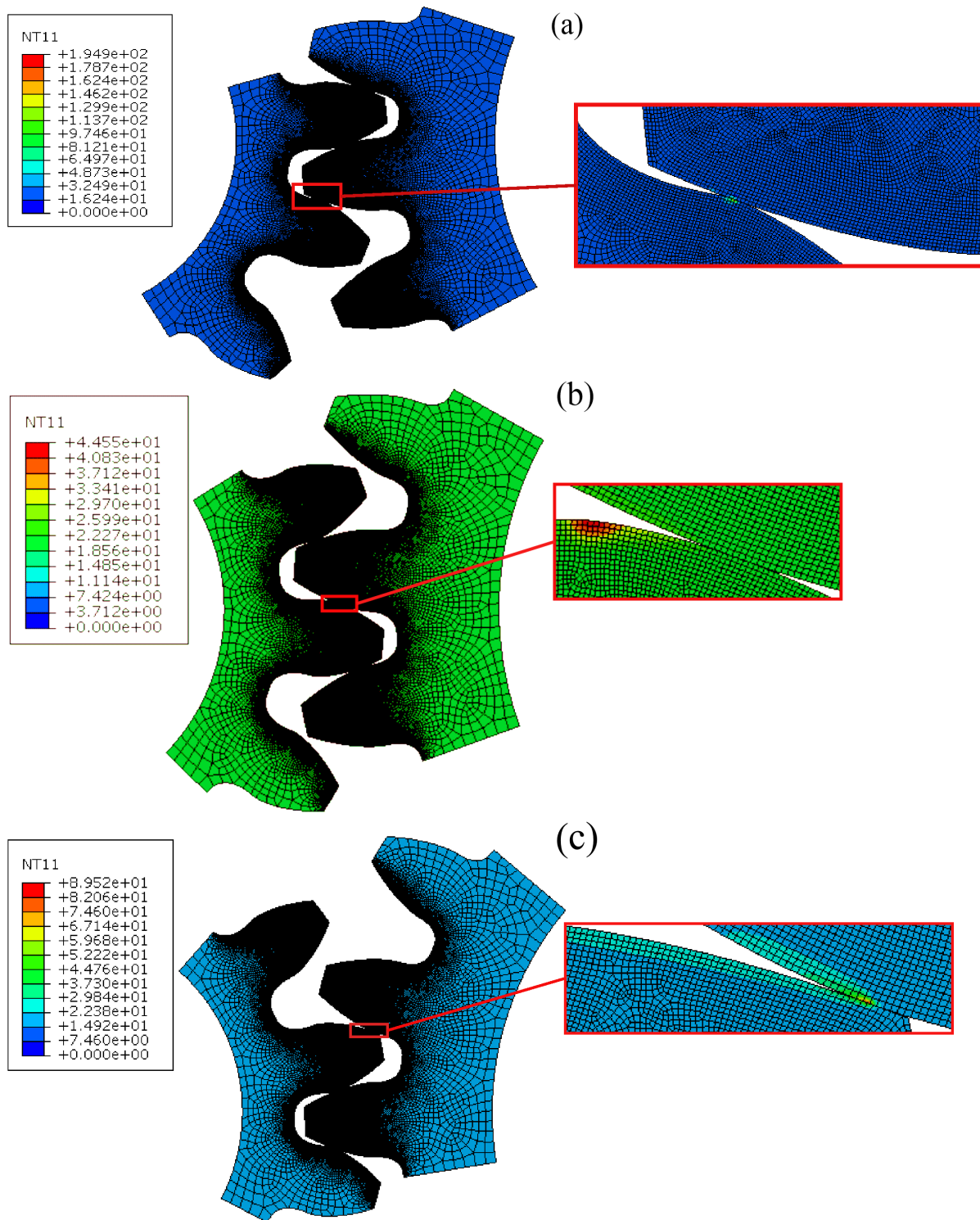


Figure 6.7: Numerical results of gear with 0 mm backlash flash temperature at: (a) mesh initiation, (b) pitch point and (c) mesh termination.

6.6.2 Data regression analysis of experimental and FE result

The FE flash temperature analysis result with 0.15 coefficient of friction has been chosen to compare with the experimental result because the flash temperature of the gear with different amounts of backlash will be predicted using FEA. The comparison will be conducted using data regression analysis. Regression analysis is a powerful statistical method that allows examining the relationship between two or more variables of interest. A regression equation is a polynomial regression equation if the power of the independent variable is more than 1.

The experimental results obtained by Tobe and his colleagues used for comparison purpose with FE results (Figure 6.8), which has been explained in Section 3.1. To analyzed how much the two results are fitted will analysis using data regression.

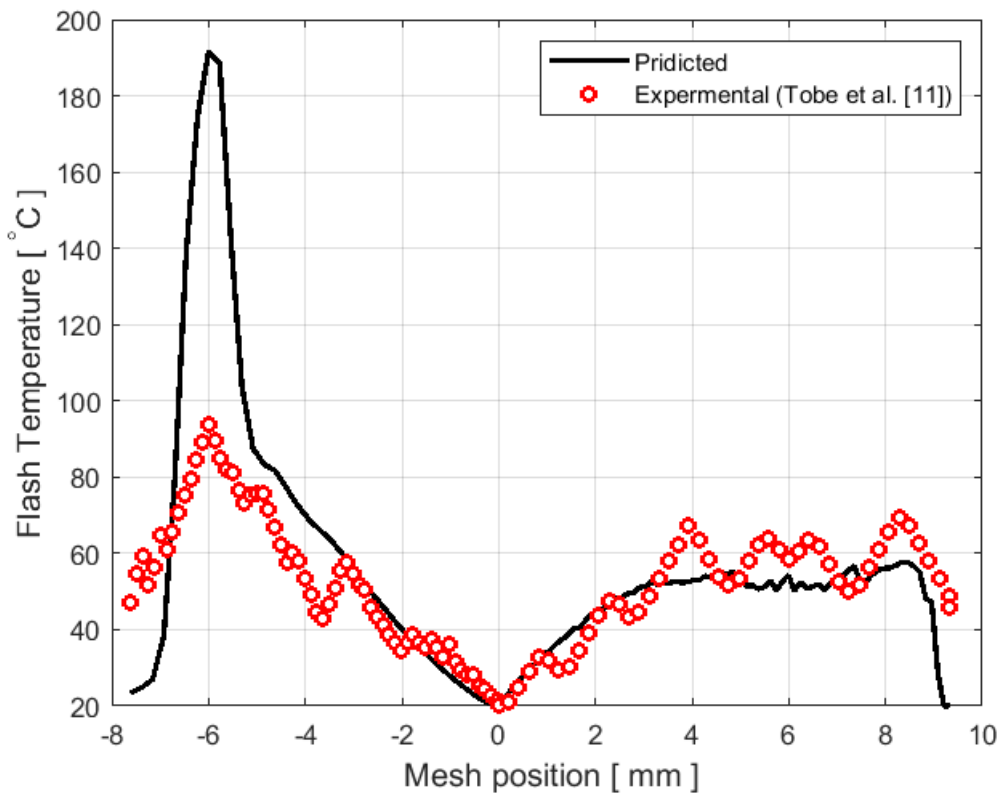


Figure 6.8: Experimental (by Tobe et al.[11]) and FE results

The regression analysis has been analyzed using Excel and MATLAB, because these software use different expressions for expression analysis. Excel uses coefficient of determination or R-square denoted R^2 , which is simply the square root of the sum of squared residuals of the equation of fitted graph and the values always between 0 and 1, while MATLAB uses norm of residuals, which varies from 0 to infinity with smaller numbers indicating better fits and zero indicating a perfect fit.

According to Kvalseth [63], if the value of R-square is close to 1, then the predicted value is within a good agreement with the experimental data, but if it's close to 0 then the residual is maximum and there is maximum deviation between experimental and predicted value. On the other hand, if the norm of residual is close to 0 then the predicted value is in close agreement with the experimental value, but if the value is maximum then this indicates that there is a very huge deviation between the two data.

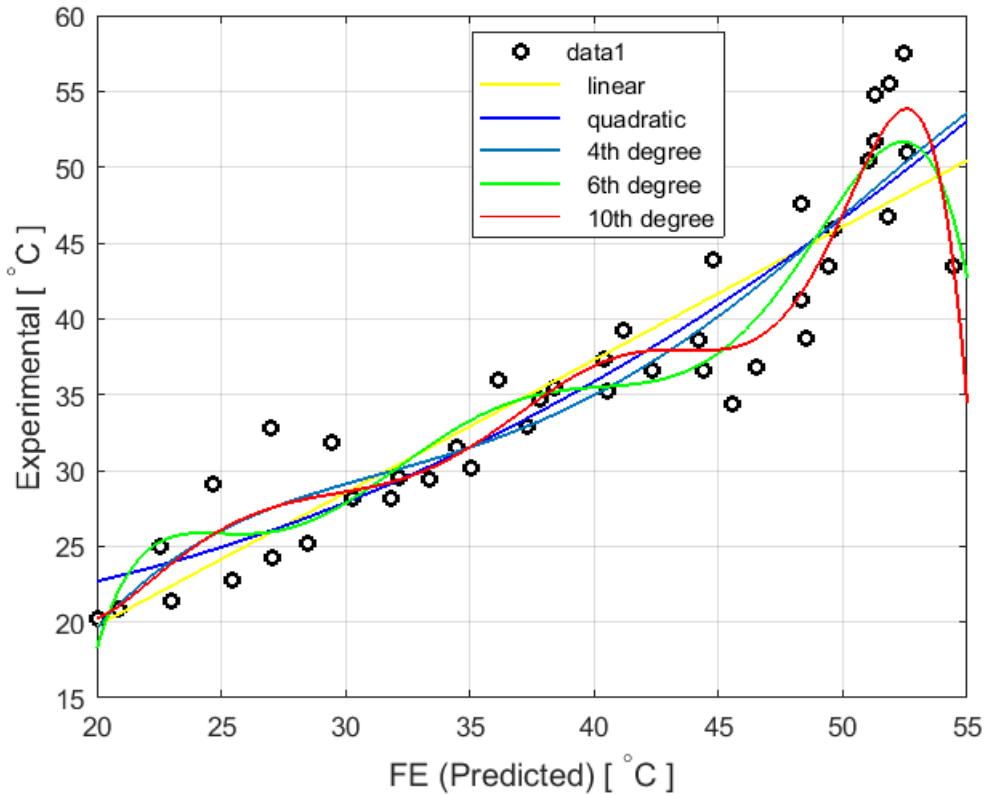


Figure 6.9: Data regression for experimental and FE results with in STC region

Figure 6.9 shows that the regression analysis of experimental and FE analysis of the gear with out backlash with 0.5 coefficient of friction. Linear and polynomial functions regression method have been used in this thesis for comparison and the expressions are given in Equations 6.9 (a) - (e). The linear regression has maximum norm of residual and this indicates that the linear function doesn't fit well. Polynomial functions such as quadratic, 4th, 6th, and 10th order degree polynomial functions have been used to find the best fitted graph, and as the figure shows the best fitted graph is found on the maximum degree (10th) degree of polynomial function. The norm of residual is given on Table 6.1 for each fitted graph.

Due to the high scatter in the data, it may be possible to say that the higher the polynomial function, the better fit you get. The disadvantage of high polynomial is that it contains several

variables as you can see in your Equation 6.9e.

$$y = p_1x + p_0 \quad (6.9a)$$

$$y = p_2x^2 + p_1x + p_0 \quad (6.9b)$$

$$y = p_4x^4 + p_3x^3 + p_2x^2 + p_1x + p_0 \quad (6.9c)$$

$$y = p_6x^6 + p_5x^5 + p_4x^4 + p_3x^3 + p_2x^2 + p_1x + p_0 \quad (6.9d)$$

$$y = p_{10}x^{10} + p_9x^9 + p_8x^8 + p_7x^7 + p_6x^6 + p_5x^5 + p_4x^4 + p_3x^3 + p_2x^2 + p_1x + p_0 \quad (6.9e)$$

Table 6.1: Regression analysis of experimental and FE results

Fitted equation	Coefficients	Norm of residuals
Linear	$p_1 = 0.87685, p_0 = 2.2163$	25.077
Quadratic	$p_2 = 0.013966, p_1 = -0.17947, p_0 = 20.691$	23.729
4th order polynomial	$p_4 = -6.6914e - 05, p_3 = 0.010968, p_2 = -0.63724, p_1 = 16.322, p_0 = -128.97$	22.964
6th order polynomial	$p_6 = -2.7522e - 06, p_5 = 0.00060506, p_4 = -0.054306, p_3 = 2.5452, p_2 = -65.656, p_1 = 884.09, p_0 = -4834$	19.829
10th order polynomial	$p_{10} = 1.6179e - 11, p_9 = -5.9742e - 09, p_8 = 9.7127e - 07, p_7 = -9.1679e - 05, p_6 = 0.0055727, p_5 = -0.22833, p_4 = 6.3991, p_3 = -121.39, p_2 = 1494.6, p_1 = -10804, p_0 = 34869$	17.253

Table 6.1 shows that the coefficients and norm of residuals of linear and polynomial functions. The norm of residual decreases from 25.077 to 17.253 for linear and 10th order polynomial function. The higher order gives a minimum norm residuals, this indicates that the polynomial function with 10 degree gives a better result, and it shows the predicted results is in close agreement with the experimental result.

The value of R Square is equals to 0.989342129 using Excel regression statistics analysis, this value is close to 1 and this indicates the predicted results in good agreement with the experimental result.

6.6.3 Comparison of Block's equation and numerical analysis

Block's equation that has been used in Section 6.4 and numerical results for 0 mm backlash at three different coefficient of friction is compared in this section.

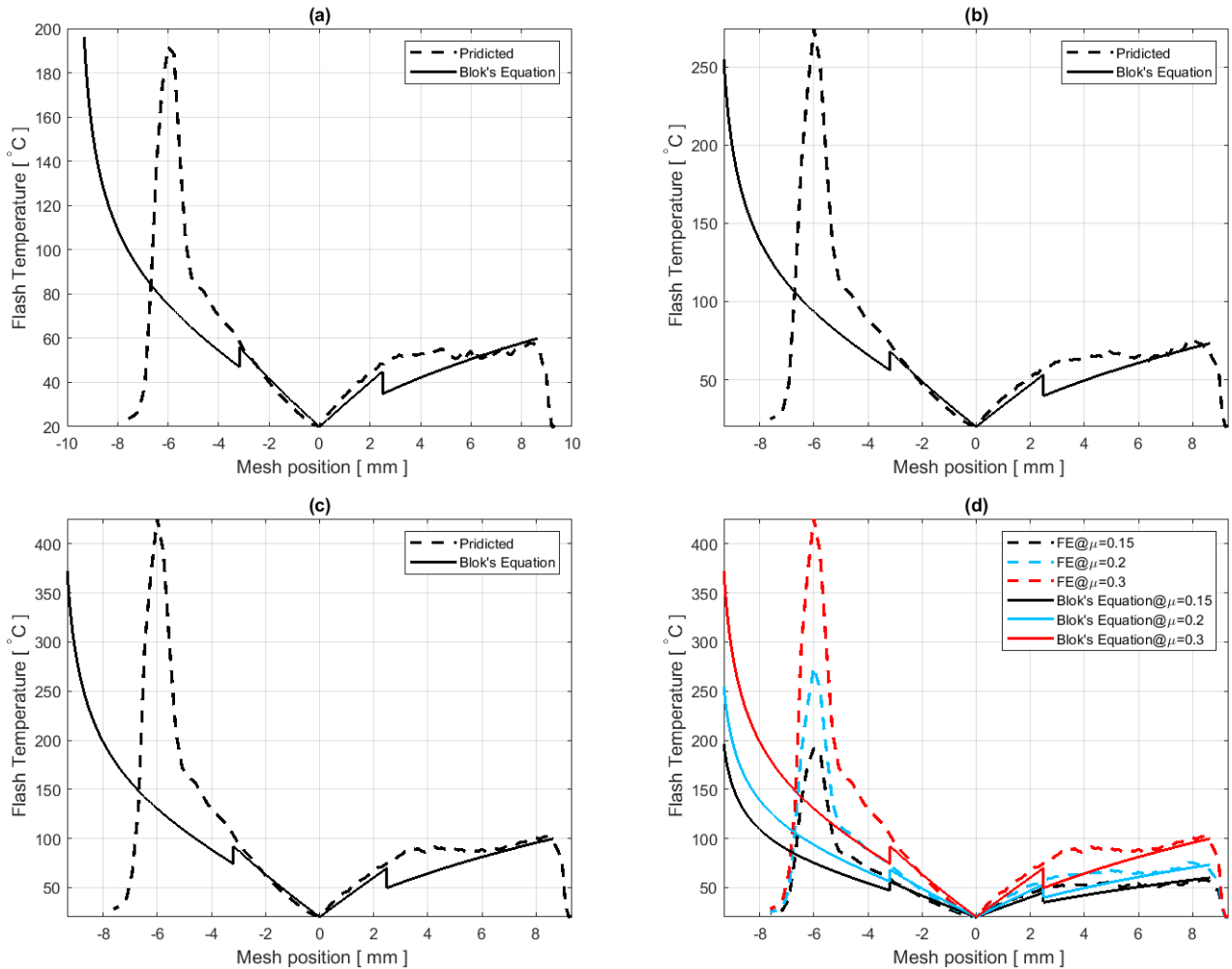


Figure 6.10: Comparison of FE and Block's equation spur gear with 0 mm backlash with: (a) $\mu = 0.15$, (b) $\mu = 0.2$ and (c) $\mu = 0.3$.

Figure 6.10 (a) - (c) show the comparison of numerical and Block's equation for 0.15, 0.2 and 0.3 coefficient of frictions of the gear with 0 mm backlash respectively.

For more clarity Figure 6.10 (d) show the FE and Block's equation analysis of flash temperature with 0.15, 0.2 and 0.3 coefficient of frictions. The numerical and Block's equations are in good agreement within a single tooth contact region, but it deviated out of single tooth contact region. The main reason for this deviation is, in Block's equation there is a single heat source, but in numerical results there is a situation in which more than a pair of tooth in contact.

6.6.4 Numerical analysis of flash temperature of spur gear at different backlash

In the previous section it's shown that the numerical results are in good agreement with Block's equation and experimental result with 0.15 coefficient of friction. Therefore, the numerical prediction will continue to predict the effect of backlash on flash temperature of spur gear.

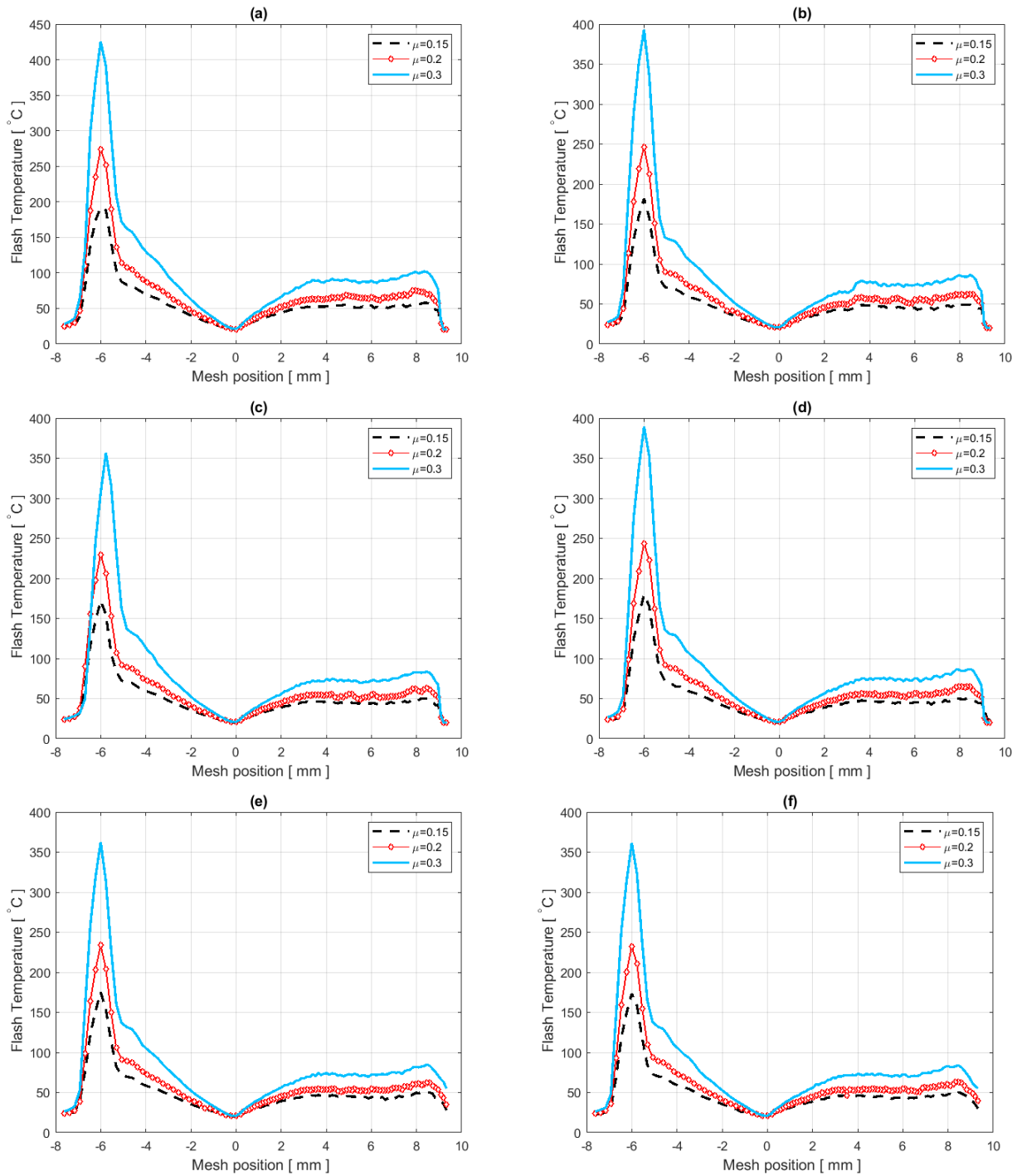


Figure 6.11: Flash temperature of gear with: (a) 0 mm, (b) 0.2 mm, (c) 0.4 mm, (d) 0.6 mm, (e) 0.8 mm and (f) 1 mm backlash.

Figure 6.11 shows that the maximum flash temperature is occurred when there is no backlash (a), 0.2 mm backlash (b) gears shows a minimum flash temperature of the gears relative to the other gears with backlash (c - f). The temperature of 0.8 mm and 1 mm backlash gears is greater than 0.6 mm and 0.4 mm backlash gear, this may be a result of impact loading.

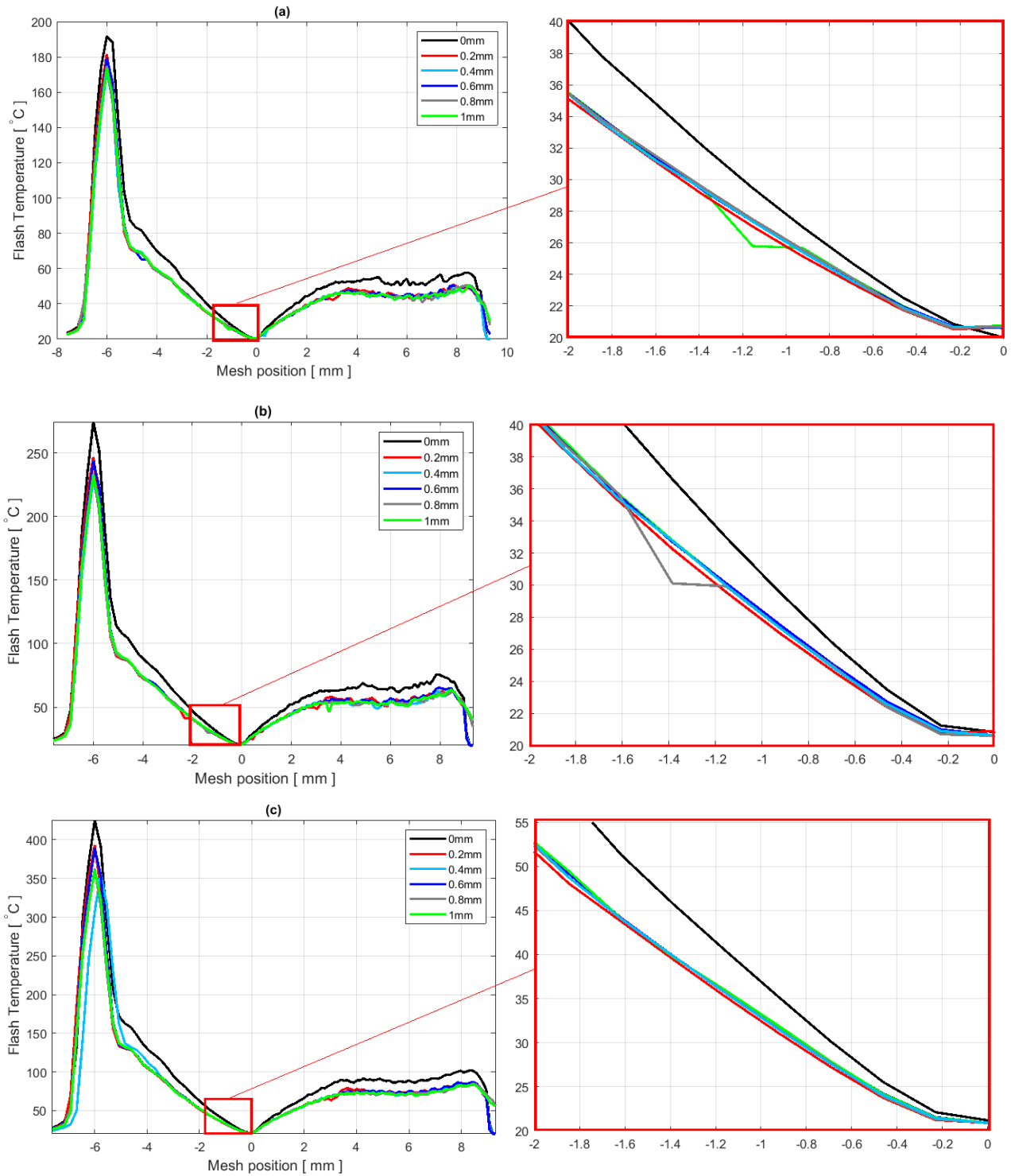


Figure 6.12: Flash temperature of gear at different backlash with:(a) $\mu = 0.15$, (b) $\mu = 0.2$ and (c) $\mu = 0.3$.

The flash temperature from pitch point to a mesh termination is not deviated much as compared to the mesh approach. For more clarity Figure 6.12 is shown flash temperature of all backlash at the different coefficients of friction, the figure shows that around the tip of the gear the flash temperature decreases as the backlash increase.

The flash temperature is increased dramatically as the friction coefficient of the gear material is increased. The maximum flash temperature for 0.15, 0.2 and 0.3 coefficient of frictions are around $194^{\circ}C$, $290^{\circ}C$ and $420^{\circ}C$. Perhaps the last flash temperature can alter the material property of the gear such as the ductility and others, this can facilitate the failurity of the gear at the early stage of the lifetime.

In addition to that, the operating temperature of the lubricant is fixed to a certain limit, as the temperature increase the functionality of the lubricant becomes decrease, this is because the viscosity of the lubricant is directly proportional to the temperature. As the viscosity decrease the lubricant splash easily without resisting the shear force, this lead a direct asperity to asperity contact between gear tooth surfaces.

The number of mesh and time for completion of the analysis is summarized in Appendix H, Table H.2. The time to complete for one analysis is set in table for a single backlash and friction of friction, therefore a 18 analysis is done for coupled temperature analysis.

This chapter provides the performance of the gear related with the flash temperature of the gear at different backlash. To determine the flash temperature of the gear there is no a single formula, to determine the formulas the pecelet number have been determined first. The pecelet number of the given gear model in this thesis shows greater than 5 around the single tooth contact region. Block's equation, FE and experimental approaches (that found by Tobe and his colleagues) have been used to compare the result of the gear for 0 mm backlash and the results are satisfactory. This shows that the numerical (FEA) is a good approach to predict the flash temperature.

The gear with 0 mm backlash exhibits maximum flash temperature of the gear, this is because there is no free play between gear tooth. The gear with 0 mm backlash shows a minimum flash temperature than the other gear with backlashes from 0.4 mm to 1 mm backlash. The other interesting phenomena is shown as the backlash increases the flash temperature of the gear, this may results from the striking between the tooth due to excess gap between tooth due to backlash.

Dynamics of Spur Gear with Backlash

7.1 Introduction

Fatigue life and noise of the gears attracted many investigators to study the dynamics of the gear. The dynamics of gear tooth forces are larger than the corresponding quasi-static forces, resulting in larger dynamic stresses, shorter bending and contact fatigue life. Time-varying mesh stiffness is the main source of dynamic forces, and these forces will be transmitted to the supportive bearings which will cause a gear noise.

The dynamic behavior of the gear tooth forces that are quite different from the quasi-static forces in both magnitude and shape. These tooth forces also reflect various nonlinear phenomena such as backlash-induced tooth separations and discontinuities. Therefore, surface wear (in this case the backlash is introduced as it's assumed as the surface of the gear is uniformly worn out) is strongly related to the contact stresses and dynamic behavior. In addition, like the dynamic response amplitudes, wear behavior should also vary with speed as well. On the other hand, the dynamic response of a gear pair is very sensitive to the deviations of the tooth surface profiles from a perfect involute.

Tooth modifications such as tip and root relieve are commonly used to reduce the dynamic forces of the gear tooth. Though, there are unavoidable errors that arise from manufacturing and assembly errors that influence the dynamic response since they act as a transmission error excitation at the gear mesh interface. Surface wear is a material removal process from the contacting surfaces that results in a deviation from the intended tooth profiles. Therefore, a gear pair with worn surfaces should have dynamic behavior that is quite different from a gear pair with no wear. This indicates that gear dynamics and gear wear are mutually dependent

on each other.

A large number of published theoretical and experimental spur gear dynamics studies focused on noise and durability because both criterion will show the dynamics of the gear pairs. Most of these studies proposed discrete models to predict the parameters that might be related to the gear noise levels.

In line with the experimental studies on spur gear dynamics, these nonlinear time-varying models used discrete gear mesh interface formulations that include periodic mesh stiffness and gear backlash-induced tooth separations. In addition, an external displacement excitation was included in some of these models to represent gear profile errors and intentional tooth modifications. Both the mesh stiffness function and the displacement excitation would be determined by using a static-elastic gear contact model.

Jian et al.[64] investigated that backlash affects the vibro-impact properties significantly, tooth separation and drive-side mesh are observed with the decrease of load coefficient, leading to drive- and back-side tooth impacts. The modeling of the dynamics is useful in case of conditional monitoring since it allows to simulate a vibration signal for different conditions of a gearbox which is difficult to conduct experiments. There are several methods to simulate the behavior of gear pairs such as mathematics modeling (MATLAB), finite element methods (ABAQUS, Ansys) and multi-body dynamic methods (MSC.Adams).

MSC.Adams is computing software used for modeling, analyzing and optimizing multi body mechanical systems. Basic procedures needed to accomplish the analysis of dynamic forces and acceleration in MSC.Adams are introduced below:

- Create physical bodies with a given dimensions.
- Apply physical characteristics such as rotational inertia, mass and coefficient friction.
- Fulfill kinematics definition such as translation and rotation.
- Simulation that relates to making motion, forces and observing model behavior.
- Record and analyses results in the MSC.Adams/ Post processing.

7.2 Modeling of spur gear with different backlash

In this section gear pairs are modeled using Adams view interface. Adams provides a machinery component that used to model different types of gear by specifying the common parameters such as module, number of teeth for both gear pairs, face width and gear tooth thickness.

The procedure is shown in Appendix-J from the beginning to the end. Once all dimensions which are summarized in Chapter 3 determined the next step is to define the gears by opening the create Gear Pair in Adams inside the machinery module. A wizard box will open where in which all parameters that need to be set is introduced. The first step is selecting the type of gears shown in Figure J.1, in this thesis spur gear is chosen. Figure J.2 show that the methods of modeling, this have options such as coupler, simplified, detailed, 3D contact and advanced 3D contact. In this case, detailed contact is chosen, this is because the detailed analysis will provide the contact forces and the accelerations of the gear components.

Next to that the dimensions and general parameters are set on the respective space as shown in Figure J.3. The gear parameters are the same as the previous and the profile of the gear can be modified. First without gear modification is done using the standard tooth thickness options and then modified the tooth thickness by subtracting the amount of the backlash as shown in the previous chapters. This will enable to model the gear with different backlash.

The material property of the gear will be specified after determining the geometric modeling of the gear as shown in Figure J.4. The kinematic connection of the gears will be determined, the rotational gear type is chosen in this case for both gears and modeling completion, these can be shown in Figure H.5.

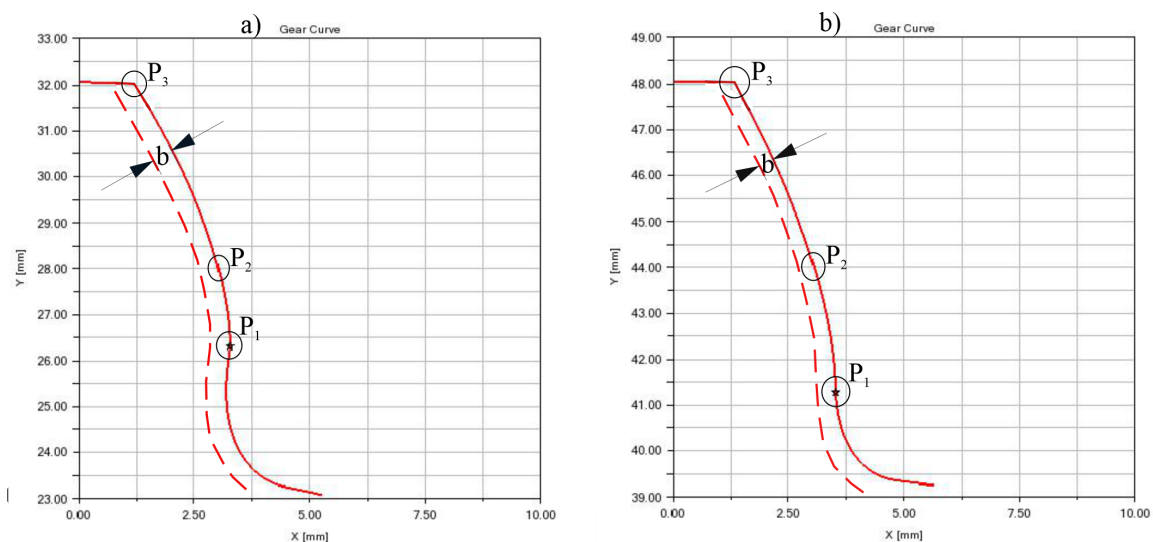


Figure 7.1: Tooth profile and contact points of (a) pinion and (b) gear.

The tooth profile of pinion and gear is shown in Figure 7.1 (a) and (b) respectively and the backlash is introduced by reducing the thickness of the gear mates. Points P_1 , P_2 , and P_3 are the point of mesh initiation, pitch point, and mesh termination respectively for both gears. The figure shows that the point at which where the mesh starts and ends for pinion and gear, according to the figure, the mesh of the gear starts at 26.4 mm from the center of rotation of pinion and 41.1 mm for gear. Six gears are modeled by modifying the gear tooth thickness and the standard tooth thickness is calculated using the following equation:

$$t = \frac{\pi m}{2} \quad (7.1)$$

As discussed in the first chapter the backlash is introduced in two ways, these are modifying tooth thickness and modifying the center distance of the gear. In this case, the backlash is introduced using the first method, the standard tooth thickness is calculates using Equation 7.1 as 6.28318 mm it is equal for pinion and gear tooth. The thickness is decreased to 5.78318 mm by 0.1 mm decrements each of gear tooth for both gear mates.

7.3 Boundary condition for dynamics analysis

Pinion and gear is fixed with the ground in all directions except the rotational degree of freedom about Z-axis. Both gear mates rotate at center of points C_1 and C_2 respectively as shown in Figure 7.2.

The gear is subjected to three load cases and the pinion is subjected to a single constant angular speed which is 2090 *RPM*. Load case 1 = 18729.92 *Nmm*, load case 2 = 37459.84 *Nmm* and load case 3 = 56189.76 *Nmm*. The contact setting (such as stiffness, friction coefficient and others) of the gear can be modified as shown in Appendix-J, Figure J.4. In this thesis the static and dynamic friction coefficients are set to 0.11 and 0.15 respectively, and the other contact parameters are set as it shown in figure.

By setting the above boundary conditions and contact settings the simulation is run for 0.2 seconds with 10^{-4} step size.

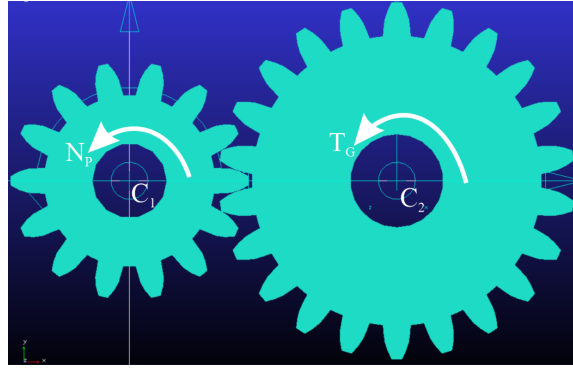


Figure 7.2: Boundary conditions and loading for dynamics.

7.4 Results and discussions for dynamics

The angular acceleration and contact forces of the gear with different backlash will clearly show the effect of backlash on the dynamics of the gear pairs. The analysis contains six models of gear with 0 mm backlash to 1 mm backlash by 0.2 mm increments. The contact forces along the radial and tangential directions will be determined and then the angular acceleration of the pinion and gear with different backlash will be examined.

7.4.1 Contact force

In designing a gear, it is important to analyze the magnitude and direction of the forces acting upon the gear teeth. In analyzing these forces, an idealized assumption is made that the tooth forces are acting upon the central part of the tooth flank. The normal contact load can be resolved into radial and tangential load, and each of these forces has its own function. The tangential load will produce the torque of the gears and the radial load is used to balance the reaction loads of the supports.

In Chapter 2 the tangential and radial loads have been determined, and that load is a static load. In the dynamics system the contact force varies due to tooth separation and discontinuities. In this section, the dynamic loads will be discussed for three loadings as discussed in Section 7.3.

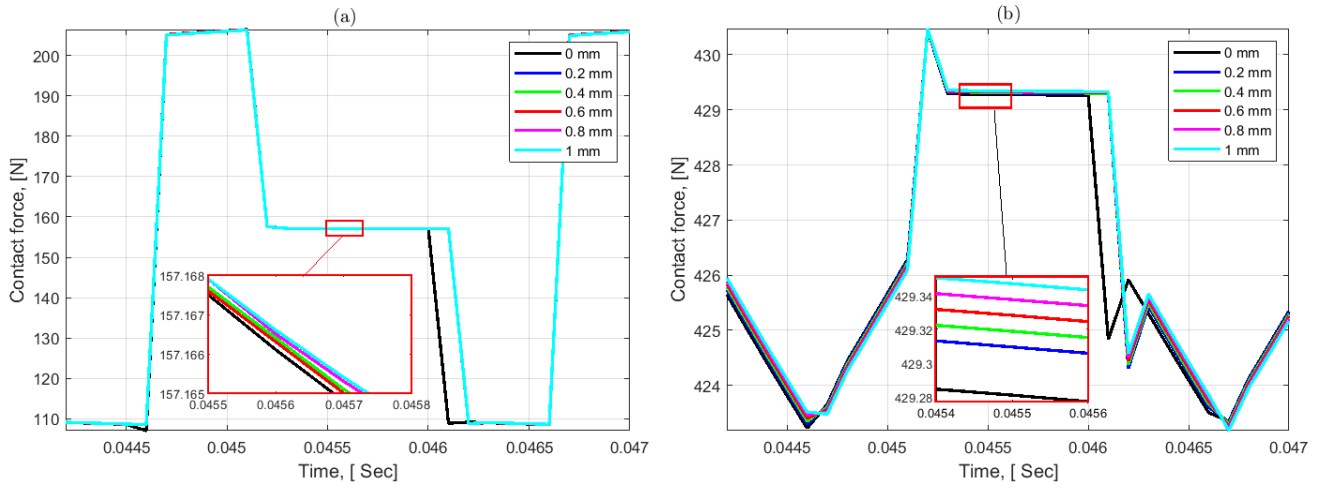


Figure 7.3: (a) Radial and (b) Tangential loads for load case 1.

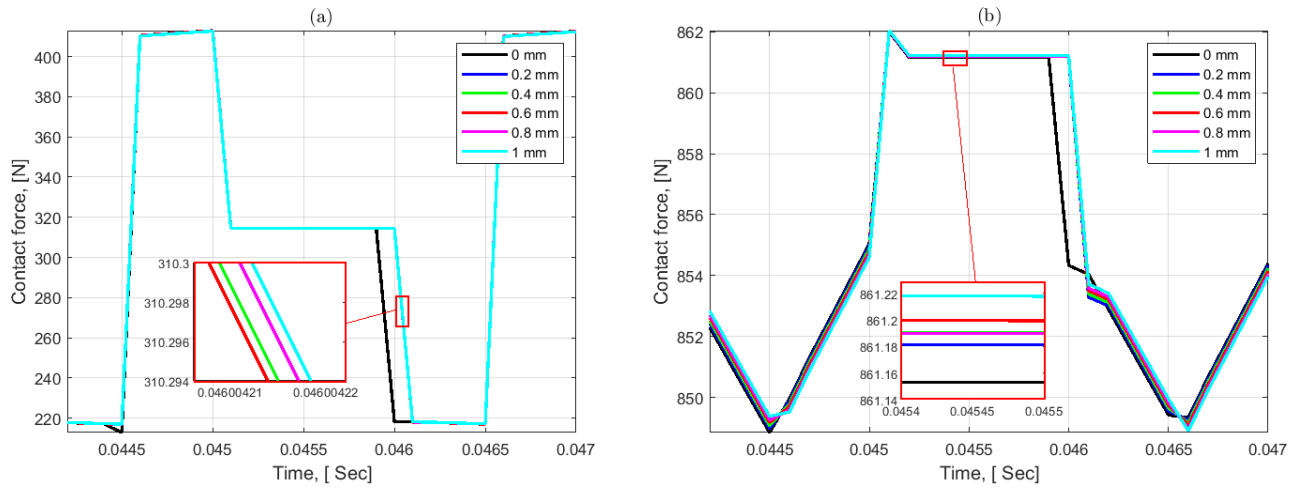


Figure 7.4: (a) Radial and (b) Tangential loads for load case 2.

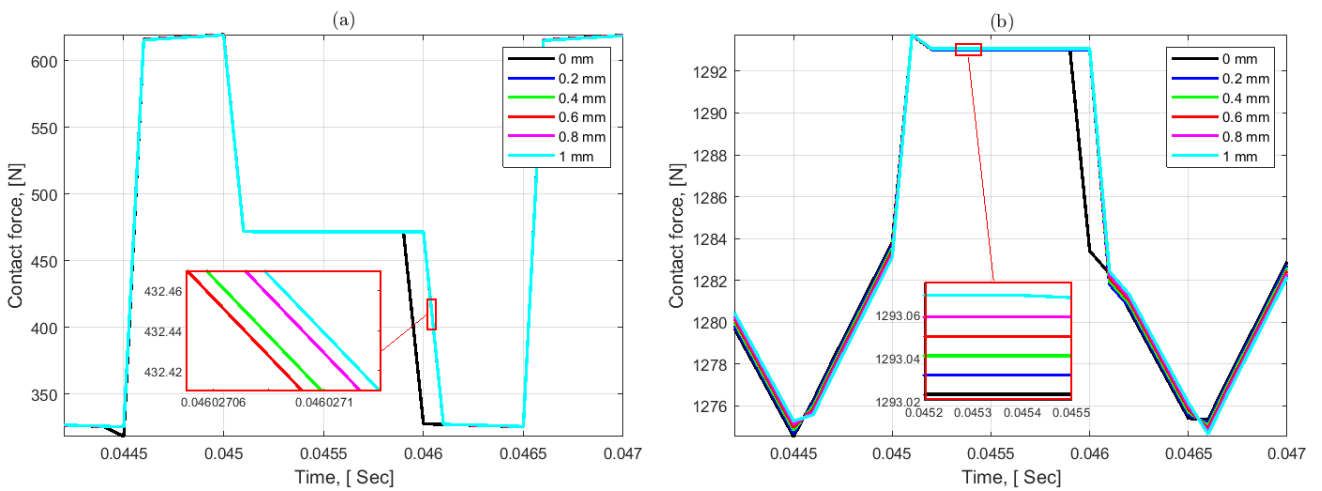


Figure 7.5: (a) Radial and (b) Tangential loads for load case 3.

Figures 7.3 - 7.5 shows the steady-state response history of the gear for contact loads form

mesh initiation to mesh termination. The designed tangential load was 425.68 N, but Figure 7.3 (b) shows that the tangential load for load case 1, and the load varies from 423 to 430.5 N due to the effect of the dynamics of backlash and discontinuities. The maximum tangential load is found in a single tooth contact region which is equal to 430.5 and it decreased to 423 N in a double tooth contact region. In addition, the tangential load shows discontinuity between the highest point of single tooth contacts the mesh termination unlike a smooth increment along approaching mesh. The backlash affects the tangential load specifically around the recess region.

The dynamic radial force is shown in Figure 7.3 (a) and it varies from 105 N to 205 N. The fluctuation of the radial load is greater than the fluctuation of tangential load, but the effect of backlash on the radial load is not significant like a tangential load.

Load case 2 and 3 shows the same thing as shown in Figure 7.4 and 7.5. For load case 2, the maximum and minimum tangential load are 862 and 848.5 N respectively, while the radial load varies between 220 and 415 N as shown in Figure 7.4 (a) and (b) respectively. Figure 7.5 (a) and (b) shows the radial and tangential load for load case 3. The tangential load is varied between 1274 and 1294 N. In addition to that, the tangential load is similar to the load share obtained using the approximate approach that has been discussed in Section 5.1.2.

In general, as the backlash increases the contact loads along radial and tangential direction will increase. In addition, the fluctuation load between the HPSTC and mesh termination becomes smooth as the load increase. The more load subjected the gear, the tangential load of spur gear with different backlash will show the same curve history with the gear without backlash. As the load of the gear increase the lower and upper limit of the contact load variation is increase, the variation of the tangential load is 7.5, 13.5 and 20 N for load case 1, 2 and 3 respectively.

7.4.2 Driving gear wheel (Pinion)

In the previous section, it's shown that the tangential and radial loads varied with time due to tooth separation and discontinuities, and these loads will produce an acceleration in the tangential and radial directions respectively. In this section, these accelerations will be discussed in detail as follows.

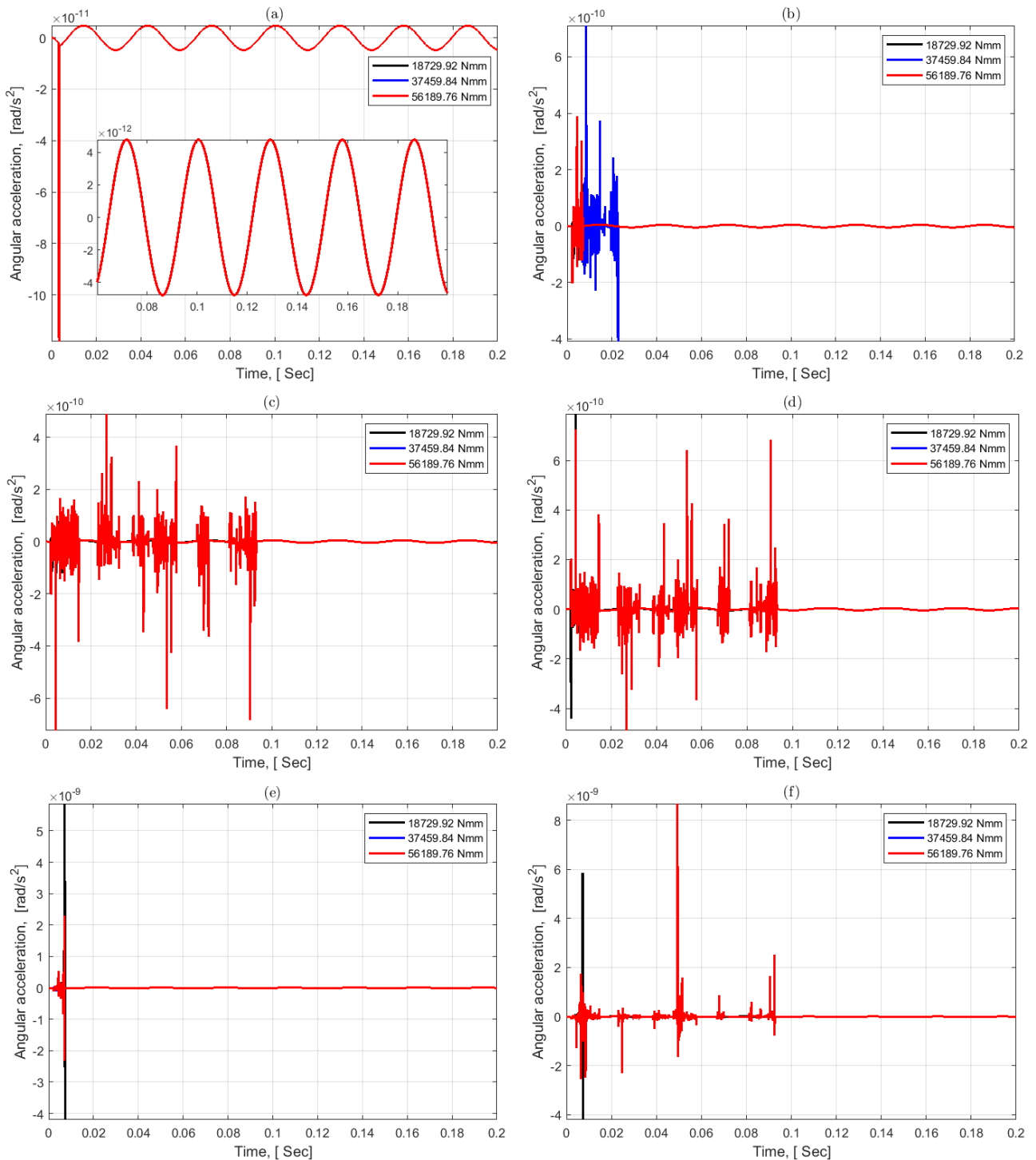


Figure 7.6: Tangential angular acceleration of pinion with: (a) 0 mm, (b) 0.2 mm, (c) 0.4 mm, (d) 0.6 mm, (e) 0.8 mm and (f) 1 mm backlash.

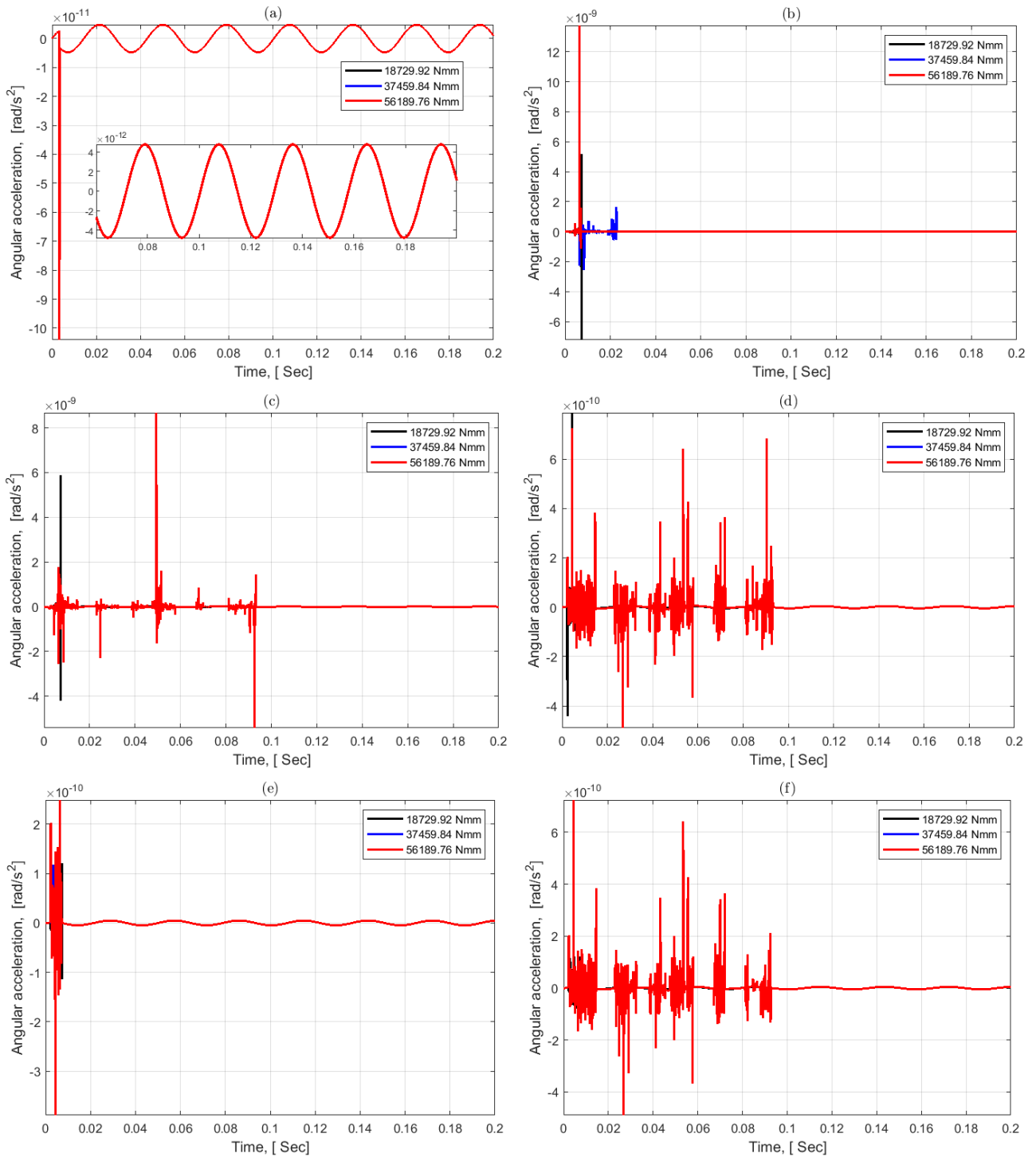


Figure 7.7: Radial angular acceleration of pinion with: (a) 0 mm, (b) 0.2 mm, (c) 0.4 mm, (d) 0.6 mm, (e) 0.8 mm and (f) 1 mm backlash.

The pinion is subjected to a constant speed and it meshes with the gear which is subjected to a load. Even-though the pinion is subjected to a constant speed, there are accelerations due to the dynamic effect of gear.

Figure 7.6 (a) shows that the gear with 0 mm backlash has a minimum angular tangential acceleration and smooth operation except at for the first few mesh cycles. In addition, it shows

that the radial acceleration of the driver gear or pinion is not affected by the load of the gear, which means it shows the same curve history for all loading cases.

The other Figures 7.6 (b) - (f) show that as the backlash increases the tangential angular acceleration will also increase. In addition, the tangential angular acceleration increases with the load. The other observations from the figures, it shows that as the backlash increases it takes a longer time to vibrate in steady-state conditions. But unexpected result have been obtained on gear with 0.8 mm backlash a shown in Figure 7.6 (e) regarding the settling time.

Figure 7.7 (a) - (f) shows that the radial angular accelerations of the gear with different amount of backlash and it is the result of a dynamic radial load. The gear without backlash has minimum radial angular acceleration. Like the tangential angular acceleration, the radial angular acceleration is increased as the backlash increase except for 0.2 and 0.4 mm backlash gears as shown Figure 7.7 (b) and (c). The radial acceleration is maximum in 0.2 mm backlash gear for the first few mesh cycles, but it shows a smooth responses after that. Therefore, the pinion with 0.2 mm backlash shows a minimum tangential and radial angular acceleration.

Interesting thing is found for the gear without backlash, the gear radial acceleration of the pinion is not affected by the load of the gear as shown in Figure 7.7 (a), this phenomena is shown for tangential angular acceleration of the pinion in Figure 7.6 (a). The gear with a backlash takes longer time relative to the gear without backlash to settle and give a steady state response.

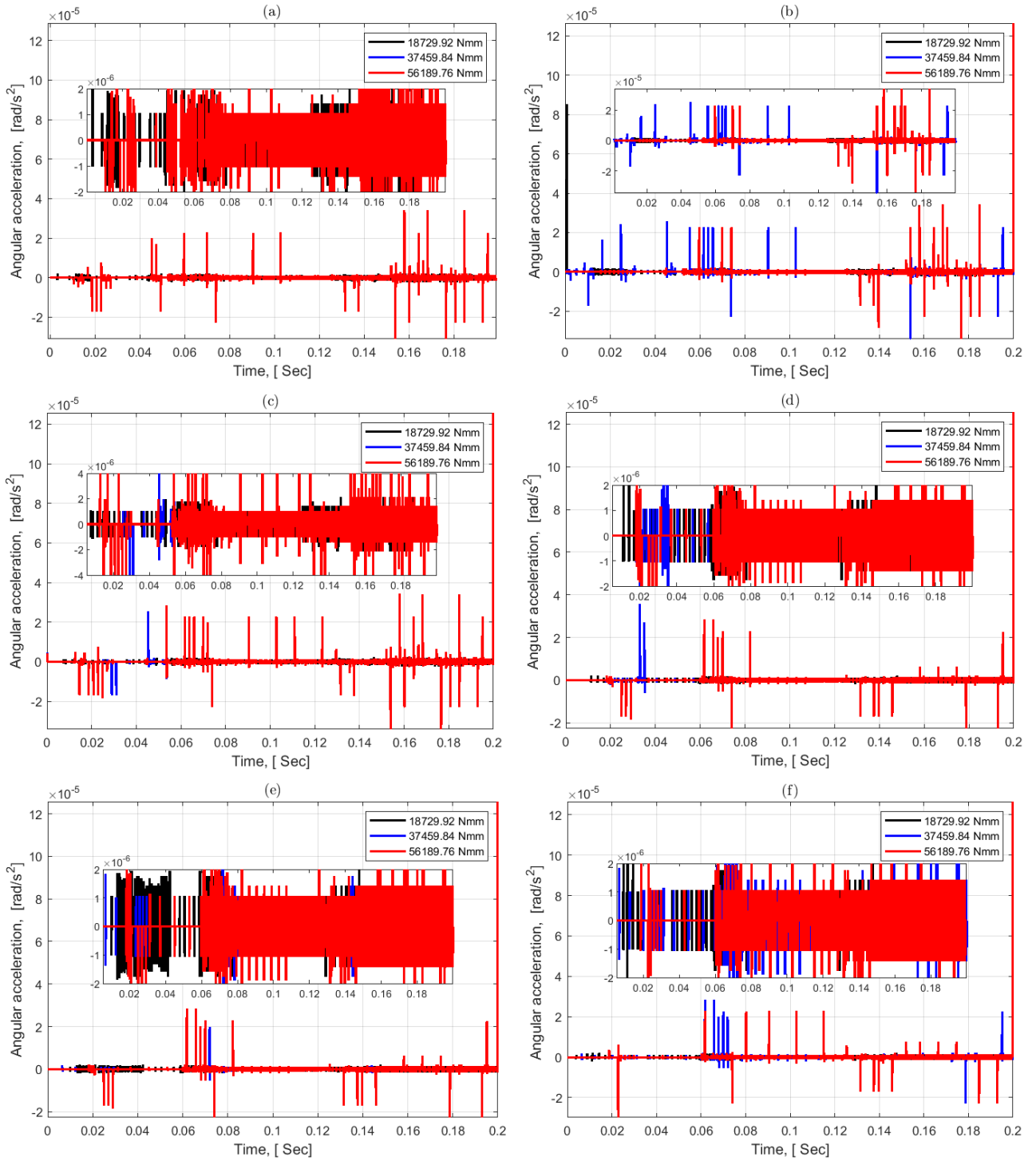


Figure 7.8: Angular acceleration of pinion along Z-axis with: (a) 0 mm, (b) 0.2 mm, (c) 0.4 mm, (d) 0.6 mm, (e) 0.8 mm and (f) 1 mm backlash.

Angular acceleration along the rotational axis is produced mainly due to the geometrical effect, such as backlash and it is shown in Figure 7.8. (a) shows that the angular acceleration of of the gear with 0 mm backlash.

The pinion is subjected to the constant angular velocity, but there is an acceleration due to the gear. Figure 7.8 (a) - (f) shows the angular acceleration of the pinion. Figure 7.8 (a) shows

that the angular acceleration for 0 mm backlash is $2 \times 10^{-6} \text{ rad/s}^2$. The pinion will accelerate and decelerate frequently due to the jamming effect, which means there is no free play.

Figure 7.8 (b) shows the angular acceleration of 0.2 mm backlash and its acceleration has less frequency than the other backlash gear responses as shown in Figure 7.8 (c) - (f) and (a). This may result due to the existence of free play, unlike the gear without backlash and less gap that may cause an impact load as compared to the gear with a backlash between 0.4 - 1 mm backlash gears.

In general, the angular acceleration of the pinion along the axis of rotation is increased for 0 mm backlash and as the backlash increased. In addition to this, the radial angular acceleration is less than the tangential acceleration of the pinion.

7.4.3 Driven gear wheel (Gear)

In the previous section the angular acceleration of the pinion has been discussed, and in this section the acceleration of the gear will be examined for different load.

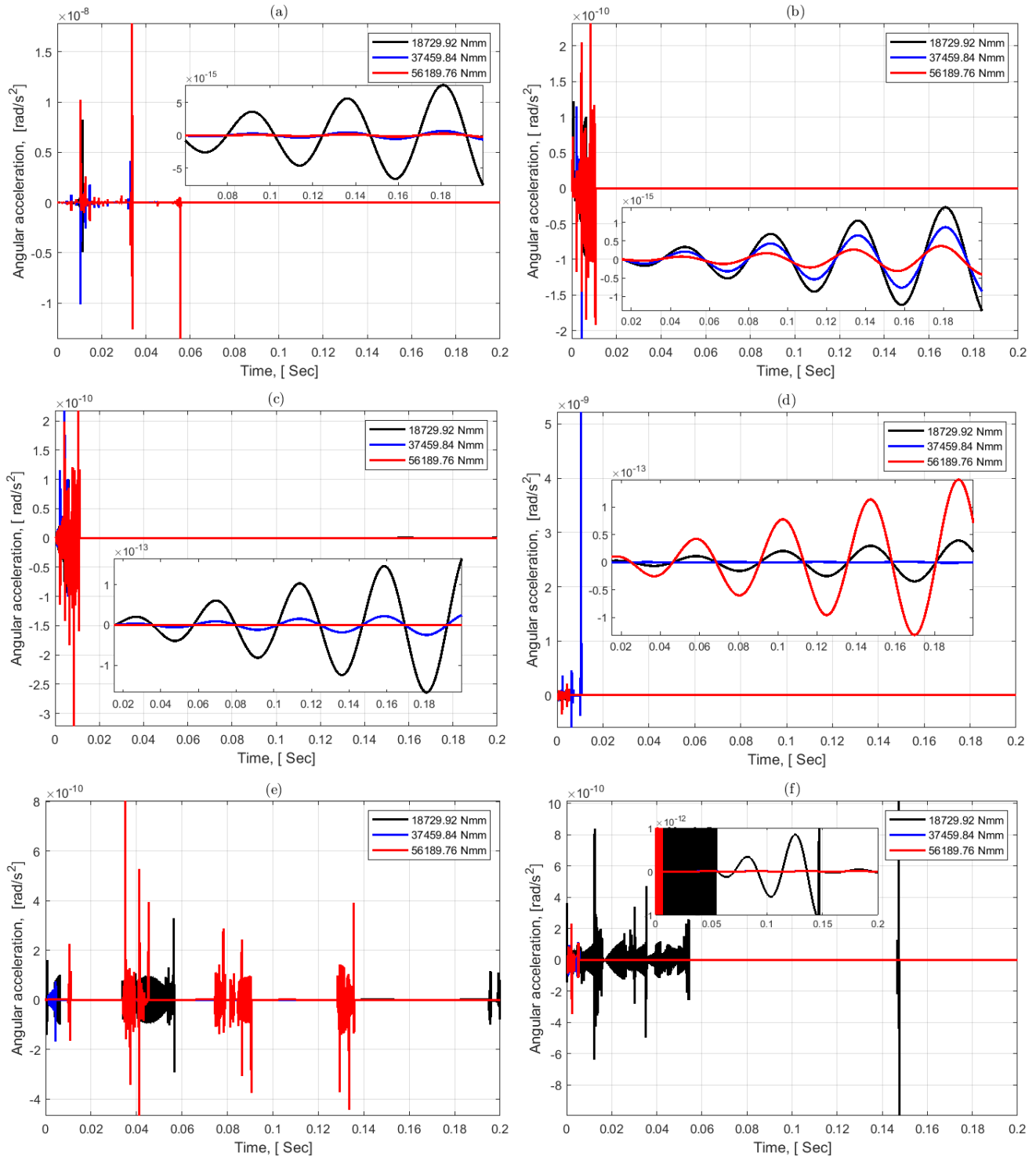


Figure 7.9: Tangential angular acceleration of gear with: (a) 0 mm, (b) 0.2 mm, (c) 0.4 mm, (d) 0.6 mm, (e) 0.8 mm and (f) 1 mm backlash.

Figure 7.9 shows the tangential load of spur gear with different backlash and under 3 load cases. Figure 7.9 (a) show the gear with 0 mm backlash, maximum tangential angular acceleration ($1.8 \times 10^{-8} \text{ rad/s}^2$) is found at load case 3. As the load increase the time to take for a steady state response will also longer. The figure shows that 10, 35 and 58 milliseconds has taken to settle the gear for load case 1, 2 and load case 3 respectively.

The tangential angular acceleration is maximum for the first few mesh cycles when the gear drives without backlash, but the steady state response of the gear with 0 mm backlash is minimum as compared to the gears with a backlash except for the gear with 0.2 mm backlash. The gear with a maximum load has minimum tangential acceleration.

Figure 7.9 (b) show the gear with 0.2 mm backlash, it shows at the instant of the meshing there is an acceleration, but its for a very short time compared to the gear without backlash, this is because a free play. The steady state response of 0.2 mm backlash gear is less than 0 mm backlash gear. The minimum load has maximum tangential angular acceleration like the gear with 0 mm backlash.

Figure 7.9 (c) show the response of gear with 0.4 mm backlash, and it shows that the tangential angular acceleration is greater than the gear with 0.2 mm backlash. Figure 7.9 (d), (e) and (f) show the same thing, and as the backlash increases the tangential angular acceleration response is also increase, however the maximum tangential acceleration is found on the gear without backlash for the first few mesh cycles and increases as the backlash increases. The optimum (minimum) tangential angular acceleration is found on the gear with 0.2 mm backlash from the given backlash of gears.

The other fascinating thing that shows in the figure is that with in the steady state response the tangential angular acceleration is maximum for a minimum load, this shown in all figures except Figure 7.9 (d) and (e) specially in 0.6 mm backlash. Perhaps the reason is the resisting torque is easily affected by the driver acceleration. The more the load subjected to the gear, less acceleration response is found. Therefore, if there is a backlash in gear mates it's better to subject the gear for more load to get less vibration.

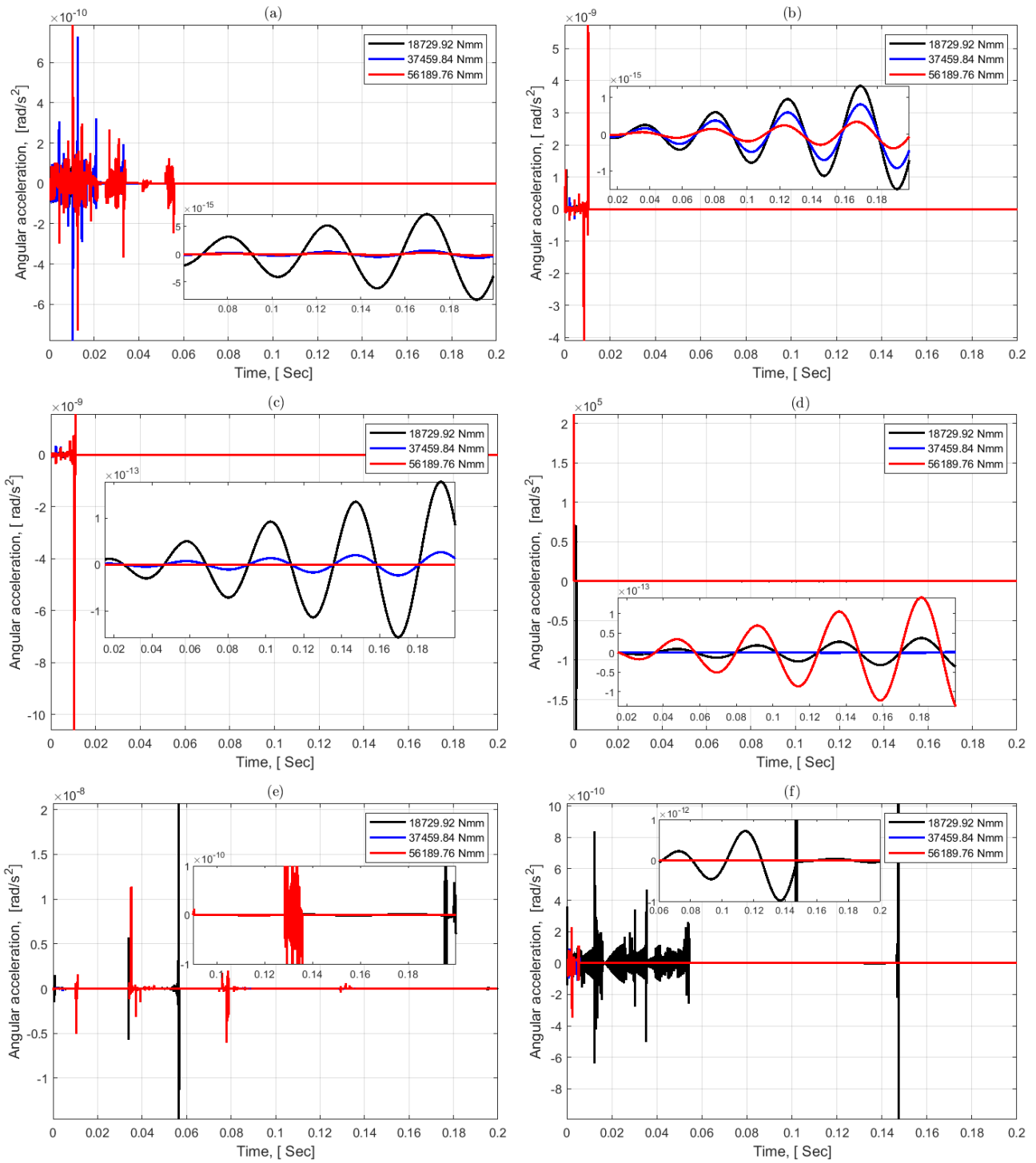


Figure 7.10: Radial acceleration of gear along Y-axis with: (a) 0 mm, (b) 0.2 mm, (c) 0.4 mm, (d) 0.6 mm, (e) 0.8 mm and (f) 1 mm backlash.

Figure 7.10 (a) show the radial angular acceleration with a minimum design load (load case 1) exceeds the gear with a larger designed load (load case 2 and 3) and the gear with 0 mm backlash has maximum tangential acceleration than the others. Like the tangential angular acceleration, the radial angular acceleration shows the same phenomena, the optimum (minimum) radial angular acceleration is found on the gear with 0.2 mm backlash. Figure 7.10 (d)

shows the response of the gear with 0.6 mm backlash, load case 2 exhibits minimum radial angular acceleration than load case 2 and 3, this is unexpected result like as shown previously on the tangential angular acceleration of the gear with 0.6 mm backlash. The gear with 1 mm backlash accelerate frequently up to 55 milliseconds with a load case 1, but for load case 2 and 3 the radial acceleration settle in a very few seconds relatively as shown in Figure 7.10 (f).

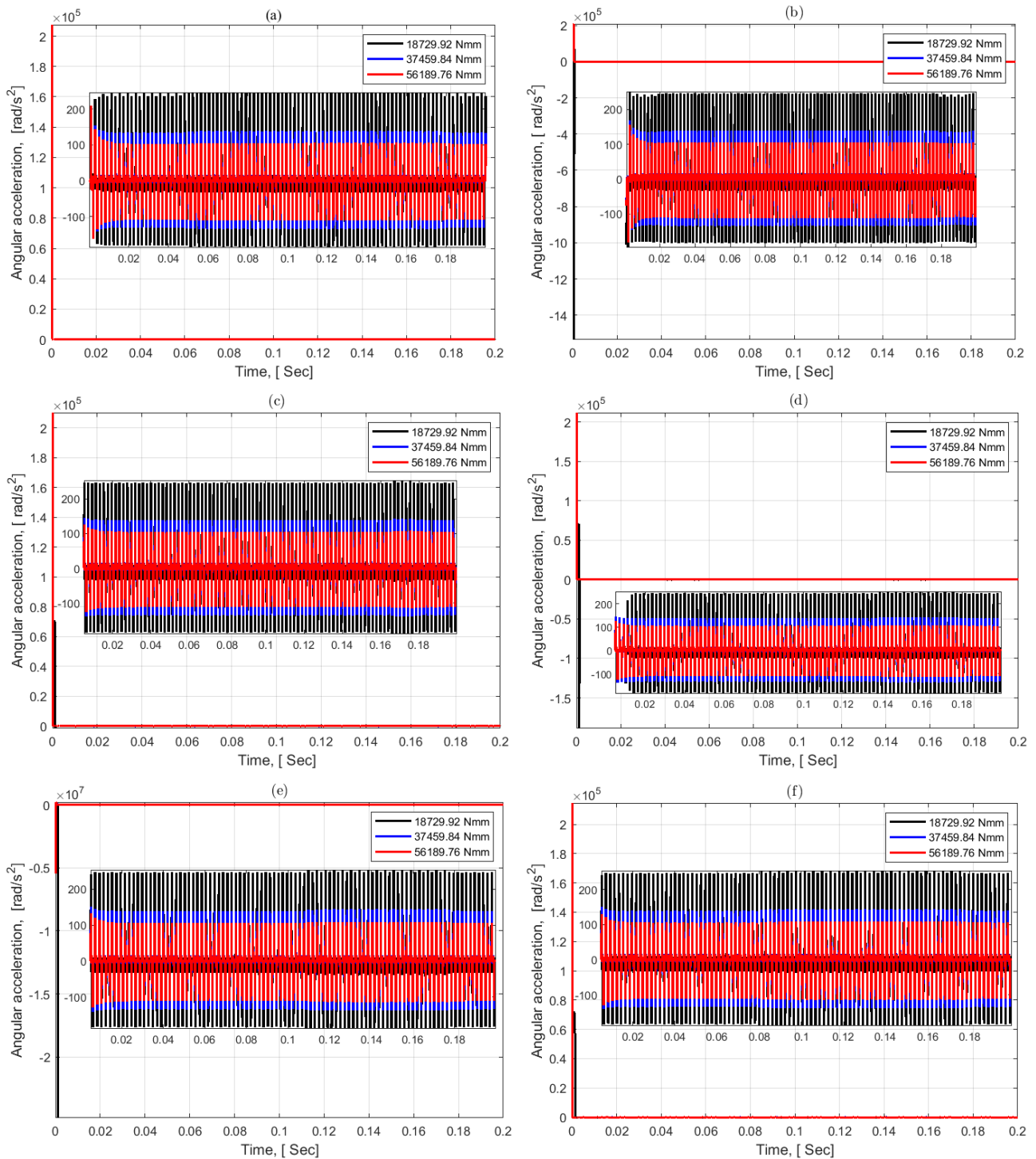


Figure 7.11: Angular angular acceleration of gear with: (a) 0 mm, (b) 0.2 mm, (c) 0.4 mm, (d) 0.6 mm, (e) 0.8 mm and (f) 1 mm backlash.

The acceleration of the gear is the measure of vibration of the gear. Figure 7.11 shows the angular acceleration for 3 different load cases along the axis of rotations. The angular acceleration of the gear decrease when the load increases. Figure 7.11 (a) - (f) shows that the angular acceleration for the first load case has oscillated within -250 and 250 rad/s , and the second load case is between -150 and 150 rad/s , and for the last load, the case is between -100 and 100 rad/s . The angular acceleration of the gear takes very few seconds to run with in a steady state fashion. The gear accelerates around $2.1 \times 10^5 rad/s^2$ for load case 3.

In this chapter the effect of backlash on the dynamics (contact force, angular acceleration) of the gear have been discussed. The vibration of the gear is affected by the non-linear parameters of the gear, such as geometrical (backlash), material non linearity. The tangential and radial angular acceleration of the gear is increases the the backlash increases, and the optimum (minimum) acceleration is found on the gear with 0.2 mm backlash. In addition, the angular acceleration (tangential and radial) of the gear is decreases as the load increases except the gear with 0.6 and 0.8 mm backlash.

Conclusions and Recommendations

8.1 Conclusion

In this thesis, the performances of spur gear related with the backlash have been studied. Backlash is important for the smooth operation of gears. In addition, gear life is limited due to loading and operational conditions. When the gear pairs transmit a load the heat is generated due to friction, and this heat alters the material property of the gear mates, the pitting and scuffing will occur during this time and the gear tooth faces is worn out. This worn-out part of the gear tooth can be modeled as a backlash to study the transmission error, flash temperature and dynamics of the gear.

The flash temperature of the contacting bodies can be determined using Block's equations and finite element method, in this thesis both methods have been implemented for 0 mm backlash gears. The result of the two methods is in good agreement between LPSTC and HPSTC region. Block's equation is using a single heat source, but in the FE analysis the source of heat generation could be more than one when the gear is out of the single tooth contact region, Therefore the value of the above methods will deviate in the double tooth contact region.

In general the following conclusions are drawn:

- Backlash affects both dynamic and static transmission error, as the backlash increases the transmission error increases drastically.
- The mesh stiffness of the gear is decreased as the backlash is increased.
- Block's and FEA results are in good agreement with the experimental results obtained by Tobe and his colleges. But the maximum flash temperature of the experimental result

is less than the FEA and Block's results, this is because the lubricant will splash over the surface of the gear.

- Flash temperature of the gear is affected by the gap between the gear tooth, the flash temperature of the gear without any backlash is maximum, this is the result of the no free play between the tooth and the minimum flash temperature is found the gear with 0.2 mm backlash. Though, as backlash increases from 0.2 mm to 1 mm the flash temperature increases, this may be because of as backlash increases the gear tooth starts strike each other which will produce an impact load and due to this the flash temperature of the gear increases. Based on this the gear should have a backlash between 0 and 0.2, but for this study, 0.2 mm backlash gives an optimum flash temperature than the rest of the backlash.
- The contact force of the gear along the tangential and radial direction has been analyzed and the contact force increased slightly as the backlash increased.
- The acceleration of the mating gear pairs is affected by the backlash, for 0 mm backlash the acceleration of the gear is greater than the gears with a backlash, and when the gear backlash varies from 0.2 mm to 1 mm backlash the angular acceleration of the gear is increased. In addition, the angular acceleration of the gear decreases as the load increases that impose the on the gear.
- The friction coefficient of the gear pair material strongly affects the transmission error and flash temperature of the gear.
- The FE analysis is a good approach to predict the flash temperature of the gear specifically in a single tooth contact region.

Based on the above conclusions the following recommendations have been made:

The gear should be designed with an optimum backlashes and tooth profile should be manufactured based on the design. Assembly error should be minimized or removed because the assembly error may cause a unwanted backlash due to deviation of center distance where it supposed to be. In addition, when the gear tooth faces are worn out it should be removed immediately because the transmission error is increased drastically, this will cause severe vibration and failure of the components that mounted on it or the mechanical elements found nearby.

8.2 Recommendations for future study

Having the above studies there is a certain direction which the future will possibly need to study.

- Fatigue life analysis of the spur gear at the different backlash.
- Developing an equation that relates backlash and flash temperature and finds an optimum backlash value to enhance the overall performance of the gear.
- Estimating the bulk temperature of the gear after a certain rotation cycle.
- Validating the effect of backlash on the flash temperature and angular acceleration using experimental work.

Bibliography

- [1] Alban, L.E., *Systematic analysis of gear failures*. ASM International, 1985.
- [2] Nordin, M., Bodin, P. and Gutman, P., “Adaptive control of nonsmooth dynamic systems,” *New Models and Identification Methods for Backlash and Gear Play*. Springer, Berlin, pp. 1–30, 2001.
- [3] Papageorgiou, D., Blanke, M., Niemann, H.H. and Richter, J.H., “Backlash estimation for industrial drive-train systems,” *IFAC-PapersOnLine*, vol. 50, no. 1, pp. 3281–3286, 2017.
- [4] Wojityla, M., Jakubiec, W. and Plowucha, W., “Comparison ISO standards 1328-1: 1995.”
- [5] Prajapat, G.P., Senroy, N. and Kar, I.N., “Modeling and impact of gear train backlash on performance of DFIG wind turbine system,” *Electric Power Systems Research*, vol. 163, pp. 356–364, 2018.
- [6] Nouby M.G., Ali, A.K. and Mousa, M.O., “Influence Of Misalignment and Backlash on Spur Gear Using FEM,” vol. 2, no. 12, 2014.
- [7] Gear failures. [Online]. Available: www.machinedesign.com/news/recognizing-gear-failures
- [8] Stachowiak, G. and Batchelor, A.W., *Engineering tribology*. Butterworth-Heinemann, 2013.
- [9] Kkaarthic. Failure modes in gears, causes of failure of gears, gears failure. [Online]. Available: www.brighthubengineering.com
- [10] Liang, X., Zuo, M.J. and Feng, Z., “Dynamic modeling of gearbox faults: A review,” *Mechanical Systems and Signal Processing*, vol. 98, pp. 852–876, 2018.

- [11] Taburdagitan, M. and Akkok, M., “Determination of surface temperature rise with thermo-elastic analysis of spur gears,” *Wear*, vol. 261, no. 5-6, pp. 656–665, 2006.
- [12] Wink, C.H. and Mantri, N.S., “AGMA Technical Paper,” 2012.
- [13] Nordin, M. and Gutman, P.O., “Controlling mechanical systems with backlash a survey,” *Automatica*, vol. 38, no. 10, pp. 1633–1649, 2002.
- [14] Lichtsinder, A. and Gutman, P.O., “Backlash and Friction Reciprocal Effect on Limit Cycle Existence,” *IFAC Proceedings Volumes*, vol. 42, no. 6, pp. 249–254, 2009.
- [15] Li, W., Liu, B., “Experimental investigation on the effect of shot peening on contact fatigue strength for carburized and quenched gears,” *International Journal of Fatigue*, vol. 106, pp. 103–113, 2018.
- [16] Liu, X., Yang, Y. and Zhang, J., “Investigation on coupling effects between surface wear and dynamics in a spur gear system,” *Tribology International*, vol. 101, pp. 383–394, 2016.
- [17] Lagerberg, A. and Egardt, B., “Estimation of backlash in automotive powertrains an experimental validation,” *IFAC Proceedings Volumes*, vol. 37, no. 22, pp. 47–52, 2004.
- [18] Merzouki, R. and Cadiou, J.C., “Estimation of backlash phenomenon in the electromechanical actuator,” *Control Engineering Practice*, vol. 13, no. 8, pp. 973–983, 2005.
- [19] Ravanbod-Shirazi, L. and Besançon-Voda, A., “Backlash identification: a two step approach,” *IFAC Proceedings Volumes*, vol. 35, no. 1, pp. 85–90, 2002.
- [20] Dyaneshwar, S., and Prof Mangrulkar, K.S., “Effect of backlash on bending stresses in spur gears ,” vol. 1, no. 7, 2016.
- [21] Moradi, H. and Salarieh, H., “Analysis of nonlinear oscillations in spur gear pairs with approximated modelling of backlash nonlinearity,” *Mechanism and Machine Theory*, vol. 51, pp. 14–31, 2012.
- [22] Chen, Q., Ma, Y., Huang, S. and Zhai, H., “Research on gears dynamic performance influenced by gear backlash based on fractal theory,” *Applied Surface Science*, vol. 313, pp. 325–332, 2014.
- [23] Lotfi, B., Zhong, Z.W. and Khoo, L.P., “A novel algorithm to generate backlash-free motions,” *Mechanism and Machine Theory*, vol. 45, no. 8, pp. 1171–1184, 2010.

- [24] Walha, L., Fakhfakh, T. and Haddar, M., “Nonlinear dynamics of a two-stage gear system with mesh stiffness fluctuation, bearing flexibility and backlash,” *Mechanism and Machine Theory*, vol. 44, no. 5, pp. 1058–1069, 2009.
- [25] J. Voros, “Identification of cascade systems with backlash,” *International Journal of Control*, vol. 83, no. 6, pp. 1117–1124, 2010.
- [26] Zhao, M. and Ji, J.C., “Nonlinear torsional vibrations of a wind turbine gearbox,” *Applied Mathematical Modelling*, vol. 39, no. 16, pp. 4928–4950, 2015.
- [27] Kacalak, W., Majewski, M. and Budniak, Z., “Innovative design of non-backlash worm gear drives,” *Archives of Civil and Mechanical Engineering*, vol. 18, no. 3, pp. 983–999, 2018.
- [28] Baumann, A. and Bertsche, B., “Experimental study on transmission rattle noise behaviour with particular regard to lubricating oil,” *Journal of Sound and Vibration*, vol. 341, pp. 195–205, 2015.
- [29] Fernandez-Del-Rincon, A., Diez-Ibarbia, A. and Theodossiades, S., “Gear transmission rattle: assessment of meshing forces under hydrodynamic lubrication,” *Applied Acoustics*, vol. 144, pp. 85–95, 2019.
- [30] Russo, R., Brancati, R. and Rocca, E., “Experimental investigations about the influence of oil lubricant between teeth on the gear rattle phenomenon,” *Journal of Sound and Vibration*, vol. 321, no. 3-5, pp. 647–661, 2009.
- [31] Kennedy Jr, F.E. and Karpe, S.A., “Thermocracking of a mechanical face seal,” *Wear*, vol. 79, no. 1, pp. 21–36, 1982.
- [32] Townsend, D.P., “Dudley’s Gear handbook: The Design, Manufacture, and Application of Gears,” *McGraw-Hill, Inc., Dudley’s Gear Handbook*, 1991.
- [33] Srirattayawong, S. and Gao, S., “Surface roughness effects on fluid flow between two rotating cylinders,” in *Key Engineering Materials*, vol. 642. Trans Tech Publ, 2015, pp. 275–280.
- [34] Li, S. and Anisetti, A., “On the flash temperature of gear contacts under the tribo-dynamic condition,” *Tribology International*, vol. 97, pp. 6–13, 2016.

- [35] Wang, Y., Tang, W., Chen, Y., Wang, T., Li, G. and Ball, A.D., “Investigation into the meshing friction heat generation and transient thermal characteristics of spiral bevel gears,” *Applied Thermal Engineering*, vol. 119, pp. 245–253, 2017.
- [36] Abel, P.B. and Ferrante, J., *Modern Tribology Handbook*, 2001.
- [37] Terauchi, Y. and Nadano, H., “Effect of tooth profile modification on the scoring resistance of spur gears,” *Wear*, vol. 80, no. 1, pp. 27–41, 1982.
- [38] Dhanasekaran, S. and Gnanamoorthy, R., “Gear tooth wear in sintered spur gears under dry running conditions,” *Wear*, vol. 265, no. 1-2, pp. 81–87, 2008.
- [39] Walton, D. and Goodwin, A.J., “The wear of unlubricated metallic spur gears,” *Wear*, vol. 222, no. 2, pp. 103–113, 1998.
- [40] Gou, X., Zhu, L. and Qi, C., “Nonlinear dynamic model of a gear-rotor-bearing system considering the flash temperature,” *Journal of Sound and Vibration*, vol. 410, pp. 187–208, 2017.
- [41] Dong, H.L., Hu, J.B. and Li, X.Y., “Temperature analysis of involute gear based on mixed elastohydrodynamic lubrication theory considering tribo-dynamic behaviors,” *Journal of Tribology*, vol. 136, no. 2, pp. 021 504–13, 2014.
- [42] Xue, J., Li, W. and Qin, C., “The scuffing load capacity of involute spur gear systems based on dynamic loads and transient thermal elastohydrodynamic lubrication,” *Tribology International*, vol. 79, pp. 74–83, 2014.
- [43] Bobach, L., Beilicke, R., Bartel, D. and Deters, L., “Thermal elastohydrodynamic simulation of involute spur gears incorporating mixed friction,” *Tribology International*, vol. 48, pp. 191–206, 2012.
- [44] Luo, B. and Li, W., “Influence factors on bulk temperature field of gear,” *Proceedings of the Institution of Mechanical Engineers, Part J: Journal of Engineering Tribology*, vol. 231, no. 8, pp. 953–964, 2017.
- [45] Norton, R.L. and Han, J., *Design of machinery*. Higher Education Press, 2007.
- [46] Harris, S.L., “Dynamic loads on the teeth of spur gears,” *Proceedings of the Institution of Mechanical Engineers*, vol. 172, no. 1, pp. 87–112, 1958.

- [47] Mark, W.D., “Analysis of the vibratory excitation of gear systems: basic theory,” *The Journal of the Acoustical Society of America*, vol. 63, no. 5, pp. 1409–1430, 1978.
- [48] Munro, R.G., “A review of the theory and measurement of gear transmission error,” *Gearbox noise and vibration*, pp. 3–10, 1990.
- [49] Technische, B., *The deformation of loaded gears and the effect on their load-carrying capacity*. Department of Scientific & Industrial Research, 1951.
- [50] Kiekbusch, T., Sappok, D., Sauer, B. and Howard, I., “Calculation of the Combined Torsional Mesh Stiffness of Spur Gears with Two-and Three-Dimensional Parametrical FE Models.” *Strojniski Vestnik/Journal of Mechanical Engineering*, vol. 57, no. 11, 2011.
- [51] Palmgren, A., “Ball and roller bearing engineering,” *Philadelphia: SKF Industries Inc.*, 1959.
- [52] Ma, H., Zeng, J., Feng, R., Pang, X. and Wen, B., “An improved analytical method for mesh stiffness calculation of spur gears with tip relief,” *Mechanism and Machine Theory*, vol. 98, pp. 64–80, 2016.
- [53] Yu, W., Shao, Y. and Mechefske, C.K., “The effects of spur gear tooth spatial crack propagation on gear mesh stiffness,” *Engineering Failure Analysis*, vol. 54, pp. 103–119, 2015.
- [54] Sainsot, P., Velex, P. and Duverger, O., “Contribution of gear body to tooth deflections—a new bidimensional analytical formula,” *J. Mech. Des.*, vol. 126, no. 4, pp. 748–752, 2004.
- [55] Philippe, V., “On the modelling of spur and helical gear dynamic behaviour,” *Mechanical Engineering*, p. 75, 2012.
- [56] Lin, T., Ou, H. and Li, R. , “ A finite element method for 3D static and dynamic contact/impact analysis of gear drives,” *Comput. Methods Appl. Mech. Eng*, vol. 196, no. 9-12, p. 1716–1728, 2007.
- [57] Howard, I., Jia,S. and Wang, J. , “The dynamic modelling of a spur gear in mesh including friction and a crack,” *Mech. Syst. Signal Process*, vol. 15, no. 5, pp. 831–853, 2001.
- [58] Wang, Q., Chen, K., Zhao, B., Ma, H.and Kong, X., “An analytical-finite-element method for calculating mesh stiffness of spur gear pairs with complicated foundation and crack,” *Engineering Failure Analysis*, vol. 94, pp. 339–353, 2018.

- [59] Liang, X., Zhang, H., Zuo, M.J. and Qin, Y., “Three new models for evaluation of standard involute spur gear mesh stiffness,” *Mechanical Systems and Signal Processing*, vol. 101, pp. 424–434, 2018.
- [60] Chen, K., Huangfu, Y., Ma, H., Xu, Z., Li, X. and Wen, B., “Calculation of mesh stiffness of spur gears considering complex foundation types and crack propagation paths,” *Mechanical Systems and Signal Processing*, vol. 130, pp. 273–292, 2019.
- [61] Sato, T., Umezawa, K. and Ishikawa, J., “Effects of contact ratio and profile correction on gear rotational vibration,” *Bulletin of JSME*, vol. 26, no. 221, pp. 2010–2016, 1983.
- [62] Chang, L., Jeng, Y.R. and Huang, P.Y., “Modeling and analysis of the meshing losses of involute spur gears in high-speed and high-load conditions,” *Journal of Tribology*, vol. 135, no. 1, 2013.
- [63] K. T.O., “Cautionary note about r^2 ,” *The American Statistician*, vol. 39, no. 4, pp. 279–285, 1985.
- [64] Shi, J., Gou, X. and Zhu, L., “Modeling and analysis of a spur gear pair considering multi-state mesh with time-varying parameters and backlash,” *Mechanism and Machine Theory*, vol. 134, pp. 582–603, 2019.

Experimental data of flash temperature

Table A.1: Experimental data of flash temperature of spur gear obtained by Tobe [11].

Time [msec]	Flash temperature [$^{\circ}C$]	Mesh position [mm]	Time [msec]	Flash temperature [$^{\circ}C$]	Mesh position [mm]
0.18941	45.323	-7.6164	0.24519	77.47	-6.3795
0.1895	45.407	-7.5575	0.25986	80.283	-6.3206
0.19664	50.122	-7.4986	0.26228	81.971	-6.2617
0.19667	50.176	-7.4397	0.27206	84.033	-6.2028
0.19675	50.282	-7.3808	0.28427	86.659	-6.1439
0.20144	58.719	-7.3219	0.29157	89.472	-6.085
0.20152	58.785	-7.263	0.30134	92.097	-6.0261
0.20386	60.407	-7.2041	0.31113	93.41	-5.9672
0.20407	52.157	-7.1452	0.32587	93.785	-5.9083
0.20628	61.907	-7.0863	0.34065	92.474	-5.8494
0.20639	57.407	-7.0274	0.3456	90.974	-5.7905
0.20869	63.407	-6.9685	0.35302	89.287	-5.7316
0.21112	64.532	-6.9096	0.3629	87.225	-5.6727
0.21354	66.032	-6.8507	0.37032	85.351	-5.6138
0.21839	68.469	-6.7918	0.37527	84.226	-5.5549
0.21844	68.457	-6.7329	0.37776	82.914	-5.496
0.22081	69.969	-6.674	0.39498	82.165	-5.4371
0.22323	71.469	-6.6151	0.41464	82.166	-5.3782
0.2256	72.971	-6.5562	0.4294	81.604	-5.3193
0.22565	72.969	-6.4973	0.44662	81.042	-5.2604
0.23294	75.97	-6.4384	0.44913	78.98	-5.2015

Time [msec]	Flash temperature [$^{\circ}C$]	Mesh position [mm]	Time [msec]	Flash temperature [$^{\circ}C$]	Mesh position [mm]
0.45655	77.293	-5.1426	0.81873	42.251	-2.9633
0.45658	77.286	-5.0837	0.82603	44.876	-2.9044
0.45909	74.106	-5.0248	0.83581	46.939	-2.8455
0.47142	72.607	-4.9659	0.85298	48.252	-2.7866
0.48127	71.857	-4.907	0.86767	50.315	-2.7277
0.4886	73.357	-4.8481	0.89466	52.004	-2.6688
0.49101	75.045	-4.7892	0.91183	53.317	-2.6099
0.59923	72.05	-4.3769	0.91915	55.005	-2.551
0.60174	69.988	-4.318	0.92401	57.442	-2.4921
0.60671	67.739	-4.2591	0.93874	58.006	-2.4332
0.61168	65.676	-4.2002	0.95109	55.381	-2.3743
0.61666	63.052	-4.1413	0.95606	53.319	-2.3154
0.62162	61.365	-4.0824	0.96593	51.82	-2.2565
0.62906	58.74	-4.0235	0.99546	50.509	-2.1976
0.63646	57.616	-3.9646	1.0127	49.01	-2.1387
0.63896	56.303	-3.9057	1.03489	46.199	-2.0798
0.65121	57.616	-3.8468	1.04232	43.949	-2.0209
0.66344	59.679	-3.7879	1.05468	41.137	-1.962
0.66834	60.617	-3.729	1.07193	39.263	-1.9031
0.67081	59.867	-3.6701	1.08672	37.577	-1.8442
0.68069	57.993	-3.6112	1.10642	36.265	-1.7853
0.69055	56.868	-3.5523	1.1212	34.766	-1.7264
0.70042	55.556	-3.4934	1.13596	34.204	-1.6675
0.71271	55.182	-3.4345	1.14574	36.267	-1.6086
0.72747	54.62	-3.3756	1.1629	37.956	-1.5497
0.74226	53.121	-3.3167	1.16533	39.081	-1.4908
0.75704	51.81	-3.2578	1.18254	38.519	-1.4319
0.77429	49.935	-3.1989	1.19243	36.457	-1.373
0.7891	47.499	-3.14	1.19737	35.52	-1.3141
0.79898	45.624	-3.0811	1.20722	34.77	-1.2552
0.8064	43.562	-3.0222	1.21946	36.646	-1.1963

Time [msec]	Flash temperature [$^{\circ}C$]	Mesh position [mm]	Time [msec]	Flash temperature [$^{\circ}C$]	Mesh position [mm]
1.23419	37.209	-1.1374	1.84871	32.365	1.287
1.2416	35.897	-1.0785	1.86105	30.303	1.404
1.25638	34.21	-1.0196	1.88565	29.554	1.521
1.26133	32.898	-0.9607	1.90527	30.868	1.638
1.27357	34.961	-0.9018	1.92487	33.494	1.755
1.28334	37.024	-0.8429	1.9469	36.869	1.872
1.3006	34.963	-0.784	1.96403	39.683	1.989
1.31785	33.089	-0.7251	1.97377	42.87	2.106
1.3302	30.839	-0.6662	2.00074	45.309	2.223
1.35233	30.278	-0.6073	2.0056	47.559	2.34
1.36955	29.529	-0.5484	2.02527	47.185	2.457
1.39416	28.218	-0.4895	2.03762	44.936	2.574
1.41137	28.218	-0.4306	2.0524	43.624	2.691
1.43104	27.657	-0.3717	2.07452	43.25	2.808
1.44336	26.533	-0.3128	2.09163	46.814	2.925
1.46306	25.034	-0.2539	2.10878	48.877	3.042
1.49504	23.91	-0.195	2.12346	51.69	3.159
1.5098	23.161	-0.1361	2.15777	55.441	3.276
1.54422	22.6	-0.0772	2.17983	57.317	3.393
1.57865	21.852	-0.0183	2.20926	59.944	3.51
1.60326	20.541	0	2.23127	63.882	3.627
1.61555	20.542	0.117	2.25329	67.633	3.744
1.65236	22.418	0.234	2.27543	66.884	3.861
1.67688	24.482	0.351	2.27794	62.248	3.978
1.69896	25.983	0.468	2.27801	62.197	4.095
1.72106	26.921	0.585	2.28299	59.76	4.212
1.73575	28.797	0.702	2.28551	57.51	4.329
1.7554	29.548	0.819	2.29786	54.886	4.446
1.77259	29.924	0.936	2.31267	52.637	4.563
1.80449	31.613	1.053	2.34218	51.701	4.68
1.83148	33.301	1.17	2.36919	52.639	4.797

Time [msec]	Flash temperature [$^{\circ}C$]	Mesh position [mm]	Time [msec]	Flash temperature [$^{\circ}C$]	Mesh position [mm]
2.39125	54.89	4.914	2.69342	59.218	7.137
2.41329	58.079	5.031	2.70563	62.406	7.254
2.43041	61.267	5.148	2.71785	64.656	7.371
2.44263	63.892	5.265	2.73502	66.157	7.488
2.46228	64.081	5.382	2.75217	68.22	7.605
2.47464	61.457	5.499	2.75951	69.533	7.722
2.48452	59.395	5.616	2.77186	66.909	7.839
2.49684	58.083	5.733	2.77932	63.722	7.956
2.51645	59.959	5.85	2.77939	63.58	8.073
2.55325	62.773	5.967	2.78684	58.097	8.19
2.58271	63.712	6.084	2.79427	55.848	8.307
2.59511	59.588	6.201	2.80659	54.536	8.424
2.60009	57.151	6.318	2.82136	53.787	8.541
2.61246	53.776	6.435	2.82876	52.475	8.658
2.61745	50.964	6.552	2.84847	50.601	8.775
2.64205	49.841	6.669	2.85344	48.726	8.892
2.6617	50.592	6.786	2.86823	46.852	9.009
2.68122	55.655	6.903	2.88055	45.728	9.327
2.68133	55.643	7.02			

Appendix B

Values of flexural endurance and surface endurance limit

Table B.1: Values of flexural endurance limit [45].

Material of pinion and gear	Brinell hardness number (B.H.N.)	Flexural endurance limit (σ_e) in MPa
Grey cast iron	160	84
Semi-steel	200	126
Phosphor bronze	100	168
Steel	150	252
	200	350
	240	420
	280	490
	300	525
	320	560
	350	595
	360	630
	400 and above	700

Table B.2: Values of surface endurance limit [45].

Material of pinion and gear	Brinell hardness number (B.H.N.)	Flexural endurance limit (σ_{es}) in MPa
Grey cast iron	160	630
Semi-steel	200	630
Phosphor bronze	100	630
Steel	150	350
	200	490
	240	616
	280	721
	300	770
	320	826
	350	910
	400	1050

Table B.3: Values of tooth error in action (e) verses module [45].

Module (m) in mm	Tooth error in action (e) in mm		
	First class commercial gears	Carefully cut gears	Precision gears
Up to 4	0.051	0.025	0.0125
5	0.055	0.028	0.015
6	0.065	0.032	0.017
7	0.071	0.035	0.0186
8	0.078	0.0386	0.0198
9	0.085	0.042	0.021
10	0.089	0.0445	0.023
12	0.097	0.0487	0.0243
14	0.104	0.052	0.028
16	0.110	0.055	0.030
18	0.114	0.058	0.032
20	0.117	0.059	0.033

Appendix C

Values of coefficients equation 5.8

Table C.1: Values of coefficients equation 5.8

	$A_i(\times 10^{-5})$	$B_i(\times 10^{-3})$	$C_i(\times 10^{-4})$	$D_i(\times 10^{-3})$	E_i	F_i
$L^*(h_{fi}, \theta_f)$	-5.574	-1.9986	-2.3015	4.7702	0.0271	6.8045
$M^*(h_{fi}, \theta_f)$	60.111	28.100	-83.431	-9.9256	0.1624	0.9086
$P^*(h_{fi}, \theta_f)$	-50.952	185.50	0.0538	53.300	0.2895	0.9236
$Q^*(h_{fi}, \theta_f)$	-6.2042	9.0889	-4.0964	7.8297	-0.1472	0.6904

Matlab code to calculate essential parameters

```
% General given parameters
Clc;clear;

rP=28; rG=44;% pitch radius of pinion and gear respectively
NP=2090;NG=1330; % RPM of pinion and gear respectively [RPM]
wP=NP*2*pi/60;wG=NG*2*pi/60;% speed of pinion and gear respectively[rad/s]
dp=56*10^-3;%Pitch diameter of pinion [m]
alpha=20*pi/180;% Pressure angle [rad]
T=75.5;% Load [N/mm]
W=453;% Normal load[N]
B=3*10^-3; % face width [m]

%Gears material properties
EG = 207*10^9; EP = EG; % Elastic modulus [MPa]
CpG = 485; CpP = CpG; %Specific heat [1000 N mm/Kg {\circ}C]
K=42.3; % Thermal conductivity [1000 N mm/mm s {\circ}C]
rogh=7.86*10^3; % Density [KG/mm^3]
poission_ratio=0.3; % Poisson ratio

% load shearing
alpha=20*pi/180;
dx=17.965/10000;
x=[-9.327:dx:8.638]
for k=1:length(x)
    if (x(k)>=-9.327) & (x(k)<=-3.18)
        y(k)=2.2*abs(-9.327-x(k))+((0.5*11919)/(6*28*cos(alpha)));
    elseif x(k)>=-3.18 & x(k)<=2.49
        y(k)=((11919)/(6*28*cos(alpha)));
    else
        y(k)=1.62*((0.5*11919)/(6*28*cos(alpha)))-2.1145*abs((8.638+x(k)));
    end
end
plot(x,y,'-b','color',[0 0 0],'LineWidth',2,'markersize',5,
'MarkerEdgeColor','auto','markerfacecolor','auto');
grid on;
xlabel('Mesh position [ mm ]','FontSize',12);
ylabel('Load shearing [N/mm]','FontSize',12);
```

```

% Gear and pinion involute radius of curvature
RP=(rP*sin(alpha)+x);%radius of curvature of pinion [mm]
RG=(rG*sin(alpha)-x);;%radius of curvature of gear [mm]
R_s=((1./RP)+(1./RG)).^-1 % Equivalent radius of curvature [mm]
plot(x,RP,'-','color',[1 0 0],'LineWidth',2,'markersize',1,
'MarkerEdgeColor','k','markerfacecolor','k'); hold on
plot(x,RG,'-','color',[0 0 0],'LineWidth',2,'markersize',1,
'MarkerEdgeColor','k','markerfacecolor','k'); hold on
plot(x,R_s,'-','color',[0 0.447 0.741],'LineWidth',2,'markersize',2,
'MarkerEdgeColor','auto','markerfacecolor','auto'); hold off
grid on,title('a')
legend('Pinion involute',' Gear involute','Equivalent radius ')
xlabel(' Mesh position [ mm ]','FontSize',12)
ylabel(' Radius of curvature [ mm ]','FontSize',12)

% Sliding velocity and surface velocities
RP=(rP*sin(alpha)+x);%radius of curvature of pinion [mm]
RG=(rG*sin(alpha)-x);;%radius of curvature of gear [mm]
R_s=((1./RP)+(1./RG)).^-1; % Equivalent radius of curvature [mm]
UP=wP*RP/1000; % surface velocity of pinion [m/s]
UG=wG*RG/1000;% surface velocity of gear [m/s]
U_s=(wP+wG)*abs(x)/1000;% sliding velocity [m/s]
plot(x,UP,'-','color',[1 0 0],'LineWidth',2,'markersize',1,
'MarkerEdgeColor','k','markerfacecolor','k'); hold on
plot(x,U2,'x','color',[0 0 0],'LineWidth',2,'markersize',1,
'MarkerEdgeColor','k','markerfacecolor','k');
plot(x,U_s,'--','color',[0 0.447 0.741],'LineWidth',2,'markersize',1,
'MarkerEdgeColor','k','markerfacecolor','k'); hold off;
legend('surface velocity of pinion','Surface velocity of gear',
'sliding velocity');
axis tight;grid on;
legend('Pinion Surface velocity','Gear Surface velocity','Slide
Velocity');
xlabel('Mesh position [ mm ]','FontSize',12);
ylabel('Velocity [ m/s ]','FontSize',12);

```

```

% Contact area
E_r=(1/2*((1-(poission_ratio)^2)/(EP) +(1-(poission_ratio)^2)/(EP)))^-1 *10^-6;%
reduced elastic of module(N/m^2);
RP=(rP*sin(alpha)+x);
RG=(rG*sin(alpha)-x);
R_s=((1./RP)+(1./RG)).^-1;
UP=wP*RP;UG=w2*RG;
b=((8*y.*(R_s)/(pi*E_r)).^0.5); % Contact width [m]
plot(x,b,'-b','color',[0 0 0],'LineWidth',2,'markersize',5,
'MarkerEdgeColor','auto','markerfacecolor','auto');
axis tight;grid on;
xlabel('Mesh position [ mm ]','FontSize',12);
ylabel('Contact width [ mm ]','FontSize',12);

% Peccelet number
XP=K/(rogh*10^-6*CpP) ; % Thermal defeasibility
LeP=(b.*U1)/(2*XP); % Pinion Peclet number
LeG=(b.*U2)/(2*XP); % Gear peclet number
plot(x,LeP,'-', 'color',[0 0 0],'LineWidth',2,'markersize',5,
'MarkerEdgeColor','auto','markerfacecolor','auto');hold on
plot(x,LeG,'--', 'color',[0 0 0],'LineWidth',2,'markersize',5,
'MarkerEdgeColor','auto','markerfacecolor','auto');hold off;
axis tight;grid on;
legend('Le_P','Le_G');
xlabel('Mesh position [ mm ]','FontSize',12);
ylabel('Peclet Number','FontSize',12);

% Maximum contact pressure
Pmax=(2.*y*1000)./(pi.*b*10^-3); % Maximum contact pressure [Pa]
plot(x,Pmax,'-b','color',[0 0 0],'LineWidth',2,'markersize',5,
'MarkerEdgeColor','auto','markerfacecolor','auto');
axis tight;grid on;
xlabel('Mesh position [ mm ]','FontSize',12);
ylabel('Contact Pressure [Pa] ','FontSize',12);

%Film thickness
WF=y./E_r.*R_s;%EHL load parameter
L_P_V_coefficient =1.2*10^-8; %Pressure-viscosity coefficient [Pa^-1]
T_V_coefficient =0.04; %Temperature-viscosity coefficient [C^-1]
L_A_V=0.01; %Lubricant ambient viscosity [Pa-s]
L_A_T=100; %Lubricant ambient temperature [{^\circ}C]
L_T_C=0.14; %Lubricant thermal conductivity [W/(m{^\circ}C)]
G=L_P_V_coefficient *E_r; %EHL material parameter
u_inte=(U2+U1)*(10^-3)/2;% Entraining velocity in the tooth contact [m/s]
C_p=(1+((0.58*10^-9*Pmax)./(1+1.68*10^-9.*Pmax)))^-1;% Compressibility reduction
factor
C_t=exp((-0.75*T_V_coefficient *L_A_V*(u_inte.^2)/(4*L_T_C));% Inlet shear-
heating reduction factor
Uf=(L_A_V.*u_inte)./(E_r.*R_s*10^-3)%EHL speed parameter
h_o=(3.06.*(C_p.*C_t.*(R_s*10^-3).*Uf.^0.69).*(G^(0.56).*(WF.^-0.1)))/10^-6;%
Film thickness [\mum]
plot(x,h_o,'-b','color',[0 0 0],'LineWidth',2,'markersize',5,'MarkerEdgeColor',
'auto','markerfacecolor','auto')
grid on;axis tight
xlabel(' Mesh position [ mm ]','FontSize',12)
ylabel(' Film thickness [ \mum ] ','FontSize',12)

```

Matlab code for heat generation and flash temperature calculation

```

%Heat generation due to friction
friction_c=[0.15 0.2 0.3]';%coefficient of friction
Q=y.*b.*abs(U1-U2).*friction_c;% Heat generation
plot(x,Q(1,:), '--', 'color', [0 0 0], 'LineWidth',2, 'markersize',5,
'MarkerEdgeColor', 'k', 'markerfacecolor', 'k'); hold on
plot(x,Q(2,:), '-b', 'color', [0 0.75 1], 'LineWidth',2, 'markersize',5,
'MarkerEdgeColor', 'auto', 'markerfacecolor', 'auto');hold on;
plot(x,Q(3,:), '-r', 'LineWidth',2, 'markersize',5, 'MarkerEdgeColor', 'r',
'markerfacecolor', 'r');hold on
axis tight;grid on;
legend('SR_P=0.6', 'SR=0.8', 'SR=1');
xlabel('Mesh position [ mm ]', 'FontSize',12);
ylabel('Generated heat [ W ]', 'FontSize',12);hold off;

% Flash Temperature calculation
Tfmax=(1.11.*friction_c.*y.*1000.*abs(sqrt(UP)-
sqrt(UG)))./(sqrt(2.*(b).*K*rogh*CpP));% flash temperature
plot(x,Tfmax(1,:), '--', 'color', [0 0 0], 'LineWidth',2, 'markersize',5,
'MarkerEdgeColor', 'k', 'markerfacecolor', 'k'); hold on
plot(x,Tfmax(2,:), '-b', 'color', [0 0.75 1], 'LineWidth',2, 'markersize',5,
'MarkerEdgeColor', 'auto', 'markerfacecolor', 'auto');hold on
plot(x,Tfmax(3,:), '-r', 'LineWidth',2, 'markersize',5, 'MarkerEdgeColor', 'r',
'markerfacecolor', 'r');hold off
grid on;
legend('SR_P=0.6', 'SR=0.8', 'SR=1');
xlabel('Mesh position [ mm ]', 'FontSize',12);
ylabel('Temperature [^\circ C] ', 'FontSize',12);

%Bulk temperature calculation
Tfmax=20+(1.11.*friction_c.*y.*1000.*abs(sqrt(U1)-
sqrt(U2)))./(sqrt(2.*(b).*K*rogh*CpP));
plot(x,Tfmax(1,:), '--', 'color', [0 0 0], 'LineWidth',2, 'markersize',5,
'MarkerEdgeColor', 'k', 'markerfacecolor', 'k'); hold on
plot(x,Tfmax(2,:), '-b', 'color', [0 0.75 1], 'LineWidth',2, 'markersize',5,
'MarkerEdgeColor', [0 0.75 1], 'markerfacecolor', 'auto');hold on
plot(x,Tfmax(3,:), '-r', 'LineWidth',2, 'markersize',5, 'MarkerEdgeColor',
'r', 'markerfacecolor', 'r');hold off
grid on;
legend('SR_P=0.6', 'SR=0.8', 'SR=1');
xlabel('Mesh position [ mm ]', 'FontSize',12);
ylabel('Temperature [^\circ C] ', 'FontSize',12);

```


Matlab code for mesh stiffness calculation

```

%%% Gear mesh tooth
function [K_a K_b K_s K_f]=Pinion_mesh_tooth(E,B,G,r,r_b,r_d,teta_f,S_f,
h_f,teta_b,alpha_0,alpha_1,beta_0)
%K_a is Axial compressive stiffness
%K_b is Bending stiffness.
%K_s is Shear stiffness
%K_f is Tooth Foundation Induced Deformation
C_pcf = [ -5.574e-5 -1.9986e-3 -2.3015e-4 4.7702e-3 0.0271 6.8045;
          60.111e-5 28.100e-3 -83.431e-4 -9.9256e-3 0.1624 0.9086;
          -50.952e-5 185.50e-3 0.0538e-4 53.300e-3 0.2895 0.9236;
          -6.2042e-5 9.0889e-3 -4.0964e-4 7.8297e-3 -0.1472 0.6904];
Ai=C_pcf(:,1); Bi=C_pcf(:,2); Ci=C_pcf(:,3);
Di=C_pcf(:,4); Ei=C_pcf(:,5); Fi=C_pcf(:,6);
for i=1:4
    Xi(i)=Ai(i)/teta_f^2 + Bi(i)*h_f^2 + Ci(i)*h_f/teta_f + Di(i)/teta_f +
Ei(i)*h_f + Fi(i);
end
L_star=Xi(1); M_star=Xi(2); P_star=Xi(3);
Q_star=Xi(4);%coefficients
dbeta=(alpha_1-alpha_0)/1000;
for i=1:1001
    beta=(i-1)*dbeta+alpha_0;
    h=r_b*((beta+teta_b)*cos(beta)-sin(beta));
    d=r_b*((beta+teta_b)*sin(beta)+cos(beta))-r;
    u_f=d+r-r_d-h*tan(beta);
    invK_f=(cos(beta)^2/(E*B))*(L_star*(u_f/S_f)^2 + M_star*(u_f/S_f) +
P_star*(1+Q_star*(tan(beta))^2));
    invK_a=0;
    invK_b=0;
    invK_s=0;
    dbetaj=(beta-beta_0)/1000;
    for j=1:1000
        beta1=(j-1)*dbetaj+beta_0;
        h1=r_b*((beta1+teta_b)*cos(beta1)-sin(beta1));
        x1=r_b*((beta1+teta_b)*sin(beta1)+cos(beta1))-r;
        beta2=(j)*dbetaj+beta_0;
        h2=r_b*((beta2+teta_b)*cos(beta2)-sin(beta2));
        x2=r_b*((beta2+teta_b)*sin(beta2)+cos(beta2))-r;
        dx=x2-x1;
        A_x=(h1+h2)*B;%Area of the section of distance 'x' measured from
the load application point
        I_x=1/12*(h1+h2)^3*B;%Area moment of inertia
        invK_a=invK_a+ (sin(beta)^2/(E*A_x))*dx;
        invK_b=invK_b+ ((d-x1)*cos(beta)-h*sin(beta))^2/(E*I_x))*dx;
        invK_s=invK_s+ (1.2*cos(beta)^2/(G*A_x))*dx;
    end
    K_a(i)=1/invK_a;
    K_b(i)=1/invK_b;
    K_s(i)=1/invK_s;
    K_f(i)=1/invK_f;
end
end

```

```

%% Pinion mesh tooth
function [K_a K_b K_s
K_f]=Pinion_mesh_tooth(E,B,G,r,r_b,r_d,teta_f,S_f,h_f,teta_b,alpha_0,alpha
_1,beta_0)
C_pcf = [ -5.574e-5 -1.9986e-3 -2.3015e-4 4.7702e-3 0.0271 6.8045;
60.111e-5 28.100e-3 -83.431e-4 -9.9256e-3 0.1624 0.9086;
-50.952e-5 185.50e-3 0.0538e-4 53.300e-3 0.2895 0.9236;
-6.2042e-5 9.0889e-3 -4.0964e-4 7.8297e-3 -0.1472 0.6904];
Ai=C_pcf(:,1); Bi=C_pcf(:,2); Ci=C_pcf(:,3);
Di=C_pcf(:,4); Ei=C_pcf(:,5); Fi=C_pcf(:,6);
for i=1:4
Xi(i)=Ai(i)/teta_f^2 + Bi(i)*h_f^2 + Ci(i)*h_f/teta_f + Di(i)/teta_f +
Ei(i)*h_f + Fi(i);
end
L_star=Xi(1); M_star=Xi(2); P_star=Xi(3); Q_star=Xi(4);
h0=r_b*teta_b;
dbeta=(alpha_1-alpha_0)/1000;
for i=1:1001
beta=(i-1)*dbeta+alpha_0;
h=r_b*((beta+teta_b)*cos(beta)-sin(beta));
d=r_b*((beta+teta_b)*sin(beta)+cos(beta))-r;
u_f=d+r-r_d-h*tan(beta);
invK_f=(cos(beta)^2/(E*B))*(L_star*(u_f/S_f)^2 + M_star*(u_f/S_f) +
P_star*(1+Q_star*(tan(beta))^2));
invK_a=0; invK_b=0; invK_s=0;
dbetaj=(beta-beta_0)/1000;
for j=1:1000
beta1=(j-1)*dbetaj+beta_0;
h1=r_b*((beta1+teta_b)*cos(beta1)-sin(beta1));
x1=r_b*((beta1+teta_b)*sin(beta1)+cos(beta1))-r;
beta2=(j)*dbetaj+beta_0;
h2=r_b*((beta2+teta_b)*cos(beta2)-sin(beta2));
x2=r_b*((beta2+teta_b)*sin(beta2)+cos(beta2))-r;
dx=x2-x1; A_x=(h1+h2)*B;
I_x=1/12*(h1+h2)^3*B;
invK_a=invK_a+ (sin(beta)^2/(E*A_x))*dx;
invK_b=invK_b+ (((d-x1)*cos(beta)-h*sin(beta))^2/(E*I_x))*dx;
invK_s=invK_s+ (1.2*cos(beta)^2/(G*A_x))*dx;
end
dx=(r_b-r_d)/1000;
for j=1:1000
x1=r_d+(j-1)*dx-r;
h1=h0;x2=r_d+(j)*dx-r;
h2=h0; dx=x2-x1; A_x=(h1+h2)*B; I_x=1/12*(h1+h2)^3*B;
invK_a=invK_a+ (sin(beta)^2/(E*A_x))*dx;
invK_b=invK_b+ (((d-x1)*cos(beta)-h*sin(beta))^2/(E*I_x))*dx;
invK_s=invK_s+ (1.2*cos(beta)^2/(G*A_x))*dx;
end
K_a(i)=1/invK_a; K_b(i)=1/invK_b; K_s(i)=1/invK_s; K_f(i)=1/invK_f;
end
end

```

```

function Meshstiffness=bsm2(y,a,b,eps)
syms x
X=(a+b)/2;
fx=subs(y,X);
E=abs(fx);
while E>eps
    fa=subs(y,a);fb=subs(y,b); fx=subs(y,X);
    if fa*fx<0
        b=X;
    else
        a=X;
    end
    X=(a+b)/2;
    fx=subs(y,X);
    E=abs(fx);
end
Meshstiffness=X;
%%%%%%%%%%%%%%%%%%%%%%%%%%%%%%%%%%%%%%%%%%%%%%%%%%%%%%%%%%%%%%%%%%%%%%%% Gear pairs input parameters %%%%%%%%%%%%%%%%%%%%%%%%%%%%%%%%%%%%%%%%%%%%%%%%%%%%%%%%%%%%%%%%%%%%%%%%%

m=4e-3;% Module [m]
TP=14;% Number of teeth of pinion
TG=22;% Number of teeth of gear
alpha=20*pi/180;% Pressure angle [rad]
EG=EP=273e9;% Modules of elasticity [Pa]
poision_ratio=0.3;
B=6e-3;% Gear width [m]
r_hP=36e-3;% Pinion hub radius [m]
r_hG=45e-3;% Gear hub radius [m]
%%%%%%%%%%%%%%%%%%%%%%%%%%%%%%%%%%%%%%%%%%%%%%%%%%%%%%%%%%%%%%%%%%%%%%%% Calculating basic parameters %%%%%%%%%%%%%%%%%%%%%%%%%%%%%%%%%%%%%%%%%%%%%%%%%%%%%%%%%%%%%%%%%%%%%%%%%
G=EP/(2*(1+poision_ratio)); % Modulus of rigidity [Pa]
rP=m*TP/2; % Pinion pitch circle radius [m]
r_aP=rP+m; % Pinion addendum circle radius [m]
r_fP=rP-0.25*m;
r_dP=rP-1.25*m; % Pinion dedendum circle radius [m]
r_bP=rP*cos(alpha); % Pinion base circle radius [m]
rG=m*TG/2; % Gear pitch circle radius [m]
r_aG=rG+1*m; % Gear addendum circle radius [m]
r_fG=rG-1*m; %
r_dG=rG-1.25*m; % Gear dedendum circle radius [m]
r_bG=rG*cos(alpha); % Gear base circle radius [m]
eps_alpha=(sqrt(r_aG^2-r_bG^2)+sqrt(r_aP^2-r_bP^2)-(rP+rG)*sin(alpha))/(pi*m*cos(alpha)); %
Contact length [m]
inv_alpha=tan(alpha)-alpha;
teta_bP=pi/(2*TP)+inv_alpha; teta_bG=pi/(2*TG)+inv_alpha;
h_fP=r_dP/r_hP; h_fG=r_dG/r_hG;
%%%%%%%%%%%%%%%%%%%%%%%%%%%%%%%%%%%%%%%%%%%%%%%%%%%%%%%%%%%%%%%%%%%%%%%% Calculating Meshing Degrees %%%%%%%%%%%%%%%%%%%%%%%%%%%%%%%%%%%%%%%%%%%%%%%%%%%%%%%%%%%%%%%%%%%%%%%%%
syms x
if r_bP<r_fP
    alpha_0P=bsm2(r_bP*((x+teta_bP)*sin(x)+cos(x))-r_fP,0,pi/2,1e-10);
    alpha_1G=bsm2(r_bG*((x+teta_bG)*sin(x)+cos(x))-r_aG,0,pi/2,1e-10);
else
    alpha_0P=0;
    alpha_1G=bsm2(r_bG*((x+teta_bG)*sin(x)+cos(x))-(r_aG-(r_bP-r_fP)),0,pi/2,1e-10);
end
if r_bG<r_fG
    alpha_0G=bsm2(r_bG*((x+teta_bG)*sin(x)+cos(x))-r_fG,0,pi/2,1e-10);
    alpha_1P=bsm2(r_bP*((x+teta_bP)*sin(x)+cos(x))-r_aP,0,pi/2,1e-10);
else
    alpha_0G=0;
    alpha_1P=bsm2(r_bP*((x+teta_bP)*sin(x)+cos(x))-(r_aP-(r_bG-r_fG)),0,pi/2,1e-10);
end
end

```

```

##### Calculating root arcs and degrees #####
syms x
if r_bP<r_dP
    beta_0P=bsmG(r_bP*((x+teta_bP)*sin(x)+cos(x))-r_dP,0,pi/2,1e-10);
    L_d1=r_b1*((beta_01+teta_b1)*cos(beta_0P)-sin(beta_0P));
else
    beta_0P=0;
    L_dP=r_bP*teta_bP;
end
if r_bG<r_dG
    beta_0G=bsmG(r_bG*((x+teta_bG)*sin(x)+cos(x))-r_dG,0,pi/2,1e-10);
    L_dG=r_bG*((beta_0G+teta_bG)*cos(beta_0G)-sin(beta_0G));
else
    beta_0G=0;
    L_dG=r_bG*teta_bG;
end
teta_fP=atan(L_dP/r_dP);
teta_fG=atan(L_dG/r_dG);
S_fP=2*teta_fP*r_dP;
S_fG=2*teta_fG*r_dG;
##### Stiffness of pinion #####
if r_dP<=r_bP
    [K_aP K_bP K_sP K_fP]=Pinion_mesh_tooth(E,B,G,rP,r_bP,r_dP,teta_fP,
S_fP,h_fP,teta_bP,alpha_0P,alpha_1P,beta_0P);
else
    [K_aP K_bP K_sP K_fP]=Gear_mesh_tooth(E,B,G,rP,r_bP,r_dP,teta_fP,S_fP,
h_fP,teta_bP,alpha_0P,alpha_1P,beta_0P);
end
##### stiffness of gear #####
if r_dG<=r_bG
    [K_aG K_bG K_sG K_fG]=Pinion_mesh_tooth(E,B,G,rG,r_bG,r_dG,teta_fG,S_fG,
h_fG,teta_bG,alpha_0G,alpha_1G,beta_0G);
else
    [K_aG K_bG K_sG K_fG]=Gear_mesh_tooth(E,B,G,rG,r_bG,r_dG,teta_fG,S_fG,
h_fG,teta_bG,alpha_0G,alpha_1G,beta_0G);
end
K_aG=fliplr(K_aG);K_bG=fliplr(K_bG);K_sG=fliplr(K_sG);K_fG=fliplr(K_fG);
##### Mesh stiffness and TVMS #####
K_a=1./(1./K_aP+1./K_aG);K_b=1./(1./K_bP+1./K_bG);K_f=1./(1./K_fP+1./K_fG);K_s=1./(1./K_s
P+1./K_sG)
K_h=(pi*E*B)/(4*(1-poisson_ratio^2));
K_h=ones(1,length(K_aP))*K_h;
K=1./(1./K_h + 1./K_a + 1./K_b + 1./K_s + 1./K_f);
PTH=length(K);
K2=[zeros(1,PTH) K zeros(1,PTH)];
Pb=floor(PTH/eps_alpha);
dbeta=360*eps_alpha/(NP*(PTH-1));
for i=1:PTH
    K_M(i)=K2(i+PTH)+K2(i+PTH+Pb)+K2(i+PTH-Pb);
    betai(i)=dbeta*(i-1);
end
##### Plotting #####
plot(betai,K,'-','color',[0 0 0],'LineWidth',2,'markersize',5,
'MarkerEdgeColor','auto','markerfacecolor','auto');
grid on;
ylabel('Mesh stiffness [N/mm]');
xlabel('Roll angle [Deg]');
plot(betai,K_M,'-','color',[0 0 0],'LineWidth',2,'markersize',5,
'MarkerEdgeColor','auto','markerfacecolor','auto');
grid on;
ylabel('Time Varying Mesh stiffness [N/mm]');
xlabel('Roll angle [Deg]');

```

```

% Mesh stiffness and Load shearing calculation using Approximate method
clc;clear;

z1=14;%Number of teeth of pinion
z2=22;% Number of teeth of gear
rpp=28;%radius of pinion pitch circle
rap=32;%radius of pinion addendum circle
rbp=26.311;% radius of pinion dedendum circle
KMmax=1;%maximum mesh stiffness
rcp=(26.311:0.01:32);% contact distance
zita_out=z1/(2*pi)*(sqrt((rap^2/(rbp^2))-1));
zita_inn=z1/(2*pi)*(sqrt((rbp^2/rbp^2))-1);
epselon=(-(zita_inn)+(zita_out)); % Contact ratio
zita_m=zita_inn + (epselon/2);
zita=((z1/(2*pi)).*(sqrt(((rcp.^2)/(rbp^2))-1)));
b_o=(0.5*((1+(epselon/2))^2)-1)^-0.5;
KM=(cos(b_o.*(zita-zita_m)));

%%%%% plot mesh stiffness%%%%%%%%%%%%%%
plot(zita,KM,'-b','color',[0 0 0],'LineWidth',2,'markersize',5,
'MarkerEdgeColor','auto','markerfacecolor','auto')
grid on;
xlabel('Contact ratio ','FontSize',12);
ylabel('Mesh stiffness [ K_M(zita) ] ','FontSize',12);

%%%%% plot load shear%%%%%%%%%%%%%%
alpha=20*pi/180;
dx=17.965/568;
x=[-9.327:dx:8.638];
for k=1:length(zita)
    if (zita_inn<=zita(k)) & (zita(k)<=zita_inn+epselon-1);
        load_shearing(k)=75.*(0.36+((0.28/(epselon-1))*(zita(k)-zita_inn)));
    elseif (zita_inn+epselon-1<=zita(k)) & (zita(k)<=zita_inn+1);
        load_shearing(k)=1.*75;
    else (zita_inn+1<=zita(k)) & (zita<=zita_inn+epselon);
        load_shearing(k)=75.*( 0.36-((0.28/(epselon-1))*(zita(k)-zita_inn-
epselon)));
    end
end
plot(zita,load_shearing,'-b','color',[0 00 0],'LineWidth',2,'markersize',
5,'MarkerEdgeColor','auto','markerfacecolor','auto');
grid on;
xlabel('Contact ratio','FontSize',12);
ylabel(' Load shearing [ N/mm ] ','FontSize',12);

```

Lubricant parameters

Table G.1: Lubricant parameter [62]

Independent parameters	Value
Lubricant ambient temperature, T_o	100 °C
Lubricant ambient viscosity, η_o	0.01 Pa s
Pressure viscosity coefficient, ψ	$1.2 \times 10^{-8} Pa^{-1}$
Temperature viscosity coefficient, β	$0.04^\circ C^{-1}$
Lubricant thermal conductivity, K_f	0.14 W/(m°C)
Lubricant density, ρ_f	800 kg/m ³
Lubricant specific heat, C_f	2290 J/(kg°C)

Finite Element analysis summary

Table H.1: Mesh convergency analysis

Mesh size (mm)	Number of Elements	Number of Nodes
1.1	264	329
0.8	340	418
0.6	403	486
0.4	531	637
0.2	941	1125
0.08	3999	4396
0.06	6320	6820
0.05	7513	8100
0.04	8866	9564

Table H.2: Finite element analysis summary

Backlash of gear	Number of Elements	Number of Nodes	Total CPU time (hrs.)
0 mm	62830	190488	10.84194
0.2 mm	62692	190048	8.161389
0.4 mm	65187	197565	10.81167
0.6 mm	62107	188319	11.99361
0.8 mm	64747	196209	15.19306
1 mm	64048	194148	11.43111

Systems of consistent units

Table I.1: Systems of consistent units

Quantity	SI	SI(mm)	US Unit(ft)	US Unit (inch)
Length	m	mm	ft	in
Force	N	N	lbf	lbf
Mass	Kg	tonne	slug	$lbf s^2/in$
Time	s	s	s	s
Stress	$Pa(N/m^2)$	$MPa(N/mm^2)$	lbf/ft^2	$psi(lbf/in^2)$
Energy	J	mJ ($10^{-3}J$)	ft lbf	in lbf
Density	Kg/m^3	$tonne/mm^3$	$slug/ft^3$	$lbf s^2/in^4$

ADAMS procedures for a dynamic analysis

Figure J.1: Insert Gear Pair wizard - Type

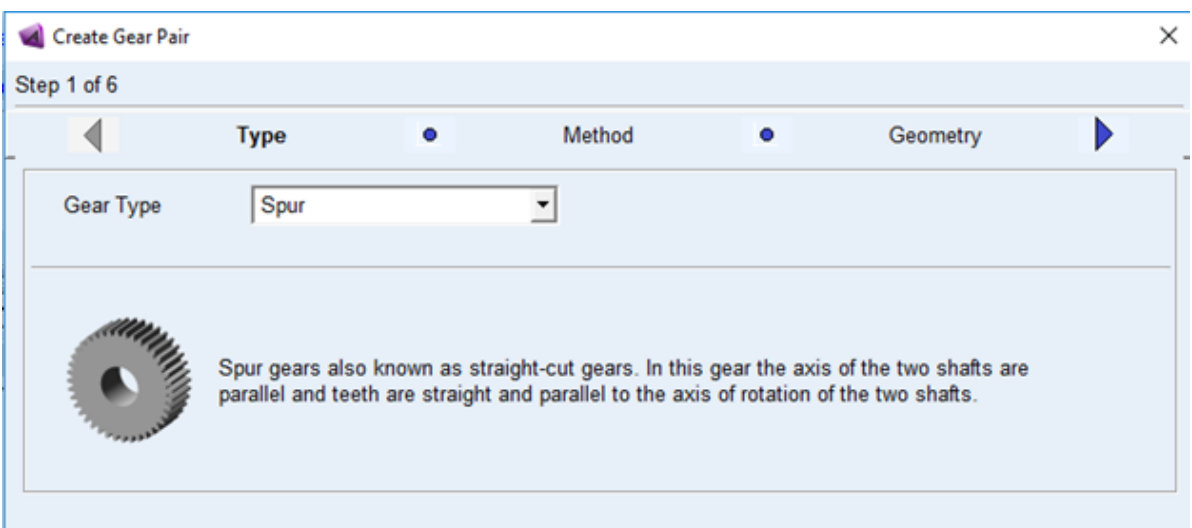


Figure J.2: Insert Gear Pair wizard - Method

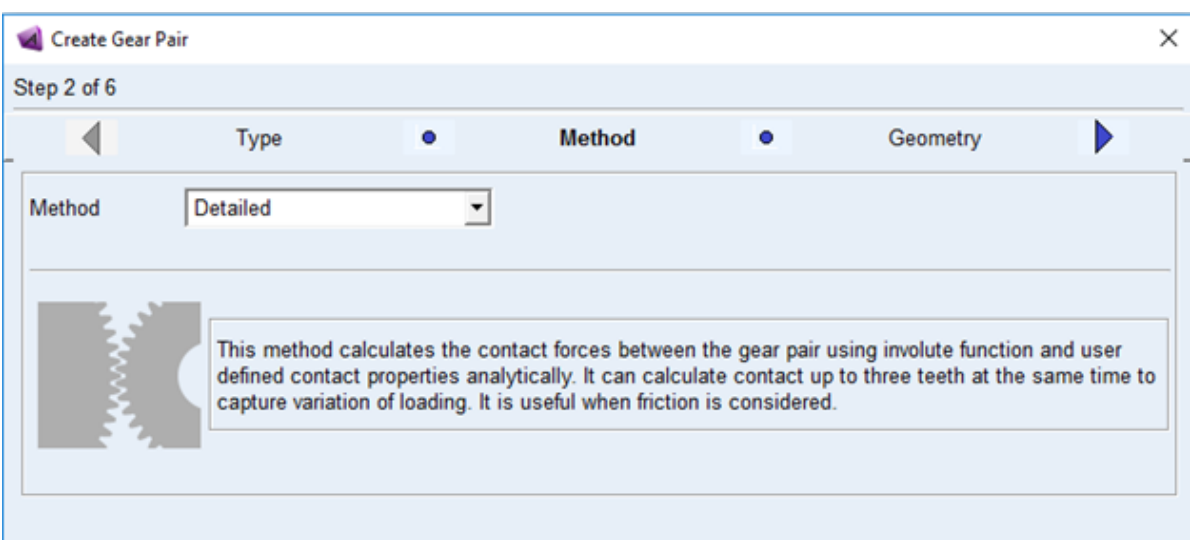


Figure J.3: Insert Gear Pair wizard – Geometry

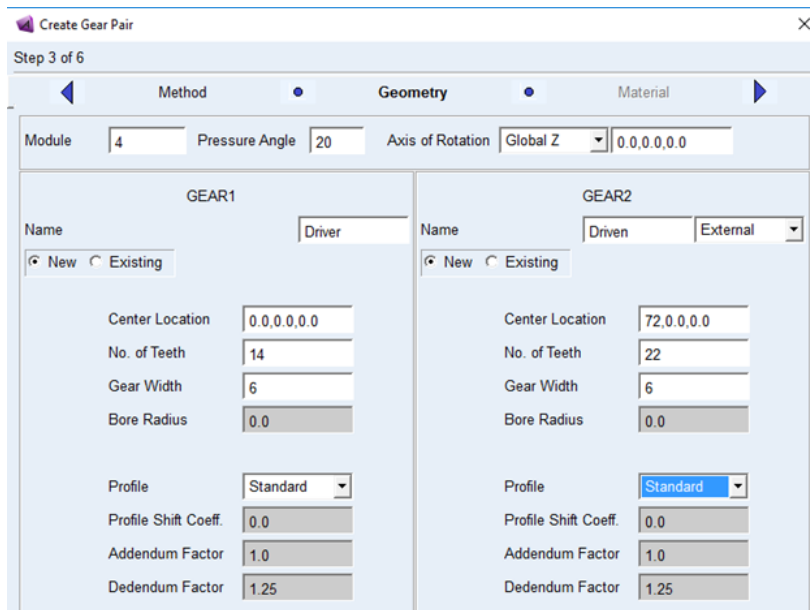


Figure J.4: Insert Gear Pair wizard - Material

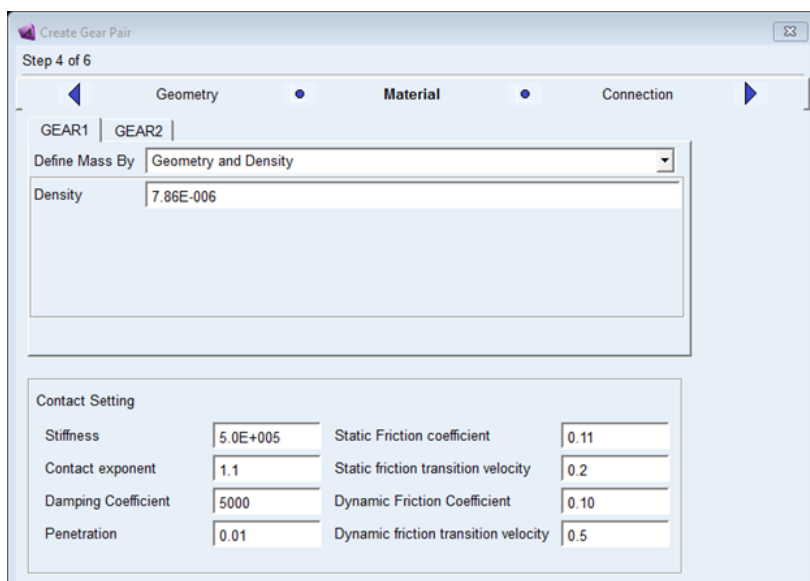


Figure J.5: Insert Gear Pair Wizard - Connection

